

**INTERFACIAL ENGINEERING OF SYNTHETIC AMPHIPHILES AND ITS
IMPACT IN THE DESIGN OF EFFICIENT
GENE AND DRUG DELIVERY SYSTEMS**

**A Dissertation
Submitted to
the Temple University Graduate Board**

**In Partial Fulfillment
of the Requirement for the Degree
DOCTOR OF PHILOSOPHY**

**By
Vishnu Dutt Sharma
May 2014**

Examining Committee Members:

Dr. Marc A. Ilies, Advisory Chair

Dr. Michael Borenstein, Pharmaceutical Sciences

Dr. Reza Fassihi, Pharmaceutical Sciences

Dr. Daniel J. Canney, Pharmaceutical Sciences

Dr. Stephanie L. Wunder, External Members, College of Science and Technology

©
Copyright
2014

by

Vishnu Dutt Sharma
All Rights Reserved

ABSTRACT

Cancer is currently the second most common cause of death in the world. Despite tremendous progress in the treatment of different forms of cancer, the five year survival rates for lung, colorectal, breast, prostate, pancreatic and ovarian cancers remain quite low. New therapies are urgently needed for the better management of these diseases. In this context, both therapeutic gene and drug delivery constitute promising approaches for cancer treatment and are addressed in this thesis.

Focusing on gene delivery, we are proposing the use new pyridinium amphiphiles for obtaining gene delivery systems with improved stability and efficiency and low toxicity (Chapters 2 and 3). The main focus was on pyridinium gemini surfactants (GSs), which possess a soft charge, a high charge/mass ratio and a high molecular flexibility – all key parameters that recommend their use in synthetic gene delivery systems with in vitro and in vivo efficiency. In Chapter 2, we optimized a novel DNA delivery systems through interfacial engineering of pyridinium GS at the level of linker, hydrophobic chains and counterions. In Chapter 3, we tested the effects of blending pyridinium cationic GS into pyridinium cationic lipid bilayers and we have evaluated these blends towards plasmid DNA compaction and delivery process. We have also correlated the cationic bilayer composition with the dynamics of the DNA compaction process, and with transfection efficiency, cytotoxicity and internalization mechanism of resulted nucleic acid complexes.

Toward improved drug delivery systems, we introduced new amphiphilic block copolymers synthesized from biocompatible and biodegradable segments. Although their capabilities for loading, transport and release of lipophilic substances stored in their

hydrophobic cores are widely known, their stability in vivo is limited due to rapid degradation by esterases present in the body. In Chapter 4, we examined the possibility to increase the enzymatic stability of PEG-PCL macromolecular amphiphiles through interfacial engineering, in a process which separates the hydrophilic/hydrophobic interface from the degradable/non-degradable block interface. We evaluated the stability, toxicity, drug loading and release properties of these new polymers using docetaxel as a model chemotherapeutic drug. The results revealed how hydrophilic/ hydrophobic interface tuning can be used to adjust key properties of polymeric drug delivery systems of this type.

DEDICATIONS

To my parents,
Tarawati and Yogendra

ACKNOWLEDGMENTS

First of all, I would like to thank God for continuously blessing – from my journey from a small town of U.P., India to becoming a well-recognized PhD from Philadelphia, USA – without his help, it would not be possible. He continues to give me strength to continue on in spite of all the obstacles life has thrown at me.

"There is no deity superior to the Guru, no gain better than the Guru's grace ... no state higher than meditation on the Guru." – Swami Muktananda

I would like to thank Dr. Marc Ilies for being the inspirational teacher in my life. He supervised me not only during my professional career, but also during my personal growth in USA. Dr. Ilies has always been supportive of me and has guided me whenever I needed him – he made me what I am today. He is my supervisor, a father figure, and a wonderful friend anyone could ask for. Even through my bouts of impatience, Dr. Ilies has been understanding and a willing listener and mentor. He gives me strength – I hope I always will have your blessing and guidance Dr. Ilies!

I am also grateful to Dr. Reza Fassihi, Dr. Michael Borenstein, Dr Daniel Canney and Dr. Stephanie Wunder for being on my thesis committee, for their support and constructive comments and suggestions. Dr. Daniel Canney was also instrumental in obtaining a TU Graduate School Scholarship for me, which allowed me to spend more time in the lab. I would also like to thank him for the Ronald F Gautieri Award and for the Rho Chi induction nomination. I would like to acknowledge Dr. Michael Borenstein for his constant support, constructive criticism, suggestions and encouragements for improvement of my work. I am especially thankful to Dr. Reza Fassihi for his advice, continuous support and suggestion for my Ph.D. project as well as for his mentoring

toward AAPS-related issues and other related projects. I thank Dr. Stephanie Wunder for accepting to serve in my graduation committee, for her support towards nanDSC access, helpful suggestions and constructive comments. I would like to give a special mention to Ms. Almira Cutler, Administrative Assistant of Office of Graduate Studies, who takes care of the copious amounts of paperwork so that graduate students, such as myself, could concentrate more on our course work and research.

I would like to thank our collaborators who helped me complete my thesis by providing support and materials. Dr. Bradford Wayland, Dr. Michael Fryd, and Dr. Xiabo Zhu – thank you for providing the materials for the drug delivery project; thanks are also addressed to Drs. Nicolas Hoffman, Eugen Brailoiu, Madesh Muniswamy for their help in the gene delivery project. I am thankful to the ACS, John Wiley and Sons, and Elsevier for granting me permission to use my published research work in my dissertation. I would like to extend my gratitude to TU Graduate School for the fellowship and for the dissertation completion grant which substantially accelerated my PhD track. Dr. Peter Doukas, Dean of TUSP – I would like to extend my appreciation and thanks for your help with a Research Assistantship during my PhD studies.

I would like to acknowledge my lab mate Suleyman for being such a wonderful friend. Suleyman is very patient – unlike me and was a great listener whenever I needed to talk with someone about my problems. Also, I would like to thank my other lab mates/colleagues, Bogdan, Julia, Eronmwon, Andrew, Han, James, Uttam, Rajesh, Utpal, Raqib, and Ahmed – all who gave a friendly, motivated, and encouraging environment to work in. I also want to thank all the graduate students for electing me the chair of AAPS

student chapter 2014. This opportunity helped me in improving my leadership, management, decision making and communication skills.

Special thanks are addressed to my best friends Parth and Vivek. They have supported me during the good and bad throughout my PhD studies. We would celebrate my successes and they also played the role of a release vessel when I was distressed and had to vent out when things got bumpy. These two individuals are very special to me and I cannot imagine my life in US without them – their support and encouragement also molded me into what I am now. Being a foreigner, it was difficult to adjust to the new environment, but they have made it feel easy and natural. I am so lucky to have these friends in my life. I would also like to acknowledge my American family Tina and Ross Stonefield, who I met during my first year of my Ph.D. They always treated me like their own son and were and are always with me, whenever I need them.

Last, but not least, I am indebted to my Mummy (Tarawati Devi), Daddy (Yogendra Kumar), and my two sisters (Poonam and Renu Sharma). My Mom is my strength and my life. My Daddy and my sisters are my role models. Whenever I feel low, they are the ones who tell me to get up and never give up hope – they give me strength to continue. My achievement is impossible without them and I owe my success to them.

TABLE OF CONTENTS

ABSTRACT.....	iii
DEDICATION.....	v
ACKNOWLEDGEMENT.....	vi
LIST OF TABLES.....	xi
LIST OF FIGURES.....	xii
LIST OF SCHEMES AND CHARTS.....	xvii
LIST OF PUBLICATIONS.....	xviii
LIST OF PRESENTATIONS.....	xx

CHAPTERS

1 OVERVIEW AND MAIN RESEARCH GOALS.....	1
2 INTERFACIAL ENGINEERING OF PYRIDINIUM GEMINI SURFACTANTS FOR THE GENERATION OF SYNTHETIC TRANSFECTION SYSTEMS.....	6
➤ Background and Rationale.....	6
➤ Materials and Methods.....	11
➤ Results and Discussion.....	36
➤ Conclusions.....	76
3. MODULATION OF PYRIDINIUM CATIONIC LIPID-DNA COMPLEX PROPERTIES BY PYRIDINIUM GEMINI SURFACTANTS AND ITS IMPACT ON LIPOPLEX TRANSFECTION PROPERTIES	77
➤ Background and Rationale.....	77
➤ Material and Methods.....	82
➤ Results and Discussion.....	92
➤ Conclusions.....	113

4. INTERFACIAL-ENGINEERED PEG₄₅-PBO_{0,6,9}-PCL_{64,58,53} AMPHIPHILIC BLOCK COPOLYMERS AS DRUG DELIVERY SYSTEMS.....	115
➤ Background and Rationale.....	115
➤ Materials and Methods.....	123
➤ Results and Discussion.....	133
➤ Conclusions.....	160
5. FUTURE STUDIES.....	161
ABBREVIATIONS.....	162
BIBLIOGRAPHY.....	164

LIST OF TABLES

Table	Page
1. D-spacing values of thermotropic self-assemblies generated from selected gemini surfactants, as revealed through SAXS data at different temperatures.....	46
2. D-spacing values of thermotropic self-assemblies generated from selected gemini surfactants, as revealed through WAXS data at different temperatures.....	47
3. Docetaxel loading and encapsulation efficiency of PEG ₄₅ PCL ₆₄ , PEG ₄₅ PBO ₆ PCL ₅₈ , PEG ₄₅ PBO ₉ PCL ₅₃ micelles at two different initial loadings ratio.....	136
4. The main physicochemical characteristics, nanoparticles yield, drug loading and drug encapsulation efficiency of docetaxel loaded polymeric micelles.....	140
5. Aging of drug loaded polymeric micelles as determined by size and zeta potential variation in time	157

LIST OF FIGURES

Figure	Page
1. Cartoon and general structures of amphiphiles used in this dissertation.....	3
2. DSC traces of gemini surfactants (GS) hexafluorophosphates and chlorides	40
3. TOPM images of GS C17 PF ₆ ⁻ , emphasizing the extent of liquid crystalline phase ordering at different temperatures.....	43
4. WAXS diffractograms of GS, revealing the higher degree of internal order induced by the Cl ⁻ counterion as compared with PF ₆ ⁻	48
5. Counterion impact on thermotropic self-assembling of pyridinium GS.....	51
6. Self-assembling in solution of GS bearing chloride as counterion.....	53
7. CMC graphs for GS C16.Br and C16.Cl.....	55
8. Impact of chain elongation and counterions on size and zeta potential of GS supramolecular assemblies.....	56
9. Size and zeta potential of supra-molecular assemblies generated from three cationic GS with 10, 14, and 17 C atoms in hydrophobic tails and co-lipids cholesterol (chol) or DOPE at three molar ratios (1/1, 1/2, and 1/4 cationic/neutral species).....	59

10. Size, zeta potential, and corresponding gel electrophoresis mobility of lipoplexes generated from formulations based on GS, either alone, or with cholesterol or DOPE at 1/1 and 1/2 molar ratios.....	61
11. Validation of DNA compaction properties of liposomes containing GSs with different chain lengths.....	63
12. Size and zeta potential of liposomes and corresponding DNA complexes generated from GSs co-formulated with DOPE, revealing the impact of GS chain length and counterion on these physicochemical properties.....	66
13. Size, zeta potential, and gel electrophoresis mobility of lipoplexes generated from formulations based on C16 GSs in mixtures with DOPE at 1/2 molar ratio.....	68
14. Transfection efficiency and associated cytotoxicity on NCI-H23 lung cancer cell line of lipoplexes generated from GSs co-formulated with DOPE liposomes, revealing the impact of GS chain length and counterion on these biological properties.....	70
15. Transfection efficiency and associated cytotoxicity of lipoplexes generated from GSs co-formulated with DOPE, on NCI-H23 lung cancer cell line, in standard media containing 0%, 5%, 10%, 20% and 40% serum.....	74
16. Comparative nanoDSC traces of cationic lipid SPYRIT-7 (lipid) formulated with DOPE or cholesterol at 1:1 and 1:2 molar ratios, in water, in the absence and in the presence of 5% GS SPYRIT-68 (GS), against the pure cationic lipid formulation.....	93

17. The impact of GS on the size and zeta potential of liposomes generated from SPYRIT-7 cationic lipid and DOPE or cholesterol at 1:1 or 1:2 molar ratios.....	96
18. The compaction of DNA by pyridinium cationic amphiphiles SPYRIT-7 and SYRIT-68 formulations as a function of the cationic amphiphile/ DNA charge ratio.....	99
19. Size, zeta potential, transfection efficiency and cytotoxicity against NCI-H23 cell line of lipoplexes formed at a +/- charge ratio of 3 from SPYRIT-68/SPYRIT-7 cationic amphiphiles formulations.....	104
20. Transfection of NCI-H23, HT-29, HCT-116 tumor spheroids by select pyridinium cationic amphiphiles formulations, as revealed by 3D images of GFP expression and luciferase quantitation.....	106
21. Cellular uptake (NCI-H23 cell line) of lipoplexes formed from SPYRIT-7/SPYRIT-68 cationic amphiphiles formulations in the presence of specific internalization inhibitors chlorpromazine, genistein and EIPA.....	109
22. Confocal images showing endolysosomal escape of the pyridinium GS-containing lipoplexes	112
23. Size of the micelles generated from the representative amphiphilic block copolymers using nanoprecipitation.....	133
24. Size of the micelles generated from the drug loaded amphiphilic block copolymer at different mass ratio using nanoprecipitation.....	135

25. Comparative DSC traces of docetaxel loaded and unloaded micelles of PEG45-PCL64, PEG45-PBO6-PCL58 and PEG45-PBO9-PCL53.....	139
26. Self assembling of the three amphiphilic block copolymers in water at 25 °C followed by DLS, revealing the Critical Aggregation Concentration (CAC) of the polymeric micelles.....	143
27. Time dependent degradation of polymeric micelle by lipase, butyrylcholinesterase, carbonic anhydrase and albumin monitored by DLS.....	147
28. GPC traces of all the products from the <i>P. cepacia</i> lipase catalyzed hydrolytic degradation of PEG ₄₅ - <i>b</i> -PBO _n - <i>b</i> -PCL ₆₀ (n = 0, 6, 9) micelles at a constant reaction time of 4.0 hours (t = 4.0 h) micelles.....	148
29. Effect of albumin alone, of a binary mixture of lipase and albumin, butyrylcholinesterase and albumin; and carbonic anhydrase and albumin on degradation of polymeric micelles at 37 °C	151
30. Hemolysis of docetaxel-loaded polymeric micelles at fixed concentration of drug (0.15 mg/mL), in PBS at 37 °C.....	153
31. Comparison of in vitro docetaxel release from drug loaded diblock and triblocks polymeric micelles under sink condition at 37 °C	155
32. Comparative NCI-H23 lung cancer cells viability exposed to docetaxel-loaded polymeric triblock micelles with tuned interfaces versus standard diblock ones and Taxotere [®] formulation.....	156

33. Long term stability of DTX-loaded polymeric micelles after seven months: aspect of formulations, size of the polymeric micelles, PEG content of formulations and drug loading.....	159
--	-----

LIST OF SCHEMES AND CHARTS

Scheme	Page
<ol style="list-style-type: none"> 1. Synthesis of the new pyridinium gemini surfactants bearing a hydrophilic linker..... 2. Cartoon revealing the interfacial engineering of PEG-PCL block copolymers and the structure and dynamic of the novel triblock copolymers as novel polymeric drug delivery systems..... 	<p>36</p> <p>145</p>
Chart	Page
<ol style="list-style-type: none"> 1. Pyridinium gemini surfactants and oligomeric surfactants, synthesized via reaction of lipophilic pyrylium salts with primary diamines..... 2. Representative cationic lipids used in synthetic gene delivery systems..... 3. Structure of PEG45-PCL64, PEG45-PBO6-PCL58 and PEG45-PBO9-PCL53 amphiphilic block copolymers..... 	<p>10</p> <p>80</p> <p>122</p>

LIST OF PUBLICATIONS

Sharma, V. D.; Ilies, M. A., Modulation of pyridinium cationic lipid-DNA complex properties by pyridinium gemini surfactants and its impact on lipoplex transfection properties. *Molecular Pharmaceutics* 2014, 11 (2), 545–559. (research article)

Sharma, V. D.; Aifuwa, E. O.; Heiney, P. A.; Ilies, M. A., Interfacial engineering of pyridinium gemini surfactants for the generation of synthetic transfection systems. *Biomaterials* 2013, 34 (28), 6906-6921. (research article)

Zhu, X.; **Sharma, V. D.;** Fryd, M.; Ilies, M. A.; Wayland, B. B., Enzyme and acid catalyzed degradation of PEG45-b-PBO0,6,9-b-PCL60 micelles: Increased hydrolytic stability by engineering the hydrophilic–hydrophobic interface. *Polymer* 2013, 54 (12), 2879-2886. (research article)

Sharma, V. D.; Ilies, M. A., Heterocyclic Cationic Gemini Surfactants: A Comparative Overview of Their Synthesis, Self-assembling, Physicochemical and Biological Properties. *Med Res Rev* 2014, 34, 1-44. published online 08/20/12, doi: 10.1002/med.21272. (review article)

Ilies, M. A.; Tiffany, V. S.; He, L.C.; Kizewski, A.; **Sharma, V. D.,** Pyridinium Amphiphiles in Gene Delivery- Present and Perspectives. In *Amphiphiles: Molecular Assembly and Applications*, American Chemical Society: 2011; Vol. 1070, pp 23-38. (book chapter)

PATENT

Sharma, V. D.; Zhu, X.; Fryd, M.; Wayland, B. B.; Ilies, M. A., Docetaxel polymeric formulation using interface-engineered amphiphilic block copolymers (Submission in process)

LIST OF PRESENTATIONS

ORAL PRESENTATIONS

- V. D. Sharma, M. A. Ilies “Interfacial engineering of amphiphiles and its impact in the design of efficient drug and gene delivery” University of Pennsylvania, Philadelphia, PA, April 3, 2014
- V. D. Sharma, M. A. Ilies “Design of efficient drug and gene delivery systems using synthetic amphiphiles” University of Chicago, Chicago, IL, March 27, 2014
- V. D. Sharma, M. A. Ilies, “Thermal Analysis of self-assembled systems of gemini surfactants, lipid and polymers: Implications in drug and gene delivery” Thermal Analysis Forum of Delaware Valley – Spring Symposium, Conshohocken, PA, March 13, 2014
- V. D. Sharma, E. A. Aifuwa, M. A. Ilies, “Interfacial engineering of pyridinium gemini surfactants in novel synthetic transfection systems with enhanced efficiency” 4th Annual Temple University Graduate Fellows Research Symposium, September 15, 2012
- V. D. Sharma “Basics in Proline Chemistry” Lyophilization Technology, Inc., Warminster, PA, July 6, 2012

POSTER PRESENTATIONS

Extramural, peer-reviewed:

- V. D. Sharma, M. A. Ilies “Dynamic stability of PEG₄₅-PBO_{0,6,9}-PCL₆₀ micelles as new drug delivery system” Abstracts of Papers AAPS National Meeting San Antonio, November 10- November 14, 2013 (W5075)
- V. D. Sharma, M. A. Ilies “Modulation of pyridinium cationic lipid-DNA complex properties by pyridinium gemini surfactants and its impact on lipoplex transfection properties” Abstracts of Papers AAPS National Meeting San Antonio, November 10- November 14, 2013 (W5074)
- V. D. Sharma, J. Lees, N. E. Hoffman, M. Madesh, S. L. Wunder, M. A. Ilies “Modulation of pyridinium cationic lipid-DNA complex properties by pyridinium gemini surfactants and its impact on lipoplex transfection properties” Gordon Research Conference of Cancer Nanotechnology, Mount Snow, VT, July 14-19
- V. D. Sharma, X. Zhu, B. B. Wayland, M. A. Ilies “Enzymatic degradation of PEG-PCL diblock copolymer micelles via esterases: the impact of hydrophilic/hydrophobic interface” Abstracts of Papers AAPS National Meeting Chicago, October 14- October 18, 2012 (W5227)
- V. D. Sharma, M. A. Ilies, R. Fassihi “Physicochemical and stability characterization of enteric-coated Omeprazole pellets with and without a protective sub-coat” Abstracts of Papers AAPS National Meeting Chicago, October 14- October 18, 2012 (W5025)

- V. D. Sharma, M. A. Ilies “Novel gene delivery systems based on gemini surfactants” Abstracts of Papers AAPS National Meeting Chicago, October 14-October 18, 2012 (R6131)
- V. D. Sharma, E. A. Aifuwa, M. A. Ilies, “Structure-activity relationships in a series of pyridinium gemini surfactants for gene delivery bearing hydrophilic linkers”, 15th American Society of Gene & Cell Therapy Annual Meeting, Philadelphia, PA, May 16-19, 2012
- V. D. Sharma, M. A. Ilies, “Self-assembling in bulk and in solution for a series of pyridinium gemini surfactants bearing a hydrophilic linker” Thermal Analysis Forum of Delaware Valley - Annual Business Meeting and Poster Session, Philadelphia, PA, December 8, 2011
- V. D. Sharma, E. O. Aifuwa, M. A. Ilies, “Pyridinium gemini surfactants: Synthesis, self-assembling, and physicochemical properties” Abstracts of Papers, 242st ACS National Meeting, Denver, CO, August 28-September 1, 2011 (COLL-239)

Intramural:

- V. D. Sharma, M. A. Ilies “Modulation of pyridinium cationic lipid-DNA complex properties by pyridinium gemini surfactants and its impact on lipoplex transfection properties” TUSP Research Day, February 21, 2014
- H. Nguyen, U. Satyal, V. D. Sharma, M. A. Ilies “Modulation of pyridinium cationic lipid-DNA complex properties by pyridinium gemini surfactants and its

impact on lipoplex transfection properties” TUSP Research Day, February 21, 2014

- J. Lees, V. D. Sharma, M. A. Ilies, “Stability of cationic lipid-DNA complexes under static and dynamic conditions: Lipoplex compaction enhancement by gemini surfactants: Lipoplex compaction enhancement by gemini surfactants”, TUSP Research Day, February 25, 2013
- V. D. Sharma, X. Zhu, B. B. Wayland, M. A. Ilies “Enzymatic degradation of PEG-PCL diblock copolymer micelles via esterases: the impact of hydrophilic/hydrophobic interface”, TUSP Research Day, February 25, 2013
- K. Thompson, V. D. Sharma, M. A. Ilies, “Self-assembling properties of novel pyridinium amphiphiles for gene delivery” TU School of Pharmacy Research Day, February 24, 2012
- V. D. Sharma, E. A. Aifuwa, M. A. Ilies, “Structure-activity relationships in a series of pyridinium gemini surfactants for gene delivery” TU School of Pharmacy Research Day, February 24, 2012
- V. D. Sharma, E. O. Aifuwa, M. A. Ilies, “Pyridinium gemini surfactants: Synthesis, self-assembling, and physicochemical properties” Temple Annual Graduate Fellows Research Symposium, September 10, 2011
- V. D. Sharma, M. A. Ilies, “Impact of chain length and counterion on self-assembling of pyridinium gemini surfactants” TU School of Pharmacy Research Day, February 25, 2011

CHAPTER 1

OVERVIEW AND MAIN RESEARCH GOALS

Lung cancer is the leading cause of cancer related mortality in the U.S. and worldwide [1]. Surgery, radiotherapy, chemotherapy and their combinations have been used for the treatment of non-small lung cancer cell lung carcinoma (NSCLC). Chemotherapy is a first line treatment and includes the use of cytotoxic agents such as cisplatin and related organoplatinum compounds, etoposide, paclitaxel gemcitabine etc, that can be used either alone or in combinations with radiotherapy to treat NSCLC [2]. Failure of first line treatment occurs due to arise of hematologic and nonhematologic toxicities and requires the use of drugs such as docetaxel, pemetrexed, and erlotinib as a second line treatment. Despite of all these efforts, five year survival rates for patients suffering from NSCLC is 13%-61% in early stages (\leq IIIa) and less than 5% for late stages (IIIB and IV) [3]. These data clearly show the urgency of developing novel and efficient method for the treatment of NSCLC, especially for late stages.

On the other hand, the lung constitutes a particularly attractive target for drug and genetic material delivery due to its high surface area. It receives 100 % of cardiac output and it is accessible non-invasively from airway (direct delivery) or from the vasculature (systemic delivery) [4].

Drug delivery systems can optimize the delivery of cytotoxic agents in late stages of NSCLC, focusing their toxicity on the tumor via enhanced permeation and retention (EPR) effect. Another promising alternative to fight lung cancer in late stages is via gene therapy, which allows partial or complete reprogramming of targeted cells to correct the

mutation or to force apoptosis of malignant cells. Main strategies currently explored include molecular chemotherapy, genetic immunopotential and mutation compensation [5]. Molecular chemotherapy involves delivering of “suicide genes” that encode enzymes capable of generating toxic metabolites that can kill the cancerous cells [6]. Herpes simplex thymidine kinase and bacterial cytosine deaminase are few examples in this case. Genetic immunopotential implies activation of the immune system against tumor cells, which have been achieved through the use of cytokines, MHC class 1 antigen, antisense TGF- β , or tumor-specific antigens [6]. The mutation compensation technologies involve either the inhibition of dominant oncogenes through antisense K-*ras*, or the augmentation of tumor suppressors wild type *p53* gene into cancer cells [7]. Importantly, the pro-apoptotic *p53* gene was found to be mutated in about 60% of human lung cancer [8]. Its mutated versions were proved to allow tumor cells to avoid apoptosis and continue to proliferate [9].

Depending upon the delivery technology used, different extracellular and intracellular barriers need to be surpassed before the genetic material reaches the nucleus of target cells. For systemic delivery, the structural characteristics of the delivery system and its ability to maintain the structural integrity of the cargo (drug/gene) in diverse, harsh environment is of utmost importance [10]. For gene delivery systems, the internalization of the genetic cargo in cytoplasm and the release of genetic material from it (endosomal escape), also constitute important points for consideration [11].

Our long term goal is to treat lung cancer with a delivery systems targeted to lung endothelium. Taking into consideration the above mentioned delivery barriers, and the particularities of NSCLC, we are advancing two alternatives to lung cancer treatment

involving amphiphiles of different size and molecular weights – one through gene therapy via delivery of plasmids encoding intact p53, for which we are proposing carrier optimization, and a second one involving focused chemotherapy via improved delivery of docetaxel via a new delivery system (Figure 1).

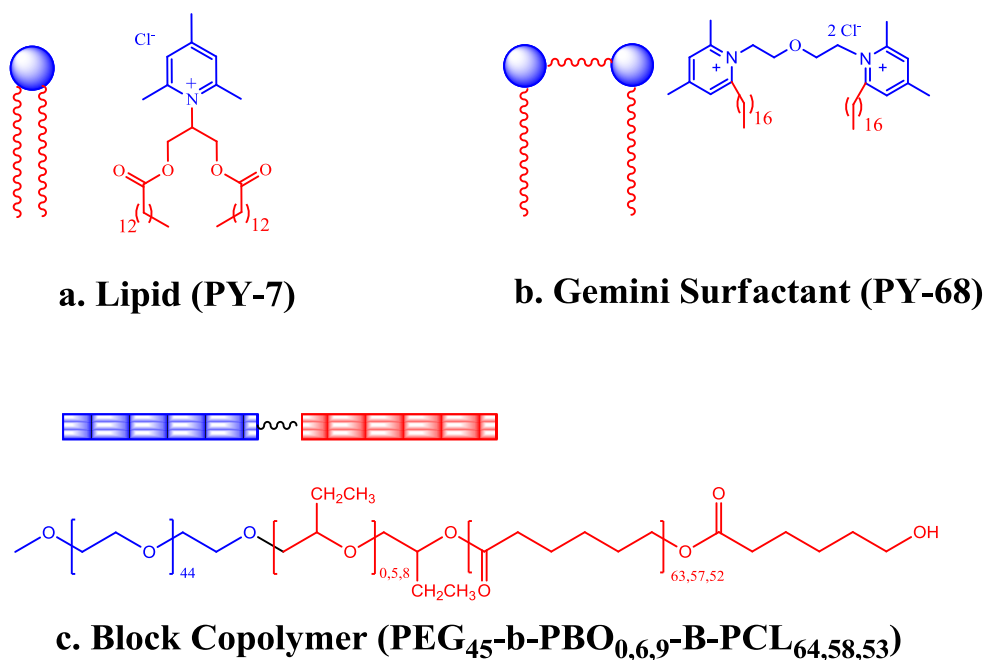


Figure 1. Cartoon and general structures of amphiphiles considered for use in this proposal: lipids (a), gemini surfactants (b) and amphiphilic block copolymers (c). Blue spheres/blocks represent hydrophilic region and red blocks/wavy line represent hydrophobic regions.

Our central hypothesis is that efficient drug and gene delivery systems can be generated by proper exploitation of the interfacial parameters (packing parameters, supramolecular size and shape) of the pyridinium amphiphiles and block copolymers. The rationale of this research is that the optimized nanosystems will allow better delivery

of genes (using pyridinium amphiphiles) or drugs (using amphiphilic block copolymers), opening new approaches for treatment of advanced lung cancer.

In the second chapter, our goal was to correlate the structural elements of new pyridinium GS bearing hydrophilic linkers, the physicochemical properties of their formulations and of their lipoplexes with transfection efficiency and cytotoxicity. The working hypothesis for this chapter is that the comprehensive optimization and fine tuning of the self-assembling process at the level of counterions and hydrophobic chains of pyridinium GS, added co-lipids, their nature and molar ratio, can generate efficient and robust self-assembled formulations with optimum charge density for efficient DNA delivery in conditions mimicking in vivo environment.

The third chapter is the continuation of chapter 2. Our goal was to correlate the structural elements and the physicochemical properties of blends of pyridinium GS with pyridinium lipids and of their lipoplexes with transfection efficiency and cytotoxicity. The working hypothesis of this chapter is that the pyridinium cationic GS/lipid blends were expected to have a higher charge density than corresponding pure cationic lipid-based formulations, while displaying reduced cytotoxicity, thus synergistically combining the properties of the two classes of cationic amphiphiles.

In the fourth chapter, we assessed comparatively the interfacial engineering of PEG-PCL diblock copolymers into PEG-PBO-PCL triblock copolymers and its impact on self assembled supramolecular micelles in terms of hydrolytic and shelf stability, drug loading capacity, drug release profile and toxicity. Based on literature data, our working hypothesis is that the insertion of a short hydrophobic non-hydrolyzable poly (1,2-

butylene oxide) (PBO) segment between the PEG and PCL blocks will prevent water from reaching the interface ester group linking the PEG to PCL block. This interface engineering will in turn increase the resilience of the polymeric material and its self-assembly in aqueous medium, will improve circulation time and shelf stability of polymeric DDS together with their drug loading and release properties, and will also reduce the toxicity of these new polymeric DDSs.

CHAPTER 2

INTERFACIAL ENGINEERING OF PYRIDINIUM GEMINI SURFACTANTS FOR THE GENERATION OF SYNTHETIC TRANSFECTION SYSTEMS

In this chapter, our goal was to correlate the structural elements of new pyridinium GS bearing hydrophilic linkers, the physicochemical properties of their formulations and of their lipoplexes with transfection efficiency and cytotoxicity. The working hypothesis for this chapter is that the comprehensive optimization and fine tuning of the self-assembly process at the level of counterions and hydrophobic chains of pyridinium GS, added co-lipids, their nature and molar ratio, can generate efficient and robust self-assembled formulations with optimum charge density for efficient DNA delivery in conditions mimicking in vivo environments.

Background and Rationale:

The success of gene therapy as a revolutionary way to treat diseases at their core level relies on finding efficient and safe delivery systems for the transfer and expression (transfection) of foreign nucleic acids into patients' cells and tissues affected by various hereditary or acquired diseases[12-15]. In recent years the technology of RNA[†] interference has broadened the potential applications of nucleic acid delivery into human therapy[16]. DNA and RNA delivery via viral vectors is efficient but rather unsafe due to elevated immunogenicity and mutagenicity of these biological vectors [12, 17, 18]. In contrast, chemical delivery methods relying on synthetic transfection systems [10, 19-21]

are much safer, and allow repeated transfection rounds without eliciting of significant immune responses. However, their efficiency must be improved by adapting the structure of these self-assembled delivery systems to the delivery barriers encountered in vivo from the point of administration to the target cells[11, 22]. Novel cationic amphiphiles (surfactants [23-26], lipids [27-29], dendrons [30], dendrimers [31-33] and polymers [32, 34-38]) with enhanced self-assembling, optimum nucleic acid binding/release profiles and reduced cytotoxicity are required for new generations of efficient synthetic gene delivery systems. The use of targeting moieties can further enhance their therapeutic index [39-41].

In this context, dimeric surfactants [42, 43] are particularly interesting and intensively researched these days as novel gene delivery vectors [44-51]. Also known as gemini surfactants [52], they consist of two simple surfactant moieties linked together at the level of the polar head. The linker restricts the movement of the two individual surfactant molecules, conferring unusual properties to this class of amphiphiles [43]. Thus, focusing on cationic gemini surfactants, it must be emphasized that although they have about the same charge per mass ratio as simple surfactants, they display a higher propensity to self-assemble and a lower critical micelle concentration as compared with their monomeric surfactant congeners. The molecular shape of cationic gemini surfactants and consequently their packing parameter [53] can vary significantly. Fine tuning of the packing parameter and hence of the dynamics of their self-assemblies is easier than in the case of cationic lipids. Small adjustments at the level of the main structural elements (polar head, linker, hydrophobic chains, counterions) can yield self-assemblies ranging in shape from spherical micelles, worm micelles, flexible bilayers, to

planar bilayers [43, 51, 54-62]. They also possess high elastic moduli and charge density, important requirements for efficient cell internalization, endosomal escape and nucleic acid cargo release [63].

It is not surprising that in recent years a large number of cationic gemini surfactants with different polar heads, hydrophobic chains, linkers and counterions were synthesized and studied in respect of their self-assembling and biological properties [42, 43, 47, 50, 51]. Heterocyclic cationic gemini surfactants in general and pyridinium gemini surfactants in particular have generated efficient gene delivery vectors [46, 51, 64]. Their soft positive charge, delocalized on an aromatic heterocyclic ring, allows a strong association with nucleic acids, and generation of robust amphiphile/nucleic acid complexes. After internalization of nucleic acid complexes it also allows the efficient release of nucleic acid cargo into the cytoplasm of the cell to be transfected [51].

These special amphiphilic properties and optimum DNA association/release profile of the pyridinium polar head, together with the high charge/mass ratio (loading capacity) of the gemini surfactant design, prompted active research in the field of pyridinium gemini surfactants. Many representatives were synthesized and their physicochemical parameters and biological properties were thoroughly assessed [46, 51, 64-69]. The vast majority of the syntheses involved the quaternization of pyridines. In contrast, Balaban, Ilies, and collaborators, proposed an alternative route and have synthesized several series of pyridinium gemini surfactants from lipophilic pyrylium salts and primary diamines [46] building on a strategy to access bis-pyridinium compounds previously reported by Balaban [70, 71]. Alternating the structure of primary diamine

allowed the generation of several series of pyridinium gemini surfactants with various linker designs and polarities (Chart 1).

In this study it was also shown that pyridinium gemini surfactants with pro-cationic hydrophilic linkers **B** and **C** were less biologically efficient than representatives bearing hydrophobic linkers **A** [46]. Interestingly, transfection efficiency could be rescued by acylating the pro-cationic amino moieties in the hydrophilic linkers. The short and long alkoxycarbonyl/acyl moieties used in representatives **D**, **E** and **F** were equally efficient, signifying that a polar but neutral linker could guarantee a good transfection profile (Chart 1). These findings were confirmed by subsequent literature reports on structurally related tetraalkylammonium gemini surfactants with polar linkers [72-74]. Therefore we have decided to evaluate in the present study the impact of a short oxyethylene-type polar linker on the transfection efficiency of pyridinium gemini surfactants. We have varied two structural components – chain length and counterion – assessing their impact on the physicochemical characteristics of the supramolecular assemblies generated with this series of pyridinium gemini surfactants, attempting to correlate the properties of these assemblies with their gene delivery ability.

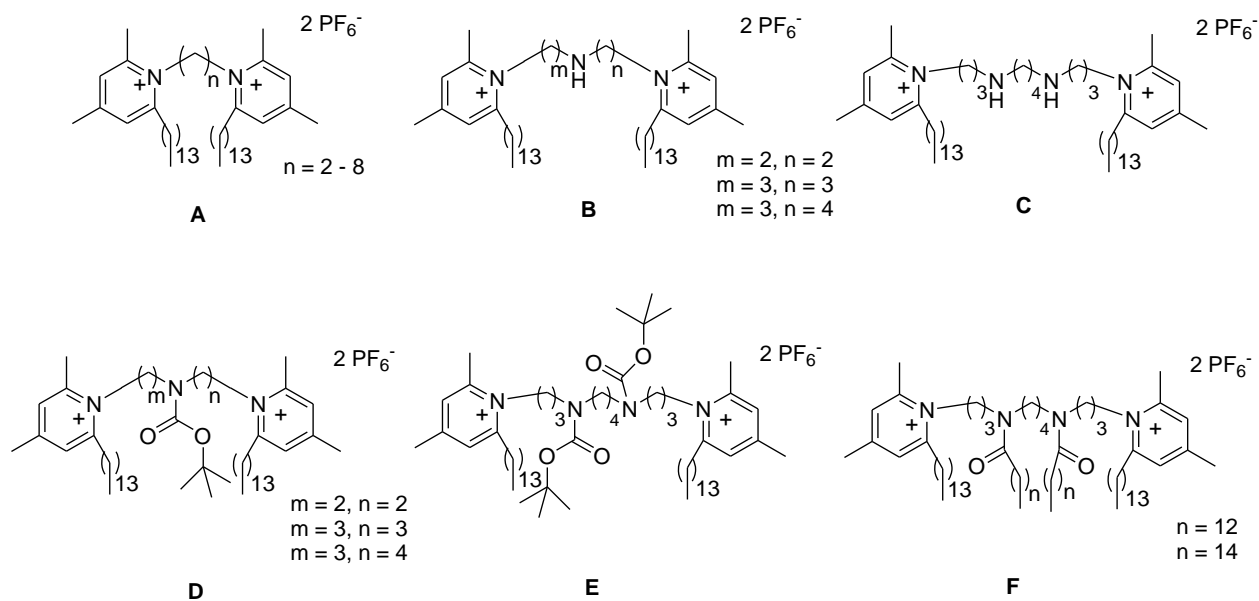


Chart 1. Pyridinium gemini surfactants and oligomeric surfactants, synthesized via reaction of lipophilic pyrylium salts with primary diamines [46] with proved efficiency in gene delivery.

Materials and Methods

Materials: 3-oxa-1,5-diaminopentane was acquired from TCI America (Portland, OR), while triethylamine, dichloromethane, acetic acid, fatty acids, salts, etc were from Acros and/or Fisher Scientific (Pittsburgh, PA) and were used without further purification. Dowex 1X8-200 was from Sigma-Aldrich (St Louis, MO) or BioRad (Hercules, CA). Solvents (HPLC quality) were from Fisher Scientific (Pittsburgh, PA), EMD (Gibbstown, NJ), and VWR International (West Chester, PA). Pyrylium salts were prepared as described elsewhere [46].

Techniques: The purity and the structure identity of the intermediary and final products were assessed by a combination of techniques that includes thin-layer chromatography (TLC), high performance liquid chromatography (HPLC), differential scanning calorimetry (DSC and nano-DSC), ^1H - and ^{13}C -NMR, and elemental analysis.

TLC was carried out on SiO_2 -precoated aluminum plates (silica gel with F254 indicator; layer thickness 200 μm ; pore size 60 \AA , from Sigma-Aldrich), eluted with $\text{MeOH}/\text{CHCl}_3$ 10/90 (v/v) unless specified otherwise.

The melting points and/or transition temperatures for cationic lipids in bulk were determined by differential scanning calorimetry, using a TA Instruments Q200 MDSC (New Castle, DE) and a heating/cooling rate of 5 $^\circ\text{C}/\text{min}$. A Thermolyne heating stage microscope (Dubuque, IA), equipped with an Olympus 5X objective, was also used for this purpose. Nano-differential scanning calorimetry (nano-DSC) measurements for the hydrates samples were obtained on a TA Instruments (New Castle, DE) NanoDSC-6300. Samples were scanned at heating/cooling rates of 1 $^\circ\text{C}/\text{min}$, using 1-2 mg lipid.

Transmission optical polarized microscopy (TOPM) was performed on a Thermolyne heating stage microscope (Dubuque, IA), equipped with an Olympus 5X objective, a polarized filter, and a Motic-1000 digital camera controlled by Motic Image Plus 2.0 software.

X-ray diffraction (XRD) measurements employed Cu-K α 1 radiation ($\lambda = 1.54178$ Å) from a Bruker Nonius FR-591 rotating anode x-ray generator, equipped with a 0.2 x 0.2 mm² filament operated at 3.4 kW. The Osmic Max-Flux focusing optics and pinhole collimation produces a bright, highly collimated beam, generating a 0.3 x 0.4 mm² spot on a two-dimensional Bruker-AXS Hi-Star multiwire area detector. An integral vacuum of 0.3 mb was maintained along the length of the flight tube and within the sample chamber to reduce both attenuation and small angle scattering by air and windows. Samples were held in glass capillaries (1.0 mm in diameter), mounted in a temperature controlled oven (temperature precision: ± 0.1 °C, temperature range from -20 °C to 300 °C). Measurements were made at fixed sample-detector distances of 11.0 cm (wide-angle configuration, or WAXS) and 54.0 cm (small-angle configuration, or SAXS), for a wider dynamic range in d-spacings. XRD peak position and intensity analysis was performed using Datasqueeze Software (version 2.29, <http://www.datasqueezesoftware.com>).

NMR spectra were recorded at ≈ 300 K with a Bruker Avance III 400 Plus spectrometer equipped with a 5 mm indirect detection probe, operating at 400 MHz for ¹H-NMR, at 100 MHz for ¹³C-NMR, and at 376 MHz for ¹⁹F-NMR. Chemical shifts are reported as δ values, using tetramethylsilane (TMS) as internal standard for proton

spectra and the solvent resonance for carbon spectra. Assignments were made based on chemical shifts, signal intensity, COSY, HMQC, and HMBC sequences.

Elemental analyses were performed by combustion, using a Perkin Elmer 2400 Series II CHNS analyzer.

General procedure for the synthesis of gemini surfactants

In an 100 mL round bottom flask 1.72 mmol of 2,4-dimethyl-6-alkylpyrylium hexafluorophosphate were dissolved in 5 mL dichloromethane (DCM) and treated under stirring with a solution made by dissolving 0.081g (0.8 mmol) of 2,2'-oxybis(ethylamine) in 10 mL of DCM. One drop of triethylamine (catalyst) was added and the reaction mixture was heated to reflux for 10 min. Acetic acid (0.5 mL) was added to the boiling solution mixture and the mixture was refluxed for 1h 30 min (TLC control). The unreacted pyrylium salt was converted into the corresponding pyridine upon treatment with 0.5 mL of 7N NH₃/MeOH and refluxing the reaction mixture for another 5 min. Solvent and excess ammonia were evaporated with a rotary evaporator under vacuum, yielding the crude product, which was purified via column chromatography using MeOH/DCM gradient elution (from 0/100 to 30/70 v/v). Useful fractions (determined by TLC) were collected and grouped, solvent was evaporated using the rotary evaporator, and the purified product was crystallized from ethanol (2-3 mL), filtered and dried under vacuum. Isolated yields varied from 47 to 75%, depending on the gemini surfactant solubility in ethanol, and were specified in each case. Comprehensive structural characterization of resulting gemini surfactants **2** is presented below.

Ion Exchange Procedure. An amount of 70 g of Dowex 1X8-200 ion exchange resin (chloride form) was suspended in 200 mL deionized water in an Erlenmeyer flask and kept at room temperature for three days to fully inflate. It was transferred into a glass column and washed with deionized water (200 mL), with 5% aqueous HCl (1 L), then again with deionised water until neutral pH was reached. After a final wash with MeOH, the resin was retrieved from the column and stored in an Erlenmeyer flask under MeOH.

Prior to counterion exchange, about 10 g resin was transferred into a small column and washed with 200 mL MeOH. Separately, an amount of 60-70 mg of pure gemini surfactant hexafluorophosphate was weighed and dissolved in MeOH (1-4 mL, depending on the solubility of the material). The methanol solution was transferred on top of the ion exchange column and the compound was eluted with methanol (flow rate 1-3 mL/min). Sample was cycled through the column repeatedly for 1 hr. ^{19}F -NMR analysis of a small aliquot taken from the eluent showed no fluorine peak corresponding to PF_6^- . Evaporation of solvent yielded the product, which was crystallized from acetone/hexane mixtures (C10-C14) or acetone (C15-C17) and dried under vacuum. Comprehensive structural characterization of novel gemini surfactants **3**, as well as details concerning the generation of bromide **4g** and dihydrogenophosphate **5g** through ion exchange and their comprehensive characterization can be found below.

Characterization of novel gemini surfactants

1,5-bis(4,6-dimethyl-2-decylpyridinium-1-yl)-3-oxapentane di-hexafluorophosphate

2a: Yield 47.8%; $^1\text{H-NMR}$ (CDCl_3 , δ , ppm): 7.46 (s, 2H, H5Py), 7.41 (s, 2H, H3Py), 4.63 (t, $J = 5.0$ Hz, 4H, 2 O-CH₂CH₂-Py), 3.89 (t, $J = 5.0$ Hz, 4H, 2 O-CH₂CH₂-Py), 2.95 (t, $J = 7.5$ Hz, 4H, 2 Py-CH₂-(CH₂)₈-CH₃), 2.71 (s, 6H, 2 Py(6)-CH₃), 2.54 (s, 6H, 2 Py(4)-CH₃), 1.67 (m, 4H, 2 Py-CH₂CH₂(CH₂)₇CH₃), 1.40 (m, 4H, 2 Py-CH₂CH₂CH₂(CH₂)₆CH₃), 1.26 (m, 24H, 12 CH₂ from alkyl chains), 0.88 (t, $J = 6.5$ Hz, 6H, 2 CH₃ from alkyl chains); $^{13}\text{C-NMR}$ (CDCl_3 , δ , ppm): 158.6 (2C, 2-Py), 158.6 (2C, 4-Py), 155.1 (2C, 6-Py), 128.8 (2C, 5-Py), 127.5 (2C, 3-Py), 68.6 (2C, O-CH₂), 50.7 (2C, Py(1)-CH₂), 33.5 (2C, Py(2)-CH₂), 31.9 (2C, Py(2)CH₂CH₂), 29.6 (2C, 2 CH₂ alkyl chains), 29.4 (2C, 2 CH₂ alkyl chains), 29.3 (4C, 4 CH₂ alkyl chains), 29.2 (2C, 2 CH₂ alkyl chains), 28.8 (2C, CH₂CH₂CH₃), 22.7 (2C, CH₂CH₃), 21.7 (2C, 2 CH₃-Py(6)), 21.6 (2C, 2 CH₃-Py(4)), 14.1 (2C, 2 CH₃ from n-alkyl chain), $^{19}\text{F-NMR}$ (CDCl_3 , δ , ppm): 73.04 (d, $J = 703$ Hz, PF₆⁻); Anal (C₃₈H₆₆F₁₂N₂OP₂) C, H, N.

1,5-bis(4,6-dimethyl-2-undecylpyridinium-1-yl)-3-oxapentane

di-

hexafluorophosphate 2b: Yield 49.1%; $^1\text{H-NMR}$ (CDCl_3 , δ , ppm): 7.48 (s, 2H, H5Py), 7.41 (s, 2H, H3Py), 4.61 (t, $J = 4.5$ Hz, 4H, 2 O-CH₂CH₂-Py), 3.87 (t, $J = 5.5$ Hz, 4H, 2 O-CH₂CH₂-Py), 2.93 (t, $J = 8.0$ Hz, 4H, 2 Py-CH₂-(CH₂)₉-CH₃), 2.68 (s, 6H, 2 Py(6)-CH₃), 2.53 (s, 6H, 2 Py(4)-CH₃), 1.67 (m, 4H, 2 Py-CH₂CH₂(CH₂)₈CH₃), 1.39 (m, 4H, 2 Py-CH₂CH₂CH₂(CH₂)₇CH₃), 1.30 (m, 28H, 14 CH₂ from alkyl chains), 0.88 (t, $J = 7.0$ Hz, 6H, 2 CH₃ from alkyl chains); $^{13}\text{C-NMR}$ (CDCl_3 , δ , ppm): 158.6 (2C, 2-Py), 158.3

(2C, 4-Py), 155.2 (2C, 6-Py), 128.8 (2C, 5-Py), 127.5 (2C, 3-Py), 68.6 (2C, O-CH₂), 50.6 (2C, Py(1)-CH₂), 33.5 (2C, Py(2)-CH₂), 31.9 (2C, Py(2)CH₂CH₂), 29.63 (4C, 4 CH₂ alkyl chains), 29.5 (2C, 2 CH₂ alkyl chains), 29.4 (2C, 2 CH₂ alkyl chains), 29.3 (2C, 2 CH₂ alkyl chains), 29.2 (2C, 2 CH₂ alkyl chains), 28.7 (2C, CH₂CH₂CH₃), 22.7 (2C, CH₂CH₃), 21.6 (2C, 2 CH₃-Py(6)), 21.6 (2C, 2 CH₃-Py(4)), 14.1 (2C, 2 CH₃ from n-alkyl chain), ¹⁹F-NMR (CDCl₃, δ, ppm): 72.92 (d, *J* = 713 Hz, PF₆⁻); Anal (C₄₀H₇₀F₁₂N₂OP₂) C, H, N.

1,5-bis(4,6-dimethyl-2-dodecylpyridinium-1-yl)-3-oxapentane di-hexafluorophosphate 2c: Yield 53.4%; ¹H-NMR (CDCl₃, δ, ppm): 7.42 (s, 2H, H5Py), 7.34 (s, 2H, H3Py), 4.54 (t, *J* = 5.0 Hz, 4H, 2 O-CH₂CH₂-Py), 3.80 (t, *J* = 5.5 Hz, 4H, 2 O-CH₂CH₂-Py), 2.85 (t, *J* = 7.5 Hz, 4H, 2 Py-CH₂-(CH₂)₁₀-CH₃), 2.60 (s, 6H, 2 Py(6)-CH₃), 2.45 (s, 6H, 2 Py(4)-CH₃), 1.59 (m, 4H, 2 Py-CH₂CH₂(CH₂)₉CH₃), 1.28 (m, 4H, 2 Py-CH₂CH₂CH₂(CH₂)₈CH₃), 1.18 (m, 32H, 16 CH₂ from alkyl chains), 0.80 (t, *J* = 7.0 Hz, 6H, 2 CH₃ from alkyl chains); ¹³C-NMR (CDCl₃, δ, ppm): 158.6 (2C, 2-Py), 158.3 (2C, 4-Py), 155.2 (2C, 6-Py), 128.8 (2C, 5-Py), 127.5 (2C, 3-Py), 68.6 (2C, O-CH₂), 50.6 (2C, Py(1)-CH₂), 33.5 (2C, Py(2)-CH₂), 31.9 (2C, Py(2)CH₂CH₂), 29.68 (2C, 2 CH₂ alkyl chains), 29.65 (2C, 2 CH₂ alkyl chains), 29.48 (4C, 4 CH₂ alkyl chains), 29.36 (2C, 2 CH₂ alkyl chains), 29.31 (2C, 2 CH₂ alkyl chains), 29.23 (2C, 2 CH₂ alkyl chains), 28.7 (2C, CH₂CH₂CH₃), 22.7 (2C, CH₂CH₃), 21.5 (2C, 2 CH₃-Py(6)), 21.5 (2C, 2 CH₃-Py(4)), 14.1 (2C, 2 CH₃ from n-alkyl chain), ¹⁹F-NMR (CDCl₃, δ, ppm): 72.88 (d, *J* = 713 Hz, PF₆⁻); Anal (C₄₂H₇₄F₁₂N₂OP₂) C, H, N.

1,5-bis(4,6-dimethyl-2-tridecylpyridinium-1-yl)-3-oxapentane di-

hexafluorophosphate 2d: Yield 54.6%; ¹H-NMR (CDCl₃, δ, ppm): 7.48 (s, 2H, H5Py), 7.41 (s, 2H, H3Py), 4.61 (t, *J* = 5.0 Hz, 4H, 2 O-CH₂CH₂-Py), 3.88 (t, *J* = 5.0 Hz, 4H, 2 O-CH₂CH₂-Py), 2.93 (t, *J* = 7.5 Hz, 4H, 2 Py-CH₂-(CH₂)₁₁-CH₃), 2.68 (s, 6H, 2 Py(6)-CH₃), 2.53 (s, 6H, 2 Py(4)-CH₃), 1.67 (m, 4H, 2 Py-CH₂CH₂(CH₂)₁₀CH₃), 1.39 (m, 4H, 2 Py-CH₂CH₂CH₂(CH₂)₉CH₃), 1.29 (m, 36H, 18 CH₂ from alkyl chains), 0.88 (t, *J* = 7.0 Hz, 6H, 2 CH₃ from alkyl chains); ¹³C-NMR (CDCl₃, δ, ppm): 158.6 (2C, 2-Py), 158.3 (2C, 4-Py), 155.1 (2C, 6-Py), 128.8 (2C, 5-Py), 127.5 (2C, 3-Py), 68.6 (2C, O-CH₂), 50.6 (2C, Py(1)-CH₂), 33.5 (2C, Py(2)-CH₂), 31.9 (2C, Py(2)CH₂CH₂), 29.71 (2C, 2 CH₂ alkyl chains), 29.69 (2C, 2 CH₂ alkyl chains), 29.68 (4C, 4 CH₂ alkyl chains), 29.49 (2C, 2 CH₂ alkyl chains), 29.37 (2C, 2 CH₂ alkyl chains), 29.32 (2C, 2 CH₂ alkyl chains), 29.24 (2C, 2 CH₂ alkyl chains), 28.8 (2C, CH₂CH₂CH₃), 22.7 (2C, CH₂CH₃), 21.6 (2C, 2 CH₃-Py(6)), 21.6 (2C, 2 CH₃-Py(4)), 14.1 (2C, 2 CH₃ from n-alkyl chain), ¹⁹F-NMR (CDCl₃, δ, ppm): 72.94 (d, *J* = 713 Hz, PF₆⁻); Anal (C₄₄H₇₈F₁₂N₂OP₂) C, H, N.

1,5-bis(4,6-dimethyl-2-tetradecylpyridinium-1-yl)-3-oxapentane di-

hexafluorophosphate 2e: Yield 55%; ¹H-NMR (CDCl₃, δ, ppm): 7.49 (s, 2H, H5Py), 7.43 (s, 2H, H3Py), 4.64 (t, *J* = 5.0 Hz, 4H, 2 O-CH₂CH₂-Py), 3.90 (t, *J* = 5.0 Hz, 4H, 2 O-CH₂CH₂-Py), 2.96 (t, *J* = 7.7 Hz, 4H, 2 Py-CH₂-(CH₂)₁₂-CH₃), 2.73 (s, 6H, 2 Py(6)-CH₃), 2.56 (s, 6H, 2 Py(4)-CH₃), 1.69 (m, 4H, 2 Py-CH₂CH₂(CH₂)₁₁CH₃), 1.40 (m, 4H, 2 Py-CH₂CH₂CH₂(CH₂)₁₀CH₃), 1.28 (m, 40H, 20 CH₂ from alkyl chains), 0.90 (t, *J* = 6.8

Hz, 6H, 2 CH₃ from alkyl chains); ¹³C-NMR (CDCl₃, δ, ppm): 158.6 (2C, 2-Py), 158.6 (2C, 4-Py), 155.1 (2C, 6-Py), 128.8 (2C, 5-Py), 127.5 (2C, 3-Py), 68.6 (2C, O-CH₂), 50.7 (2C, Py(1)-CH₂), 33.5 (2C, Py(2)-CH₂), 31.9 (2C, Py(2)CH₂CH₂), 29.72 (2C, 2 CH₂ alkyl chains), 29.7 (2C, 2 CH₂ alkyl chains), 29.68 (4C, 4 CH₂ alkyl chains), 29.65 (2C, 2 CH₂ alkyl chains), 29.5 (2C, 2 CH₂ alkyl chains), 29.4 (2C, 2 CH₂ alkyl chains), 29.3 (2C, 2 CH₂ alkyl chains), 29.2 (2C, 2 CH₂ alkyl chains), 28.8 (2C, CH₂CH₂CH₃), 22.7 (2C, CH₂CH₃), 21.7 (2C, 2 CH₃-Py(6)), 21.6 (2C, 2 CH₃-Py(4)), 14.1 (2C, 2 CH₃ from n-alkyl chain), ¹⁹F-NMR (CDCl₃, δ, ppm): 72.96 (d, *J* = 712 Hz, PF₆⁻); Anal (C₄₆H₈₂F₁₂N₂OP₂) C, H, N.

1,5-bis(4,6-dimethyl-2-pentadecylpyridinium-1-yl)-3-oxapentane dihexafluorophosphate 2f: Yield 63.6%; ¹H-NMR (CDCl₃, δ, ppm): 7.44 (s, 2H, H5Py), 7.40 (s, 2H, H3Py), 4.64 (t, *J* = 5.0 Hz, 4H, 2 O-CH₂CH₂-Py), 3.90 (t, *J* = 5.0 Hz, 4H, 2 O-CH₂CH₂-Py), 2.97 (t, *J* = 8.0 Hz, 4H, 2 Py-CH₂-(CH₂)₁₃-CH₃), 2.74 (s, 6H, 2 Py(6)-CH₃), 2.55 (s, 6H, 2 Py(4)-CH₃), 1.68 (m, 4H, 2 Py-CH₂CH₂(CH₂)₁₂CH₃), 1.41 (m, 4H, 2 Py-CH₂CH₂CH₂(CH₂)₁₁CH₃), 1.26 (m, 44H, 22 CH₂ from alkyl chains), 0.88 (t, *J* = 6.8 Hz, 6H, 2 CH₃ from alkyl chains); ¹³C-NMR (CDCl₃, δ, ppm): 158.6 (2C, 2-Py), 158.3 (2C, 4-Py), 155.1 (2C, 6-Py), 128.8 (2C, 5-Py), 127.5 (2C, 3-Py), 68.6 (2C, O-CH₂), 50.7 (2C, Py(1)-CH₂), 33.5 (2C, Py(2)-CH₂), 31.9 (2C, Py(2)CH₂CH₂), 29.73 (8C, 8 CH₂ alkyl chains), 29.7 (2C, 2 CH₂ alkyl chains), 29.68 (2C, 2 CH₂ alkyl chains), 29.5 (2C, 2 CH₂ alkyl chains), 29.38 (2C, 2 CH₂ alkyl chains), 29.33 (2C, 2 CH₂ alkyl chains), 29.24 (2C, 2 CH₂ alkyl chains), 28.8 (2C, CH₂CH₂CH₃), 22.7 (2C, CH₂CH₃), 21.63 (2C, 2 CH₃-

Py(6)), 21.61 (2C, 2 CH₃-Py(4)), 14.1 (2C, 2 CH₃ from n-alkyl chain), ¹⁹F-NMR (CDCl₃, δ, ppm): 72.96 (d, *J* = 713 Hz, PF₆⁻); Anal (C₄₈H₈₆F₁₂N₂OP₂) C, H, N.

1,5-bis(4,6-dimethyl-2-hexadecylpyridinium-1-yl)-3-oxapentane

di-

hexafluorophosphate 2g: Yield 55.6%; ¹H-NMR (CDCl₃, δ, ppm): 7.41 (s, 2H, H5Py), 7.33 (s, 2H, H3Py), 4.54 (t, *J* = 5.0 Hz, 4H, 2 O-CH₂CH₂-Py), 3.80 (t, *J* = 5.0 Hz, 4H, 2 O-CH₂CH₂-Py), 2.86 (t, *J* = 8.0 Hz, 4H, 2 Py-CH₂-(CH₂)₁₄-CH₃), 2.61 (s, 6H, 2 Py(6)-CH₃), 2.46 (s, 6H, 2 Py(4)-CH₃), 1.58 (m, 4H, 2 Py-CH₂CH₂(CH₂)₁₃CH₃), 1.28 (m, 4H, 2 Py-CH₂CH₂CH₂(CH₂)₁₂CH₃), 1.18 (m, 48H, 24 CH₂ from alkyl chains), 0.81 (t, *J* = 7.0 Hz, 6H, 2 CH₃ from alkyl chains); ¹³C-NMR (CDCl₃, δ, ppm): 158.6 (2C, 2-Py), 158.3 (2C, 4-Py), 155.2 (2C, 6-Py), 128.8 (2C, 5-Py), 127.5 (2C, 3-Py), 68.6 (2C, O-CH₂), 50.6 (2C, Py(1)-CH₂), 33.5 (2C, Py(2)-CH₂), 31.9 (2C, Py(2)CH₂CH₂), 29.74 (10C, 10 CH₂ alkyl chains), 29.68 (4C, 4 CH₂ alkyl chains), 29.51 (2C, 2 CH₂ alkyl chains), 29.38 (2C, 2 CH₂ alkyl chains), 29.34 (2C, 2 CH₂ alkyl chains), 29.25 (2C, 2 CH₂ alkyl chains), 28.75 (2C, CH₂CH₂CH₃), 22.7 (2C, CH₂CH₃), 21.58 (2C, 2 CH₃-Py(6)), 21.58 (2C, 2 CH₃-Py(4)), 14.1 (2C, 2 CH₃ from n-alkyl chain), ¹⁹F-NMR (CDCl₃, δ, ppm): 72.90 (d, *J* = 713 Hz, PF₆⁻); Anal (C₅₀H₉₀F₁₂N₂OP₂) C, H, N.

1,5-bis(4,6-dimethyl-2-heptadecylpyridinium-1-yl)-3-oxapentane

di-

hexafluorophosphate 2h: Yield 75.1%; ¹H-NMR (CDCl₃, δ, ppm): 7.49 (s, 2H, H5Py), 7.42 (s, 2H, H3Py), 4.63 (t, *J* = 5.0 Hz, 4H, 2 O-CH₂CH₂-Py), 3.89 (t, *J* = 5.0 Hz, 4H, 2 O-CH₂CH₂-Py), 2.95 (t, *J* = 8.0 Hz, 4H, 2 Py-CH₂-(CH₂)₁₅-CH₃), 2.70 (s, 6H, 2 Py(6)-

CH₃), 2.54 (s, 6H, 2 Py(4)-CH₃), 1.68 (m, 4H, 2 Py-CH₂CH₂(CH₂)₁₄CH₃), 1.37 (m, 4H, 2 Py-CH₂CH₂CH₂(CH₂)₁₃CH₃), 1.31 (m, 52H, 26 CH₂ from alkyl chains), 0.89 (t, *J* = 7.0 Hz, 6H, 2 CH₃ from alkyl chains); ¹³C-NMR (CDCl₃, δ, ppm): 158.6 (2C, 2-Py), 158.3 (2C, 4-Py), 155.2 (2C, 6-Py), 128.8 (2C, 5-Py), 127.5 (2C, 3-Py), 68.6 (2C, O-CH₂), 50.6 (2C, Py(1)-CH₂), 33.5 (2C, Py(2)-CH₂), 31.9 (2C, Py(2)CH₂CH₂), 29.74 (10C, 10 CH₂ alkyl chains), 29.68 (6C, 6 CH₂ alkyl chains), 29.51 (2C, 2 CH₂ alkyl chains), 29.38 (2C, 2 CH₂ alkyl chains), 29.34 (2C, 2 CH₂ alkyl chains), 29.25 (2C, 2 CH₂ alkyl chains), 28.75 (2C, CH₂CH₂CH₃), 22.7 (2C, CH₂CH₃), 21.58 (2C, 2 CH₃-Py(6)), 21.58 (2C, 2 CH₃-Py(4)), 14.1 (2C, 2 CH₃ from n-alkyl chain), ¹⁹F-NMR (CDCl₃, δ, ppm): 72.91 (d, *J* = 713 Hz, PF₆⁻); Anal (C₅₂H₉₄F₁₂N₂OP₂) C, H, N.

1,5-bis(4,6-dimethyl-2-decylpyridinium-1-yl)-3-oxapentane di-chloride 3a: Yield 95.9%; ¹H-NMR (DMSO-d₆, δ, ppm): 7.70 (s, 2H, H5Py), 7.68 (s, 2H, H3Py), 4.58 (t, *J* = 5.0 Hz, 4H, 2 O-CH₂CH₂-Py), 3.77 (t, *J* = 5.0 Hz, 4H, 2 O-CH₂CH₂-Py), 2.82 (t, *J* = 8 Hz, 4H, 2 Py-CH₂-(CH₂)₈-CH₃), 2.60 (s, 6H, 2 Py(6)-CH₃), 2.54 (s, 6H, 2 Py(4)-CH₃), 1.67 (m, 4H, 2 Py-CH₂CH₂(CH₂)₇CH₃), 1.40 (m, 4H, 2 Py-CH₂CH₂CH₂(CH₂)₆CH₃), 1.20 (m, 24H, 12 CH₂ from alkyl chains), 0.80 (t, *J* = 6.5 Hz, 6H, 2 CH₃ from alkyl chains); ¹³C-NMR (DMSO-d₆, δ, ppm): 158.0 (2C, 2-Py), 157.5 (2C, 4-Py), 155.0 (2C, 6-Py), 127.9 (2C, 5-Py), 126.8 (2C, 3-Py), 68.1 (2C, O-CH₂), 50.5 (2C, Py(1)-CH₂), 32.6 (2C, Py(2)-CH₂), 31.26 (2C, Py(2)CH₂CH₂), 28.97 (2C, 2 CH₂ alkyl chains), 28.92 (2C, 2 CH₂ alkyl chains), 28.75 (2C, 2 CH₂ alkyl chains), 28.68 (2C, 2 CH₂ alkyl chains), 28.63 (2C, 2 CH₂ alkyl chains), 28.36 (2C, CH₂CH₂CH₃), 22.1 (2C, CH₂CH₃), 21.16 (2C, 2 CH₃-

Py(6)), 20.9 (2C, 2 CH₃-Py(4)), 13.9 (2C, 2 CH₃ from n-alkyl chain); Anal (C₃₈H₆₆Cl₂N₂O) C, H, N.

1,5-bis(4,6-dimethyl-2-undecylpyridinium-1-yl)-3-oxapentane di-chloride 3b: Yield 90.3%; ¹H-NMR (DMSO-d⁶, δ, ppm): 7.72 (s, 2H, H5Py), 7.41 (s, 2H, H3Py), 4.63 (t, *J* = 5.5 Hz, 4H, 2 O-CH₂CH₂-Py), 3.82 (t, *J* = 5.0 Hz, 4H, 2 O-CH₂CH₂-Py), 2.87 (t, *J* = 8.0 Hz, 4H, 2 Py-CH₂-(CH₂)₉-CH₃), 2.65 (s, 6H, 2 Py(6)-CH₃), 2.53 (s, 6H, 2 Py(4)-CH₃), 1.67 (m, 4H, 2 Py-CH₂CH₂(CH₂)₈CH₃), 1.55 (m, 4H, 2 Py-CH₂CH₂CH₂(CH₂)₇CH₃), 1.26 (m, 28H, 14 CH₂ from alkyl chains), 0.86 (t, *J* = 7.0 Hz, 6H, 2 CH₃ from alkyl chains); ¹³C-NMR (DMSO-d⁶, δ, ppm): 158.0 (2C, 2-Py), 157.5 (2C, 4-Py), 155.0 (2C, 6-Py), 127.9 (2C, 5-Py), 126.7 (2C, 3-Py), 68.1 (2C, O-CH₂), 50.5 (2C, Py(1)-CH₂), 32.6 (2C, Py(2)-CH₂), 31.2 (2C, Py(2)CH₂CH₂), 29.0 (4C, 4 CH₂ alkyl chains), 28.9 (2C, 2 CH₂ alkyl chains), 28.7 (2C, 2 CH₂ alkyl chains), 28.69 (2C, 2 CH₂ alkyl chains), 28.64 (2C, 2 CH₂ alkyl chains), 28.35 (2C, CH₂CH₂CH₃), 22.1 (2C, CH₂CH₃), 21.1 (2C, 2 CH₃-Py(6)), 20.9 (2C, 2 CH₃-Py(4)), 13.9 (2C, 2 CH₃ from n-alkyl chain); Anal (C₄₀H₇₀Cl₂N₂O) C, H, N.

1,5-bis(4,6-dimethyl-2-dodecylpyridinium-1-yl)-3-oxapentane di-chloride 3c: Yield 81.6%; ¹H-NMR (DMSO-d⁶, δ, ppm): 7.74 (s, 2H, H5Py), 7.73 (s, 2H, H3Py), 4.64 (t, *J* = 5.0 Hz, 4H, 2 O-CH₂CH₂-Py), 3.83 (t, *J* = 5.0 Hz, 4H, 2 O-CH₂CH₂-Py), 2.88 (t, *J* = 8.0 Hz, 4H, 2 Py-CH₂-(CH₂)₁₀-CH₃), 2.67 (s, 6H, 2 Py(6)-CH₃), 2.45 (s, 6H, 2 Py(4)-CH₃), 1.55 (m, 4H, 2 Py-CH₂CH₂(CH₂)₉CH₃), 1.25(m, 36H, 18 CH₂ from alkyl chains),

0.86 (t, $J = 7.0$ Hz, 6H, 2 CH₃ from alkyl chains); ¹³C-NMR (DMSO-d⁶, δ , ppm): 158.0 (2C, 2-Py), 157.53 (2C, 4-Py), 155.0 (2C, 6-Py), 127.99 (2C, 5-Py), 126.7 (2C, 3-Py), 68.1 (2C, O-CH₂), 50.5 (2C, Py(1)-CH₂), 32.6 (2C, Py(2)-CH₂), 31.2 (2C, Py(2)CH₂-CH₂), 29.1 (2C, 2 CH₂ alkyl chains), 29.02 (2C, 2 CH₂ alkyl chains), 29.00 (2C, 2 CH₂ alkyl chains), 28.93 (2C, 2 CH₂ alkyl chains), 28.75 (2C, 2 CH₂ alkyl chains), 28.69 (2C, 2 CH₂ alkyl chains), 28.64 (2C, 2 CH₂ alkyl chains) 28.35 (2C, CH₂CH₂CH₃), 22.06 (2C, CH₂CH₃), 21.1 (2C, 2 CH₃-Py(6)), 20.9 (2C, 2 CH₃-Py(4)), 13.9 (2C, 2 CH₃ from n-alkyl chain); Anal (C₄₂H₇₄Cl₂N₂O) C, H, N.

1,5-bis(4,6-dimethyl-2-tridecylpyridinium-1-yl)-3-oxapentane di-chloride 3d: Yield 96.8%; ¹H-NMR (DMSO-d⁶, δ , ppm): 7.70 (s, 2H, H5Py), 7.68 (s, 2H, H3Py), 4.58 (t, $J = 5.0$ Hz, 4H, 2 O-CH₂-CH₂-Py), 3.77 (t, $J = 5.0$ Hz, 4H, 2 O-CH₂-CH₂-Py), 2.82 (t, $J = 7.5$ Hz, 4H, 2 Py-CH₂-(CH₂)₁₁-CH₃), 2.62 (s, 6H, 2 Py(6)-CH₃), 2.53 (s, 6H, 2 Py(4)-CH₃), 1.49 (m, 4H, 2 Py-CH₂-CH₂-(CH₂)₁₀CH₃), 1.22(m, 40H, 20 CH₂ from alkyl chains), 0.80 (t, $J = 6.5$ Hz, 6H, 2 CH₃ from alkyl chains); ¹³C-NMR (DMSO-d⁶, δ , ppm): 158.0 (2C, 2-Py), 157.5 (2C, 4-Py), 155.0 (2C, 6-Py), 128.0 (2C, 5-Py), 126.7 (2C, 3-Py), 68.1 (2C, O-CH₂), 50.5 (2C, Py(1)-CH₂), 32.6 (2C, Py(2)-CH₂), 31.2 (2C, Py(2)CH₂-CH₂), 29.05 (6C, 6 CH₂ alkyl chains), 29.00 (2C, 2 CH₂ alkyl chains), 28.94 (2C, 2 CH₂ alkyl chains), 28.76 (2C, 2 CH₂ alkyl chains), 28.69 (2C, 2 CH₂ alkyl chains), 28.65 (2C, 2 CH₂ alkyl chains), 28.36 (2C, 2 CH₂ alkyl chains), 22.06 (2C, CH₂CH₃), 21.1 (2C, 2 CH₃-Py(6)), 20.9 (2C, 2 CH₃-Py(4)), 13.9 (2C, 2 CH₃ from n-alkyl chain); Anal (C₄₄H₇₈Cl₂N₂O) C, H, N.

1,5-bis(4,6-dimethyl-2-tetradecylpyridinium-1-yl)-3-oxapentane di-chloride 3e: Yield 96.3%; $^1\text{H-NMR}$ (DMSO-d^6 , δ , ppm): 7.75 (s, 2H, H5Py), 7.74 (s, 2H, H3Py), 4.63 (t, $J = 5.0$ Hz, 4H, 2 O-CH₂CH₂-Py), 3.83 (t, $J = 5.0$ Hz, 4H, 2 O-CH₂CH₂-Py), 2.88 (t, $J = 7.5$ Hz, 4H, 2 Py-CH₂-(CH₂)₁₂-CH₃), 2.66 (s, 6H, 2 Py(6)-CH₃), 2.55 (s, 6H, 2 Py(4)-CH₃), 1.54 (m, 4H, 2 Py-CH₂CH₂(CH₂)₁₁CH₃), 1.27(m, 44H, 22 CH₂ from alkyl chains), 0.87 (t, $J = 6.5$ Hz, 6H, 2 CH₃ from alkyl chains); $^{13}\text{C-NMR}$ (DMSO-d^6 , δ , ppm): 158.0 (2C, 2-Py), 157.5 (2C, 4-Py), 155.0 (2C, 6-Py), 128.0 (2C, 5-Py), 126.7 (2C, 3-Py), 68.1 (2C, O-CH₂), 50.5 (2C, Py(1)-CH₂), 32.6 (2C, Py(2)-CH₂), 31.2 (2C, Py(2)CH₂CH₂), 29.05 (6C, 6 CH₂ alkyl chains), 29.00 (2C, 2 CH₂ alkyl chains), 28.95 (4C, 4 CH₂ alkyl chains), 29.76 (2C, 2 CH₂ alkyl chains), 28.69 (2C, 2 CH₂ alkyl chains), 28.66 (2C, 2 CH₂ alkyl chains), 28.36 (2C, CH₂CH₂CH₃), 22.06 (2C, CH₂CH₃), 21.1 (2C, 2 CH₃-Py(6)), 20.9 (2C, 2 CH₃-Py(4)), 13.9 (2C, 2 CH₃ from n-alkyl chain); Anal (C₄₆H₈₂Cl₂N₂O) C, H, N.

1,5-bis(4,6-dimethyl-2-pentadecylpyridinium-1-yl)-3-oxapentane di-chloride 3f: Yield 82.5%; $^1\text{H-NMR}$ (DMSO-d^6 , δ , ppm): 7.80 (s, 2H, H5Py), 7.78 (s, 2H, H3Py), 4.69 (t, $J = 5.0$ Hz, 4H, 2 O-CH₂CH₂-Py), 3.88 (t, $J = 5.0$ Hz, 4H, 2 O-CH₂CH₂-Py), 2.93 (t, $J = 7.5$ Hz, 4H, 2 Py-CH₂-(CH₂)₁₃-CH₃), 2.73 (s, 6H, 2 Py(6)-CH₃), 2.55 (s, 6H, 2 Py(4)-CH₃), 1.60 (m, 4H, 2 Py-CH₂CH₂(CH₂)₁₂CH₃), 1.33(m, 48H, 24 CH₂ from alkyl chains), 0.91 (t, $J = 7.0$ Hz, 6H, 2 CH₃ from alkyl chains); $^{13}\text{C-NMR}$ (DMSO-d^6 , δ , ppm): 157.9 (2C, 2-Py), 157.4 (2C, 4-Py), 154.8 (2C, 6-Py), 127.8 (2C, 5-Py), 126.6 (2C, 3-Py), 68.0

(2C, O-CH₂), 50.4 (2C, Py(1)-CH₂), 32.5 (2C, Py(2)-CH₂), 31.1 (2C, Py(2)CH₂CH₂), 28.9 (12C, 12 CH₂ alkyl chains), 28.85 (2C, 2 CH₂ alkyl chains), 28.82 (2C, 2 CH₂ alkyl chains), 28.63 (2C, 2 CH₂ alkyl chains), 28.54 (2C, 2 CH₂ alkyl chains), 28.22 (2C, CH₂CH₂CH₃), 21.9 (2C, CH₂CH₃), 21.0 (2C, 2 CH₃-Py(6)), 20.7 (2C, 2 CH₃-Py(4)), 13.7 (2C, 2 CH₃ from n-alkyl chain); Anal (C₄₈H₈₆Cl₂N₂O) C, H, N.

1,5-bis(4,6-dimethyl-2-hexadecylpyridinium-1-yl)-3-oxapentane di-chloride 3g: Yield 74.2%; ¹H-NMR (DMSO-d⁶, δ, ppm): 7.69 (s, 2H, H5Py), 7.67 (s, 2H, H3Py), 4.54 (t, *J* = 5.0 Hz, 4H, 2 O-CH₂CH₂-Py), 3.77 (t, *J* = 5.0 Hz, 4H, 2 O-CH₂CH₂-Py), 2.83 (t, *J* = 8.0 Hz, 4H, 2 Py-CH₂-(CH₂)₁₄-CH₃), 2.60 (s, 6H, 2 Py(6)-CH₃), 2.46 (s, 6H, 2 Py(4)-CH₃), 1.49 (m, 4H, 2 Py-CH₂CH₂(CH₂)₁₃CH₃), 1.20(m, 52H, 26 CH₂ from alkyl chains), 0.79 (t, *J* = 7.0 Hz, 6H, 2 CH₃ from alkyl chains); ¹³C-NMR (DMSO-d⁶, δ, ppm): 158.0 (2C, 2-Py), 157.5 (2C, 4-Py), 155.0 (2C, 6-Py), 128.0 (2C, 5-Py), 126.7 (2C, 3-Py), 68.2 (2C, O-CH₂), 50.5 (2C, Py(1)-CH₂), 32.6 (2C, Py(2)-CH₂), 31.2 (2C, Py(2)CH₂CH₂), 29.05 (10C, 10 CH₂ alkyl chains), 28.98 (4C, 4 CH₂ alkyl chains), 28.96 (2C, 2 CH₂ alkyl chains), 28.76 (4C, 4 CH₂ alkyl chains), 28.67 (2C, 2 CH₂ alkyl chains), 28.36 (2C, 2 CH₂ alkyl chains), 22.1 (2C, CH₂CH₃), 21.1 (2C, 2 CH₃-Py(6)), 20.9 (2C, 2 CH₃-Py(4)), 13.9 (2C, 2 CH₃ from n-alkyl chain); Anal (C₅₀H₉₀Cl₂N₂O) C, H, N.

1,5-bis(4,6-dimethyl-2-heptadecylpyridinium-1-yl)-3-oxapentane di-chloride 3h: Yield 90.1%; ¹H-NMR (DMSO-d⁶, δ, ppm): 7.80 (s, 2H, H5Py), 7.79 (s, 2H, H3Py), 4.69 (t, *J* = 5.0 Hz, 4H, 2 O-CH₂CH₂-Py), 3.89 (t, *J* = 5.0 Hz, 4H, 2 O-CH₂CH₂-Py), 2.94 (t, *J*

= 8.0 Hz, 4H, 2 Py-CH₂-(CH₂)₁₅-CH₃), 2.73 (s, 6H, 2 Py(6)-CH₃), 2.54 (s, 6H, 2 Py(4)-CH₃), 1.61 (m, 4H, 2 Py-CH₂CH₂(CH₂)₁₄CH₃), 1.30(m, 56H, 28 CH₂ from alkyl chains), 0.91 (t, *J* = 7.0 Hz, 6H, 2 CH₃ from alkyl chains); ¹³C-NMR (DMSO-d⁶, δ, ppm): 157.9 (2C, 2-Py), 158.4 (2C, 4-Py), 154.9 (2C, 6-Py), 127.8 (2C, 5-Py), 126.6 (2C, 3-Py), 68.0 (2C, O-CH₂), 50.4 (2C, Py(1)-CH₂), 32.5 (2C, Py(2)-CH₂), 31.1 (2C, Py(2)CH₂CH₂), 28.92 (10C, 10 CH₂ alkyl chains), 28.9 (6C, 6 CH₂ alkyl chains), 28.84 (2C, 2 CH₂ alkyl chains), 28.63 (2C, 2 CH₂ alkyl chains), 28.54 (4C, 4 CH₂ alkyl chains), 28.22 (2C, CH₂CH₂CH₃), 21.9 (2C, CH₂CH₃), 21.0 (2C, 2 CH₃-Py(6)), 20.7 (2C, 2 CH₃-Py(4)), 13.7 (2C, 2 CH₃ from n-alkyl chain); Anal (C₅₂H₉₄Cl₂N₂O) C, H, N.

1,5-bis(4,6-dimethyl-2-hexadecylpyridinium-1-yl)-3-oxapentane di-bromide 4g. The DOWEX 1X8-200 (chloride form) was first converted to OH⁻ form using 5% aqueous sodium hydroxide, and subsequently washed with DI water to neutral pH. The full exchange of Cl⁻ was tested in the eluent using a concentrated aqueous AgNO₃ solution. The Dowex OH form was converted into the Br⁻ form using 5% aqueous hydrobromic acid, followed by DI water until pH = 7. The resin was subsequently washed with methanol and stored overnight in the same solvent to fully inflate. The next day it was loaded into a column, and washed with fresh methanol. An amount of 46.8 mg of hexadecyl pyridinium gemini surfactant dihexafluorophosphate **3g** was dissolved in 6 mL of methanol with gentle heating and the solution was transferred on top of the ion exchange column. The dibromide compound was eluted with methanol (flow rate 1-3 mL/min). Sample was cycled through the column repeatedly for 1 hr. ¹⁹F-NMR analysis of a small aliquot taken from the eluent showed no fluorine peak corresponding to PF₆⁻.

Evaporation of solvent yielded the product, which was crystallized from hexane and dried under vacuum, yielding 30.1 mg of dibromide (77.5 % yield).

$^1\text{H-NMR}$ (CDCl_3 , δ , ppm): 7.61 (s, 2H, H5Py), 7.45 (s, 2H, H3Py), 4.81 (t, $J = 5.0$ Hz, 4H, 2 O-CH₂CH₂-Py), 3.9 (t, $J = 5.0$ Hz, 4H, 2 O-CH₂CH₂-Py), 3.0 (t, $J = 8.0$ Hz, 4H, 2 Py-CH₂-(CH₂)₁₄-CH₃), 2.89 (s, 6H, 2 Py(6)-CH₃), 2.52 (s, 6H, 2 Py(4)-CH₃), 1.63 (m, 4H, 2 Py-CH₂CH₂(CH₂)₁₃CH₃), 1.24(m, 52H, 26 CH₂ from alkyl chains), 0.82 (t, $J = 7.0$ Hz, 6H, 2 CH₃ from alkyl chains); $^{13}\text{C-NMR}$ (CDCl_3 , δ , ppm): 158.5 (2C, 2-Py), 158.1 (2C, 4-Py), 155.6 (2C, 6-Py), 129.1 (2C, 5-Py), 127.5 (2C, 3-Py), 69.0 (2C, O-CH₂), 51.77 (2C, Py(1)-CH₂), 33.97 (2C, Py(2)-CH₂), 31.9 (2C, Py(2)CH₂CH₂), 29.71 (10C, 10 CH₂ alkyl chains), 29.66 (4C, 4 CH₂ alkyl chains), 29.49 (2C, 2 CH₂ alkyl chains), 29.4 (4C, 4 CH₂ alkyl chains), 29.3 (2C, 2 CH₂ alkyl chains), 29.0 (2C, 2 CH₂ alkyl chains), 23.0 (2C, CH₂CH₃), 22.6 (2C, 2 CH₃-Py(6)), 21.9 (2C, 2 CH₃-Py(4)), 14.12 (2C, 2 CH₃ from n-alkyl chain); Anal ($\text{C}_{50}\text{H}_{90}\text{Br}_2\text{N}_2\text{O}$) C, H, N.

1,5-bis(4,6-dimethyl-2-hexadecylpyridinium-1-yl)-3-oxapentane

di-

hydrogenophosphate 5g. The DOWEX 1X8-200 (chloride form) was first converted to OH form using 5% aqueous sodium hydroxide, and subsequently washed with DI water to neutral pH. The full exchange of Cl⁻ was tested in the eluent using a concentrated aqueous AgNO₃ solution. The Dowex OH form was converted into the H₂PO₄⁻ form using 5% aqueous phosphoric acid, followed by DI water until pH = 4. The resin was subsequently washed with methanol and stored overnight in the same solvent to fully inflate. The next day it was loaded into a column, and washed with fresh methanol. An

amount of 60 mg hexadecyl pyridinium gemini surfactant dihexafluorophosphate **3g** was dissolved in 6 mL methanol with gentle heating and the solution was transferred on top of the ion exchange column. The dihydrogenophosphate compound was eluted with methanol (flow rate 1-3 mL/min). Sample was cycled through the column repeatedly for 1 hr. ^{19}F -NMR analysis of a small aliquot taken from the eluent showed no fluorine peak corresponding to PF_6^- . Evaporation of solvent yielded the product, which was crystallized from chloroform and dried under vacuum, yielding 30.0 mg of dihydrogenophosphate (67.2 % yield).

1,5-bis(4,6-dimethyl-2-hexadecylpyridinium-1-yl)-3-oxapentane

di-

hydrogenophosphate 5g: Yield 75.1%; ^1H -NMR (CDCl_3 , δ , ppm): 7.72 (s, 2H, H5Py), 7.70 (s, 2H, H3Py), 4.62 (t, $J = 5.0$ Hz, 4H, 2 O- CH_2CH_2 -Py), 3.81 (t, $J = 5.0$ Hz, 4H, 2 O- CH_2CH_2 -Py), 2.87 (t, $J = 8.0$ Hz, 4H, 2 Py- CH_2 -(CH_2)₁₄-CH₃), 2.64 (s, 6H, 2 Py(6)- CH_3), 2.50 (s, 6H, 2 Py(4)- CH_3), 1.56 (m, 4H, 2 Py- $\text{CH}_2\text{CH}_2(\text{CH}_2)_{13}\text{CH}_3$), 1.24 (m, 52H, 26 CH_2 from alkyl chains), 0.84 (t, $J = 7.0$ Hz, 6H, 2 CH_3 from alkyl chains); ^{13}C -NMR (CDCl_3 , δ , ppm): 158.5 (2C, 2-Py), 158.1 (2C, 4-Py), 155.6 (2C, 6-Py), 129.1 (2C, 5-Py), 127.5 (2C, 3-Py), 69.0 (2C, O- CH_2), 51.77 (2C, Py(1)- CH_2), 33.97 (2C, Py(2)- CH_2), 31.9 (2C, Py(2) CH_2CH_2), 29.71 (10C, 10 CH_2 alkyl chains), 29.66 (4C, 4 CH_2 alkyl chains), 29.49 (2C, 2 CH_2 alkyl chains), 29.4 (4C, 4 CH_2 alkyl chains), 29.3 (2C, 2 CH_2 alkyl chains), 29.0 (2C, 2 CH_2 alkyl chains), 23.0 (2C, CH_2CH_3), 22.6 (2C, 2 CH_3 -Py(6)), 21.9 (2C, 2 CH_3 -Py(4)), 14.12 (2C, 2 CH_3 from n-alkyl chain); Anal ($\text{C}_{50}\text{H}_{94}\text{N}_2\text{O}_9\text{P}_2$) C, H, N.

Critical micelle concentration (cmc) measurement procedure. The critical micelle concentration of the gemini surfactants was determined using the conductivity method [75]. Concentrated solutions of novel gemini surfactants were transferred into Zetasizer Nano dip cell (ZEN1002, Malvern Instruments, Malvern, UK) and their conductivities (mS/cm) were measured using a Zetasizer Nano (Malvern Instruments, Malvern, UK) upon sequential dilution with deionized water. The plot of conductivity k against the surfactant concentration C (mM) was drawn and the cmc was determined as the intersection between the two linear variation regimes. All measurements were reported at 25 °C.

Krafft temperature measurement procedure. The Krafft temperature of the novel gemini surfactants were estimated by visual inspection of the clearing point of amphiphile suspension in water (1 mg in 200 μ L DI water), using a Thermolyne heating stage microscope (Dubuque, IA), equipped with an Olympus 5X objective. Precise determination was done using the conductivity method [67].

Liposomal preparation and characterization

Liposome Preparation. Stock solutions (3 mM) of the gemini surfactants (GSs) were prepared from powder in glass vials using $\text{CHCl}_3/\text{MeOH}$ (2/1) as solvent (organic stock). For DOPE and cholesterol, solutions of the same concentration (3 mM) were

made in CHCl_3 . All solutions were swirled, purged with nitrogen, and capped securely; when not in use they were stored in the -20°C freezer.

Two preparations were made for each GS alone, GS mixed with cholesterol in 1:1, 1:2, 1:4 molar ratio, and GS mixed with DOPE in 1:1, 1:2, 1:4 molar ratio. Thus, 20 μL of the corresponding organic stock was transferred into eppendorf vials, along with appropriate amount of co-lipids (total GS in each eppendorf was 60 nmol). The samples were diluted with $\text{CHCl}_3/\text{MeOH}$ (2/1) to a final volume of 500 μL . The organic solvent was evaporated to dryness in the SpeedVac for 1 h, and then the samples were further dried under vacuum in a dessicator for another 1 h. The dry lipid films were hydrated with 600 μL of deionised water yielding a 0.1 mM cationic GS suspension. The vials were purged with sterile nitrogen passed through a 0.22 μm filter, sonicated at room temperature for 1 min, and then left overnight to hydrate. The next day, each vial was freeze-thawed 5 times ($-70^\circ\text{C}/65^\circ\text{C}$) and subsequently sonicated twice for 15 minutes at 65°C with a 15 minute pause between cycles yielding homogeneous liposomal formulations.

Liposome Characterization. A volume of 500 μL of each liposomal preparation was introduced into a disposable Malvern DTS 1060 measurement cell. The size and zeta potential of the liposomes were measured using a Zetasizer Nano (Malvern Instruments). The readings were all made at 25°C at normal resolution, using the instrument's automated feature. For the size measurements, the volume results were used in all cases, and the results were reported as the average of 10-20 runs. Zeta potentials were measured in millivolts (mV).

Lipoplex preparation and characterization

Lipoplex preparation. Solutions of plasmid DNA (gWiz™ Luc plasmid, Aldevon, ND), and ladder Lambda DNA/*Hind* III (Promega, WI), both 0.05 µg/µL, were prepared in sterile conditions, using nuclease-free water.

In six eppendorf tubes, 5 µL of diluted DNA stock were treated with 8 µL, 16 µL, 24 µL, 32 µL, 40 µL, and 64 µL of diluted liposomal preparation (0.1mM) (GS/DNA ratios of 1/1, 2/1, 3/1, 4/1 and 8/1). The tubes were tapped gently for 1 min to ensure proper mixing, and then allowed to rest at room temperature for 30 min for proper lipoplex compaction. This lipoplexes stock solution was used for both gel electrophoresis and size/zeta potential measurements.

Gel electrophoresis of lipoplexes. For the 1/1 and 2/1 +/- charge ratio, 4 µL of lipoplex were aliquoted out in small eppendorf vials. Similarly, 6 µL, 8 µL, 10 µL, 15 µL of lipoplexes were aliquoted out from the lipoplexes stock solution having 3/1, 4/1, 5/1 and 8/1 charge ratio respectively. All these lipoplexes were then accordingly diluted to a final volume of 15 µL with nuclease-free water. Each eppendorf tube subsequently received 3 µL of Blue/Orange Loading dye (Promega, WI). A DNA standard was made by mixing 3 µL of diluted DNA stock with 12 µL of nuclease free water and 3 µL of Blue/Orange Loading dye. A ladder reference standard was made by mixing 2 µL of Lambda DNA/*Hind* III marker with 13 µL of nuclease free water and 3 µL of Blue/Orange Loading dye. The final volume in all vials was 18 µL. The lipoplex/dye mixtures were loaded into a 1% Agarose gel made in 1X TAE buffer, pre-stained with

GelStar® (Lonza) nucleic acid stain (10 μ L in 35 mL gel suspension). Gel electrophoresis was carried out at 75 mV for 90 min. DNA bands were visualized with a Mighty Bright transilluminator (Hoefer), and the gel was photographed with an Olympus C-5060 digital camera.

Lipoplex characterization. The remaining lipoplexes from each lipoplex stock solution was diluted to a final volume of 500 μ L with nuclease-free water and transferred into a disposable Malvern DTS 1060 measurement cell. The size and zeta potential of the lipoplexes were measured using a Zetasizer Nano (Malvern Instruments) at 25°C at normal resolution. Volume results were used for size data, and results were reported as the average of 10-20 runs. Zeta potentials were measured in millivolts (mV).

General procedure for transfection and cytotoxicity experiments

Preparation of lipoplexes. In a typical experiment, for each cationic liposomal formulation to be tested an amount of 3 μ L of a 0.5 mg/mL gWiz™ Luc plasmid DNA solution was aliquoted out in a sterile eppendorf tubes and was diluted with 13 μ L nuclease-free water. The diluted DNA was then treated with 144 μ L of the liposomal formulation 0.6 mM, prepared as indicated above. The vials were tapped gently to ensure proper mixing, and then allowed to rest at room temperature for 30 min for complete lipoplex compaction. This lipoplex stock solution was used for transfection, cytotoxicity, size, and zeta potential measurements.

Transfection and viability experiments. From the lipoplex stock solution, an amount of 135 μ L was aliquoted out for each cationic lipid formulation to be tested, and was diluted with 765 μ L Optimem.

The lipoplexes were tested for their ability to transfect NCI-H23 cancer cell lines. The cells were maintained in 10% fetal bovine serum (FBS) enriched medium at 37 °C in a humidified atmosphere of 95% air/5% CO₂. The media RPMI 1640 (CellGro, Houston, TX) was used for NCI-H23. Twenty-four hours prior to transfection, cells were transferred to 96-well microtiter plates (Cellstar 655180, Greiner Bio-One) at a density of 20,000 cells/well. Each well received 100 μ L of appropriate medium, and the plate was incubated in the same conditions as above. All experiments were done in quadruplicate. Two plates were made for each experiment, one for transfection, and another one for cytotoxicity. The error bars in figures represent one standard deviation from the average value.

Immediately before transfection the medium was removed, and the cells from each well were briefly washed with 200 μ L sterile PBS. After removal of the PBS solution each well received 100 μ L of lipoplex stock solution, and the plates were returned to the incubator. After 90 min incubation time with cells the lipoplex suspension was removed, cells were washed with sterile PBS and then each well received 200 μ L of medium. Cell plates were incubated for further 48 hours, after which the transfection efficacy was determined using the first cell plate and the associated cytotoxicity was assessed using the second cell plate, transfected in similar conditions as the first one.

Transfection efficiency: luciferase and protein content assay. Forty-eight hours after transfection, the medium was aspirated and the wells were washed briefly with 200 μ L PBS. After removal of PBS the cells were lysed by adding 100 μ L 1X reporter lysis buffer (Promega) to each well and incubating the plate at 37 °C for 15 minutes. The cell lysate was collected and used for luciferase and protein assays.

For the luciferase assay, 20 μ L of cell lysate was transferred to a test tube and assessed directly by means of BD Monolight 3010 luminometer (BD Biosciences, San Jose, CA) using a luciferase assay kit (E4030) from Promega.

The protein content was quantified using a bicinchoninic acid (BCA) assay (Thermo Scientific, Rockford, IL). The BCA assay was prepared as specified in its manufacturer's instructions; 40 μ L of cell lysate were treated with 1 mL of BCA reagent in an acryl cuvette and the solution was incubated for 1 hour at 37 °C. The light absorption of the solution was then read at 562 nm by means of a Hach DR/4000U UV-VIS Spectrometer (Loveland, CO), and the protein content was estimated by comparison to bovine serum albumin standards. The luciferase activity was normalized by the protein content and expressed as relative luminescence units/ μ g of protein (RLU/ μ g protein).

Viability assay. In order to quantify the relative cytotoxicity of the non-viral cationic vectors, a WST-1 standard viability method[76] was performed along with the luciferase and BCA assays. Forty-eight hours post-transfection, 20 μ L of WST-1 tetrazolium dye solution (Roche, Mannheim, Germany) was added to each well (still containing 200 μ L of medium). A blank was prepared by mixing 200 μ L of medium and 20 μ L of tetrazolium dye solution, and the plate was incubated at 37 °C in the CO₂

incubator. After 3 hours the colorimetric measurement was performed at 450 nm (with a reference wavelength of 650 nm that was subtracted) by means of a SpectramaxM2 microplate reader (Molecular Devices, Sunnyvale, CA). The value corresponding to the blank was deducted from the value corresponding to each well. Viability was expressed as percentage of the control, represented by cells that underwent the same treatments but did not receive any cationic lipoplexes.

Lipoplex characterization. The remaining 25 μL from each lipoplex preparation was diluted to a final volume of 500 μL with nuclease-free water and transferred into a disposable Malvern DTS 1060 measurement cell. The size and zeta potential of the lipoplexes were measured using a Zetasizer Nano (Malvern Instruments) at 25°C at normal resolution. Volume results were used for size data, and results were reported as the average of 10-20 runs. Zeta potentials were measured in millivolts (mV).

General procedure for transfection experiments in the presence of variable amounts of serum

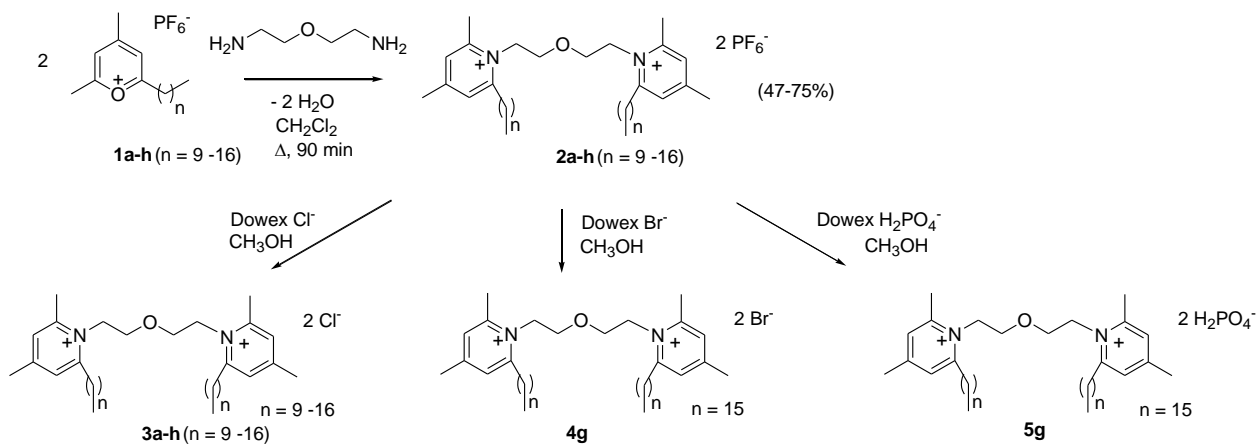
The preparation and characterization of the liposomes and lipoplexes were done as indicated above, using a lipid/DNA charge ratio of 3/1. Lipofectamine transfection reagent (Invitrogen, Carlsbad, CA) was used as a positive control, following the manufacturer's protocol. In this case, 3.75 μL of reagent was diluted to 24 μL nuclease-free water and added over 3 μL plasmid DNA stock solution (0.5 mg/mL) pre-diluted to 50 μL water. The vial was tapped gently to ensure proper mixing, and then allowed to rest at room temperature for 30 min for complete lipoplex compaction. Nuclease-free

water (50 μ L) was used to dilute lipoplex preparation. This lipoplex stock solution was used for transfection, size, and zeta potential measurements.

From all lipoplex stock solutions, an amount of 100 μ L was aliquoted out for each cationic lipid formulation to be tested, including the two positive controls, and was diluted with 800 μ L of media containing the amount of serum indicated in each case (0%, 5%, 10%, 20%, and 40%). The lipoplexes were tested for their ability to transfect the NCI-H23 cell line, following the same protocol and experimental conditions as indicated above. Immediately before transfection the medium was removed, and the cells from each well were briefly washed with 200 μ L sterile PBS. After removal of the PBS solution each well received 100 μ L of lipoplex stock solution (containing in this case variable amounts of serum), and the plates were returned to the incubator for 2 hours. After 2h incubation with cells in pulse transfection the lipoplexes were removed, cells were washed with sterile PBS and then each well received 200 μ L of medium. Cell plates were incubated for further 48 hours, after which the transfection efficacy was determined via luminometry and was corrected for protein content in the standard way (indicated above).

Results and Discussion

The synthesis of the new cationic gemini surfactants is depicted in Scheme 1 and it is based on the high-yield, original procedure for generation of pyridinium compounds via reaction of pyrylium salts with primary amines developed by Balaban, Ilies, and collaborators [46, 77]. Thus, two moles of lipophilic pyrylium salts **1** were reacted with 3-oxa-1,5-diaminopentane in dichloromethane, yielding the desired gemini surfactants as hexafluorophosphates **2** in good isolated yields, after purification via flash chromatography and crystallization from ethanol. Since an essential structural element that impacts the shape of the individual gemini surfactant molecules and their self-assembling is the length of the hydrophobic chains [42, 43, 61], we have varied this parameter from 10 to 17 carbon atoms using the lipophilic pyrylium salts **1a-1h** [46] (Scheme 1).



Scheme 1. Synthesis of the new pyridinium gemini surfactants bearing a hydrophilic linker. The hexafluorophosphate counterion introduced by the lipophilic pyrylium salts

used as synthons was exchanged for the more biocompatible chloride, bromide and dihydrogenophosphate using Dowex 1X8 resin.

Besides the hydrophobic chains, the counterion of the cationic amphiphiles plays an important role in the self-assembling of these charged molecules in bulk and in solution and was shown to have a decisive impact on the physicochemical and biological properties of their DNA complexes [46, 77-83]. It is known that lipoplex formation is a complex process that occurs at the aqueous/organic interface and involves large scale lipid rearrangement, driven by the electrostatic attraction between the positively charged lipid headgroups and the negatively charged phosphate group on the DNA, and entropically-favored by the release of counterions from both amphiphile and DNA [10, 84-86]. Therefore, we have exchanged the PF_6^- anion of compounds **2a-h** for the more biocompatible Cl^- counterion (compounds **3a-h**) using Dowex anion exchange resin. The hexafluorophosphate and chloride ions were selected for their optimum biological properties (transfection efficiency/cytotoxicity ratio) manifested in conjunction with the pyridinium polar head [46, 77]. These anions are very different in their hydration properties – the first one is lipophilic and chaotropic, while the second one is borderline kosmotropic [87]. In order to study the counterion impact on the physicochemical, self-assembling and biological properties of novel pyridinium gemini surfactants we have investigated two other counterions for the C16 representative – the bromide **4g** (chaotropic) and the dihydrogenophosphate **5g** (kosmotropic). Both **4g** and **5g** were obtained from their hexafluorophosphate congener **2g** through anion exchange on Dowex resin and crystallization from acetone/hexane mixtures (Scheme 1).

The formation and stability of the lipoplexes is directly dependent on the packing and self-assembling properties of the amphiphilic cationic compound. Therefore we analyzed the self-assembling properties of novel cationic gemini surfactants **2**, **3**, **4g** and **5g** in bulk, as well as in hydrated form, using a combination of analytical methods that involved differential scanning calorimetry (DSC), small-angle X-ray scattering (SAXS), wide-angle X-ray scattering (WAXS), transmission optical polarized microscopy (TOPM), nanoDSC, conductivity measurements, dynamic light scattering (DLS) and zeta potential measurement experiments. Our goal was to establish how the main structural elements such as the length of hydrophobic tail and the counterion are influencing the thermotropic and lyotropic supramolecular assemblies of these amphiphiles, in order to subsequently correlate them with the biological properties of their lipoplexes.

Thus, DSC thermal analysis experiments (Figure 2) reveal major differences between self-assembling in bulk of hexafluorophosphates **2** and chlorides **3**, evidencing a major impact of the counterion on formation and dynamics of supra-molecular assemblies. During first heating of the gemini surfactants (Figure 2a), the initial crystalline phases templated by the crystallization solvent are destroyed. While cooling the isotropic liquids (Figure 2b) the difference in polarity between the cationic heads associated with counterions and the alkyl tails is expected to generate microphase segregation and to induce ordering of the molecules of amphiphile. It can be observed that in the case of hexafluorophosphates **2** this ordering effect cannot be induced upon cooling of the isotropic solution of amphiphile. No transitions were observed for amphiphiles **2**, irrespective of chain length. This is probably due to the fact that both the

pyridinium cation and the PF_6^- anion are bulky and differ significantly in internal symmetry. Moreover, since both partners are lipophilic, their interaction is relatively strong, with the PF_6^- sitting in close proximity of the pyridinium cation(s), as shown in a recently solved crystal structure of pyridinium cationic lipid hexafluorophosphate [88]. Their association greatly reduces the difference in polarity between the pyridinium polar area and the hydrophobic chains and also increases the steric demand of the polar area. The result is a diminished tendency for microphase segregation and difficulties in spontaneous molecular packing for hexafluorophosphates **2**, similar to the mechanism of formation of ionic liquids [89].

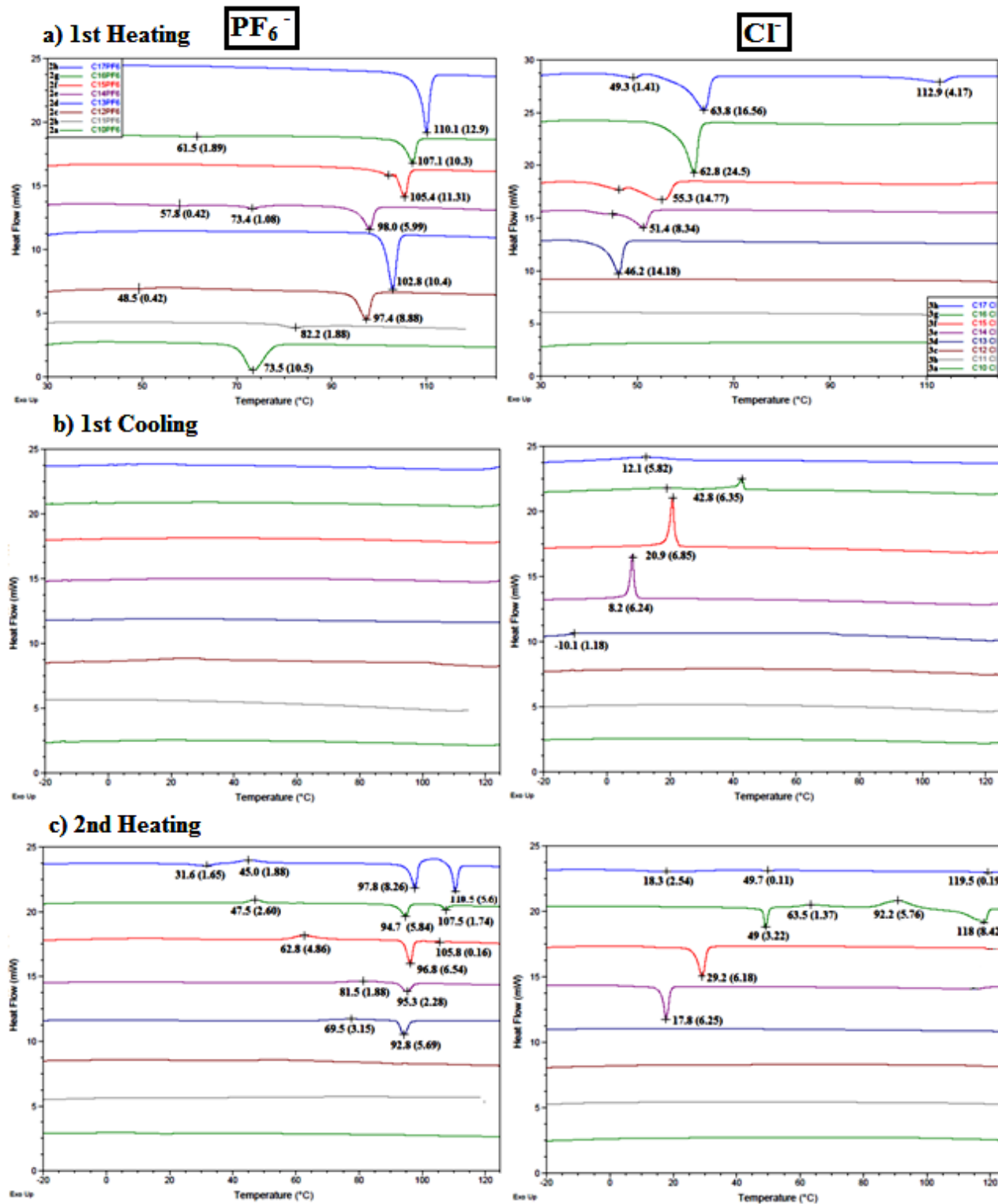
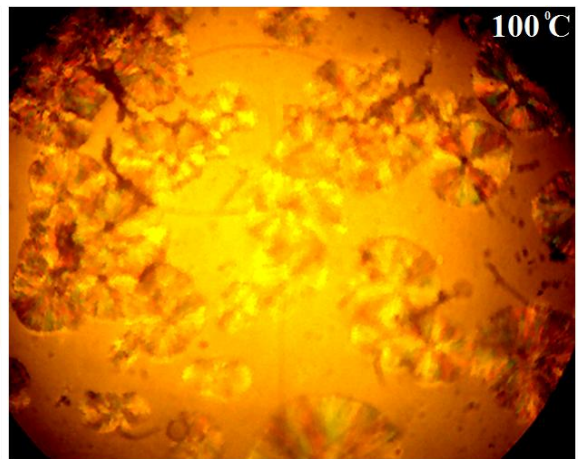
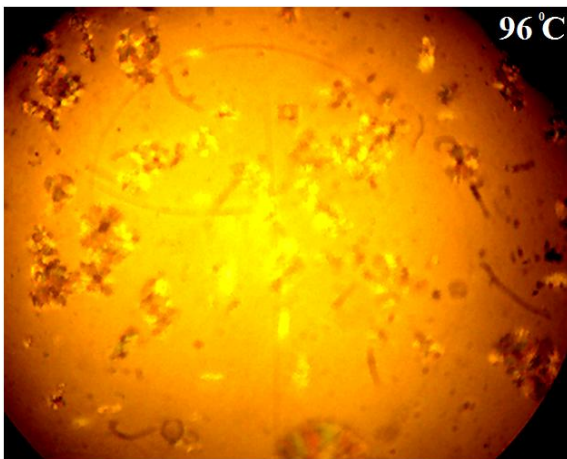
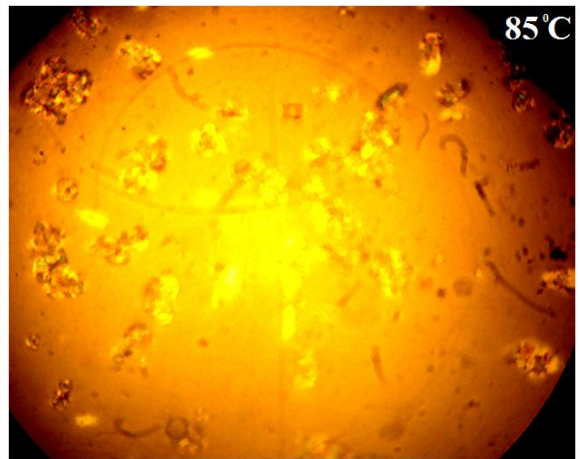
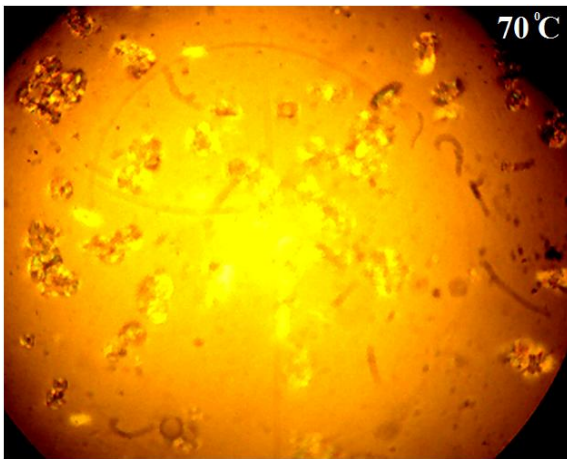
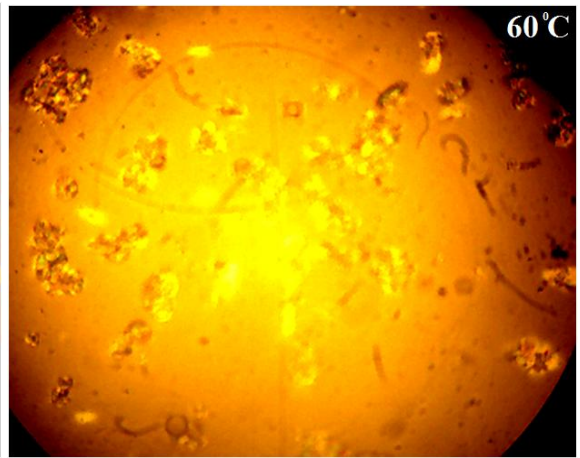
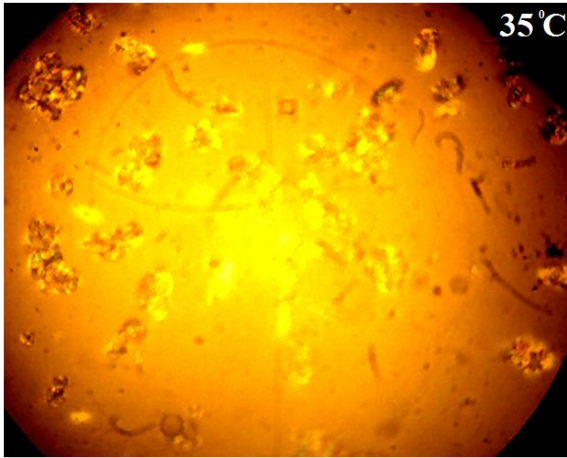


Figure 2. DSC thermograms (5 °C/min) for the first heating (a), first cooling (b), and second heating (c) of gemini surfactants hexafluorophosphates **2** (left panels) and

chlorides **3** (right panels). Transition temperatures and associated enthalpies (Kcal/mol) are shown in each case.

This internal disorder (amorphous state) is confirmed upon reheating of lower hexafluorophosphates **2a-2c** for which no transitions could be observed (Figure 2c). For chain lengths over 12 C atoms an internal reorganization occurred upon reheating. The endothermic ordering transition temperature diminished with the increase of alkyl chain length, as expected, showing that alkyl chains are the main ordering elements in this case, triggering the microphase segregation and the formation of an LC smectic phase (Figure 3). The difference in isotropisation temperature between congeners **2d** and **2e** is rather small, and indicates that lattice stabilization through interaction between lipophilic cations and PF_6^- anions is stronger than the energetic gain conferred through chain length increase. For alkyl chains longer than 15 C atoms (amphiphiles **2f-2h**) another ordered liquid crystalline smectic phase can be observed also at high temperatures (see Figure 3 for thermal behavior of **2h**), whose stability increases from **2f** to **2h** with the increase of chain length, as revealed by the increase in enthalpy of the isotropisation transition from 0.2 Kcal/mol for **2f** to 5.6 Kcal/mol for **2h** (Figure 2c, Figure 3).



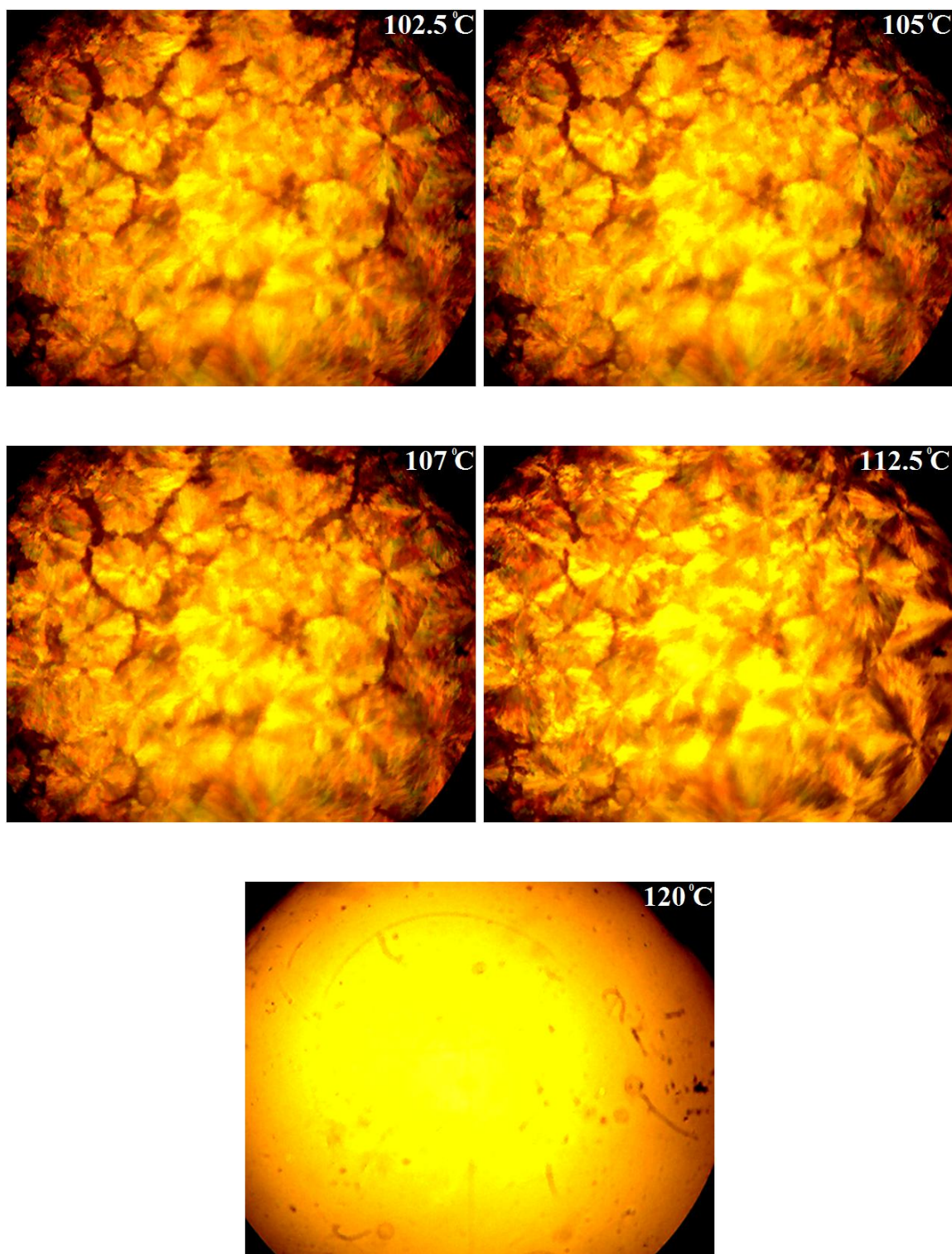


Figure 3. TOPM images of GS **2h** (C17 PF₆⁻) during the second heating cycle, emphasizing the extent of liquid crystalline phase ordering at different temperatures. One

may observe the broken fan texture characteristic to the smectic phase and the enhancement of internal ordering with the increase of temperature.

The above-mentioned self-assembly mechanism in bulk and the significant contribution of the counterions become evident when comparing the thermal behavior of hexafluorophosphates **2** with chlorides **3** (Figure 2, compare left and right panels) and the thermal behavior of the C16 representative with four different counterions: hexafluorophosphate (**2g**), bromide (**4g**), chloride (**3g**), and dihydrogenophosphate (**5g**) (Figure 5). Data from Figures 2 and 5 reveal the combined impact of counterion size, symmetry and lipophilicity on the thermotropic self-assembling of these novel pyridinium amphiphiles. Thus, the bulkiness of hexafluorophosphate anion and its different symmetry as compared with the pyridinium cation induces molecular disorder upon cooling the isotropic liquid, as mentioned above. The SAXS diffractogram of GS **2h** measured at 35 °C (Figure 2c and 5d) confirms the low level of structural order of the assembly post-cooling, revealing a broad diffraction peak corresponding to a d-spacing of about 35 Å. The corresponding TOPM texture (Figure 5e, left panel) also shows lack of ordering, with the exception of some nucleation points with broken fan texture, which indicate a smectic phase. Upon reheating, the highly lipophilic PF₆⁻ eventually repositions itself and its compatibility with the lipophilic alkyl-substituted pyridinium [88], in conjunction with the long alkyl chains, generates organized liquid crystalline smectic structures [90] (Figure 5e, right panel, and Figure 3). In these supramolecular LC phases individual GSs are probably associated in-layer with PF₆⁻ counterions that bridge the positively charged polar heads (Figure 5f) as recently observed in crystal structures of

pyridinium amphiphiles [88]. The d-spacing drops from about 35 Å at 35 °C to 27-28 Å upon increasing the temperature to 85 °C, reflects the combined ordering effect of PF₆⁻ anions and lipophilic chains (Table 1). A second smectic LC phase displaying an intermediate d-spacing value of 33.9 Å is observed at high temperature, before isotropisation (Figures 3, 4 and Tables 1 and 2). The stability of this high temperature LC phase increases with the increase of chain length from 0.16 Kcal/mol in **2f** to 5.6 Kcal/mol in **2h**). We assume that the ionic interactions between PF₆⁻ and pyridinium polar head were fully compensated while passing through the endothermic transition at 97.8 °C. The mobility of the counterions and polar heads increases and facilitates the generation of a highly ordered smectic phase observed before isotropisation, templated predominantly via hydrophobic chains.

Table 1: D-spacing values of thermotropic self-assemblies generated from selected gemini surfactants, as revealed through SAXS data at different temperatures

Compound	Thermal Cycle	Temperature (°C)	d-spacing (Å)*
2h (C17 PF ₆)	Sample as prepared	20	26.4
	1 st Heating	125	33.7
	1 st Cooling	-20	34.8
	2 nd Heating	35	34.8
		85	27.2
		105	33.9
3g (C16 Cl)	Sample as prepared	20	36.4, 29.5, 18.2
	1 st Heating	103	36.2
	1 st Cooling	-20	36.8
	2 nd Heating	32	38.1
		47	37.9
		62	37.6
77		37.0	
92		36.5	
107		36.0	
5g (C-16 H ₂ PO ₄)	Sample as prepared	20	46.5, 31.0, 27.1, 24.5
	1 st Heating	100	37.7, 35.3, 32.6
	1 st Cooling	100	38.2, 35.6, 33.0
		-20	50.5, 39.2, 33.5
	2 nd Heating	20	49.1, 39.4, 36.8, 34.0
		100	38.2, 35.8, 33.1

* the d spacing uncertainty in SAXS configuration is ± 0.1 Å

The WAXS experiments performed at the same temperatures as SAXS ones (Table 2) confirmed the position of diffraction peaks obtained by SAXS and allowed the observation of additional diffraction peaks generated by self-assemblies of **2h** and **3g** that correspond to smaller d-spacing values.

Table 2: D-spacing values of thermotropic self-assemblies generated from selected gemini surfactants, as revealed through WAXS data at different temperatures

Compound	Thermal Cycle	Temperature (°C)	D-spacing (Å)*
2h (C17 PF ₆)	Sample as prepared	20	26.4, 13.2, 8.8
	1st Heating	125	33.6
	1st Cooling	-20	35.1
	2nd Heating	35	34.2
		85	28.4, 20.5
		105	33.9
3g (C16 Cl)	Sample as prepared	20	37.1, 18.7, 12.3, 9.3
	1st Heating	103	36.1
	1st Cooling	32	36.1, 17.7, 11.8, 8.8
	2nd Heating	47	38.3
		62	37.4
		77	37.1
		92	36.1
		107	36.1

* the d spacing uncertainty in WAXS configuration is ± 0.5 Å

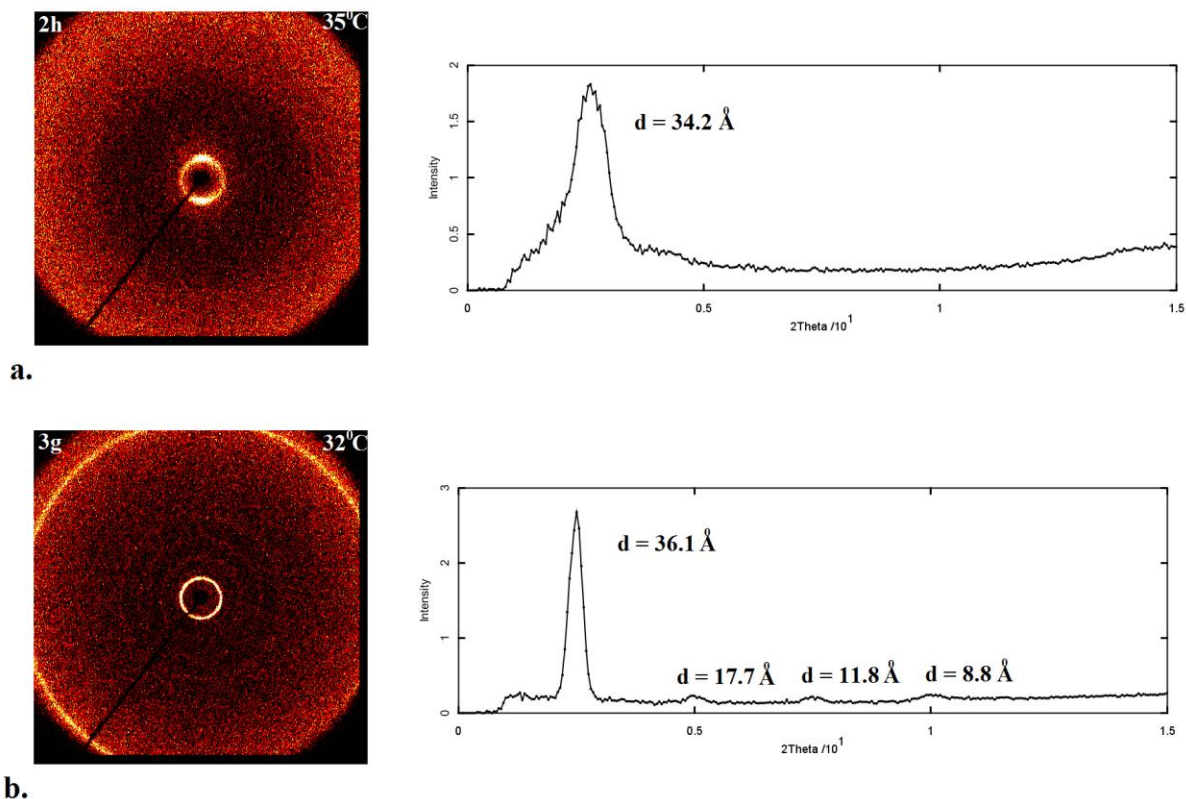


Figure 4. WAXS diffractograms of **2h** at 35 °C (a) and **3g** at 32 °C (b) after 1st cooling cycle, revealing the higher degree of internal order induced by the Cl⁻ counterion as compared with PF₆⁻.

While stepping from PF₆⁻ to Br⁻ and Cl⁻ the size of the counterion and its lipophilicity diminishes and templation of thermotropic smectic phases becomes more facile, due to the higher mobility of the counterion, greater polarity difference in between the polar core and hydrophobic chains and closer proximity of the hydrophobic tails that allows tighter packing. The bromide anion is sufficiently bulky and lipophilic to prevent the organization of individual molecules upon cooling, similar to PF₆⁻; however, its reduced lipophilicity as compared with PF₆⁻ prevents the templation of LC phases upon reheating, probably being unable to efficiently bridge the pyridinium polar heads in **4g**

(Figure 5a-c). The smaller, less lipophilic and therefore more mobile Cl^- allows facile formation of organized structures of GS **3**, upon cooling from isotropic phase, for chain lengths longer than 14 C atoms (Figure 2b, Figure 5; see also Table 2 and Figure 4 for a direct comparison of **2h** and **3g** supramolecular assemblies after 1st cooling through WAXS). The supercooling interval decreases with the increase in chain length, as expected. The lower impact of counterion on self-assembling properties and the increased impact of hydrophobic chains are clearly visible upon second heating cycle of lipids **3**. The SAXS diffractogram of GS **3g** at 35 °C (Figure 5d) reveals a sharper diffraction peak as in the case of hexafluorophosphate **2h**, proving improved self-assembling and a higher degree of order within the smectic LC phase. The d-spacing was 38.1 Å at 32 °C, slightly higher than for **2h**. At higher temperature the very long alkyl chains of **3g** and **3h** stabilize secondary smectic liquid crystalline phases, similarly to hexafluorophosphate congeners **2g** and **2h**. The d-spacing decreases monotonically from 38.1 Å to 36.0 Å upon heating, (Table 1). The isotropisation temperatures of chlorides **3** are superior to PF_6^- lipids **2**, reflecting a higher degree of order induced by the Cl^- counterion (Figure 2c).

The very polar and relatively bulky dihydrogenophosphate anion enhances the polarity of the pyridinium core and allows the fast formation of well-defined LC phases in **5g** upon cooling (Figure 5b). Dihydrogenophosphate is a soft anion, perfectly compatible with the soft pyridinium cation. The strength of this interaction is relevant for the formation of pyridinium GSs/DNA complexes (lipoplexes) in which the pyridinium polar head directly associates with the phosphate groups from the nucleic acid backbone. The SAXS diffractogram of GS **5g** at 20 °C (Figure 5d) reveals several strong diffraction

peaks characteristic of a crystalline lattice, corresponding to d-spacing values of 49.1 Å, 39.4 Å, 36.8 Å, 34.0 Å. The order is maintained at higher temperature as demonstrated by SAXS (Table 1). The thermal stability of the LC phase was the highest among all counterions, **5g** having an isotropisation temperature slightly higher than the isotropisation temperature of chloride **3g**. The enthalpy for the isotropisation process was smaller in **5g** as compared with **3g**, proving that both polarity and size of the counterion play important roles in formation and stability of LC phases in these GSs (Figure 5c).

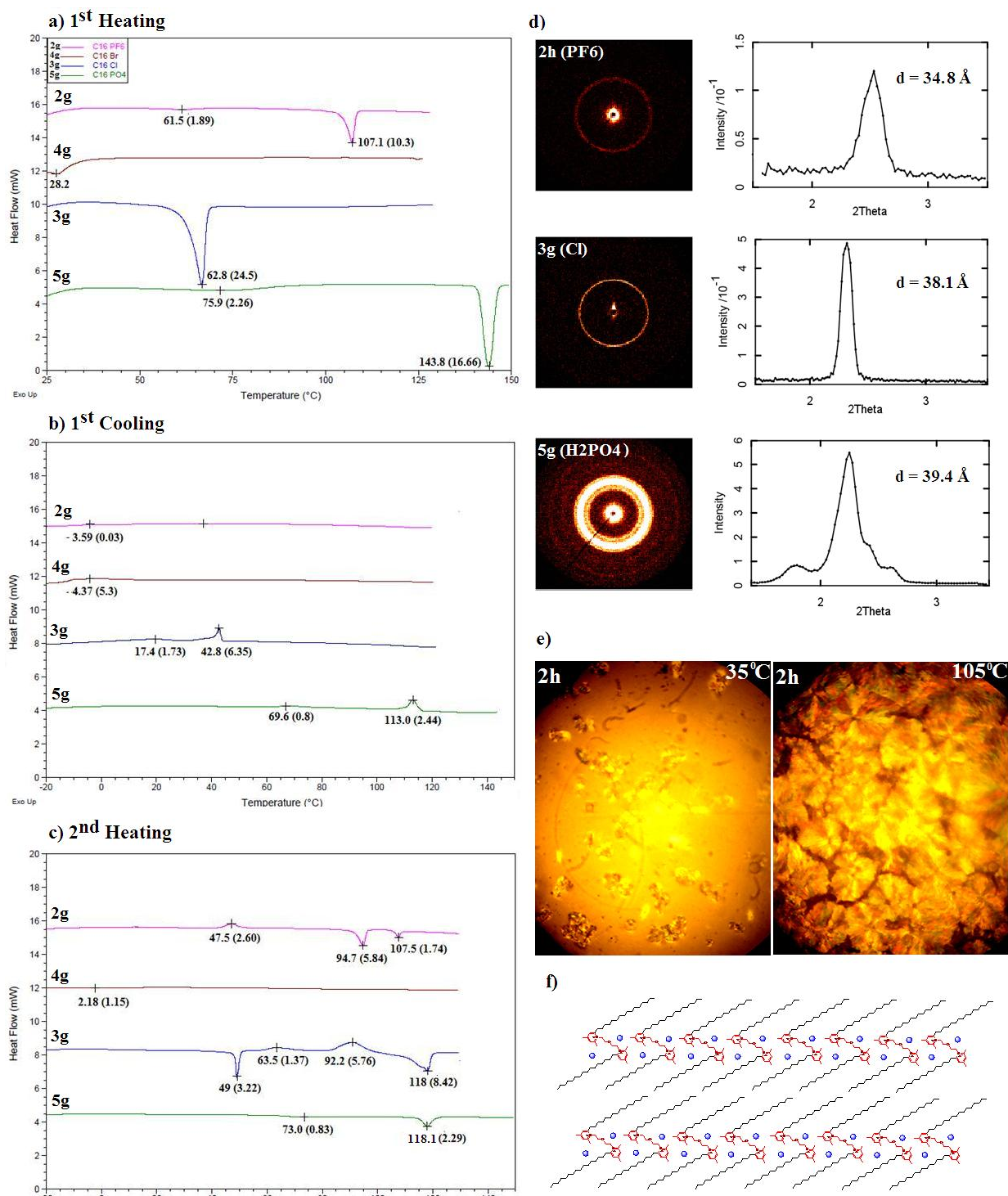


Figure 5. Counterion impact on thermotropic self-assembling of pyridinium gemini surfactants. DSC thermograms (5 °C/min) for the first heating (a), first cooling (b), and second heating (c) of C16 gemini surfactant as bis-hexafluorophosphate (**2g**, red traces),

bis-bromide (**4g**, brown traces), bis-chloride (**3g**, blue traces), and bis-dihydrogenophosphate (**5g**, green traces). Transition temperatures and enthalpies (Kcal/mol) are shown in each case. SAXS diffractograms (d) for **2h**, **3g**, and **5g** revealing the impact of counterion on the strength of self-assembling and the main d-spacing observed around room temperature. TOPM image of the smectic phases observed for **2h** at 35 and 105 °C, displaying the typical broken-fan texture (e), and proposed in-plane packing of pyridinium gemini surfactants (f).

When the amphiphiles are hydrated through repeated freeze-thaw cycles, water penetrates the supramolecular assemblies, hydrating all ionic species and the hydrophilic linker. The strong hydrophobic effect, which increases steeply with hydrophobic tail(s) elongation remodels the supramolecular assembly, folding the molecules and generating micellar aggregates. Thus, nanoDSC experiments performed on hydrated gemini surfactants of type **2-5** did not reveal any thermal transition, ruling out bilayer assemblies.

The decoupling of intra-bilayer interactions from inter-bilayer ones allows a better estimation of the impact of hydrophobic tail on the self-assembling of these novel lipids. Critical micelle concentration (CMC) for the gemini surfactants **3**, bearing chloride as a counterion decreases monotonically from 15.67 mM to 4.19 mM with the elongation of chain length from 10 to 17 C atoms, as expected (Figure 6). Interestingly, the conductivity increases after micellization, in contrast to single chain surfactants and

gemini surfactants with hydrophobic linkers (Figure 6) [43, 67]. We attribute this behavior to the shielding effect of the oxygen atom of the polar linker, which tends to place itself at the oil/water interface, buffering the electrostatic repulsions of the polar heads. Hence, shielding of positively-charged polar head repulsions with counterions is less needed and thus a greater mobility of the Cl^- counterions can be observed above CMC. The degree of counterion dissociation α decreases monotonically with the increase of chain length, similar to other simple and gemini surfactants, due to the increase of charge density of the micelle (Figure 6).

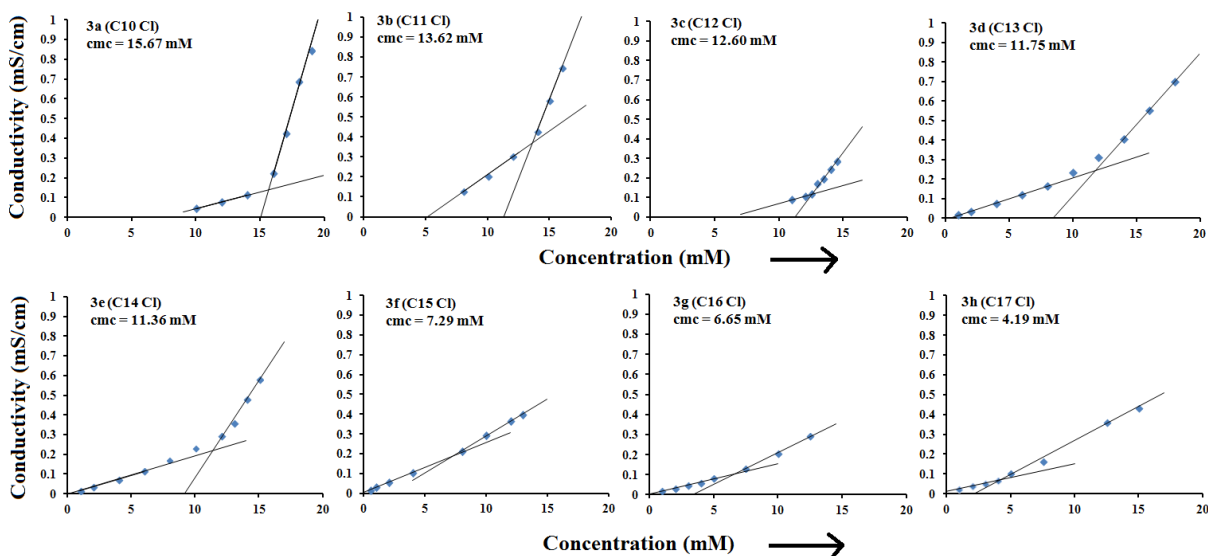


Figure 6. Self-assembling in solution of gemini surfactants **3a-h** bearing chloride as counterion, investigated via conductivity measurements. Critical aggregation concentration and the mobility of the counterions are decreasing monotonously with the increase in chain length.

The chain elongation within the series of gemini surfactants **3** has also a significant effect on the size and zeta potential of the supramolecular assemblies, as depicted in Figures 3a, 3c. Thus, the size of assemblies increases while passing from C10 representative **3a** to C17 congener **3h** due to the decrease of molecular curvature of the tapered molecules and increase in packing parameter, as expected. Gemini surfactants having an odd number of C atoms in their hydrophobic chains have generally smaller sizes than their even-numbered homologs, probably due to better packing in the corresponding supramolecular assemblies, already observed in their thermotropic assemblies (Figure 8a). Zeta potentials (Figure 8c) varied between 10 and 20 mV, slightly increasing with chain elongation due to increased localization of the Cl⁻ counterion in the Stern layer, as predicted by CMC graphs presented above.

Hexafluorophosphates congeners **2** displayed Krafft points over 60 °C, therefore their CMC was not determined. The elevated Krafft temperature of these surfactants is probably due to the very lipophilic PF₆⁻ counterions, which bridge the lipophilic pyridinium polar heads as in their thermotropic LC assemblies presented above and in recent X-ray crystal structure of a structurally related pyridinium amphiphile [88]. When lipophilicity of the counterion is reduced the Krafft temperature diminishes and solubility of the amphiphile increases substantially. Bromide **4g** has a Krafft temperature of 17.9 °C and a CMC of 5.46 mM (Figure 7), while chlorides **3** and hydrogenophosphate **5g** have Krafft temperatures below 0 °C and excellent water solubility.

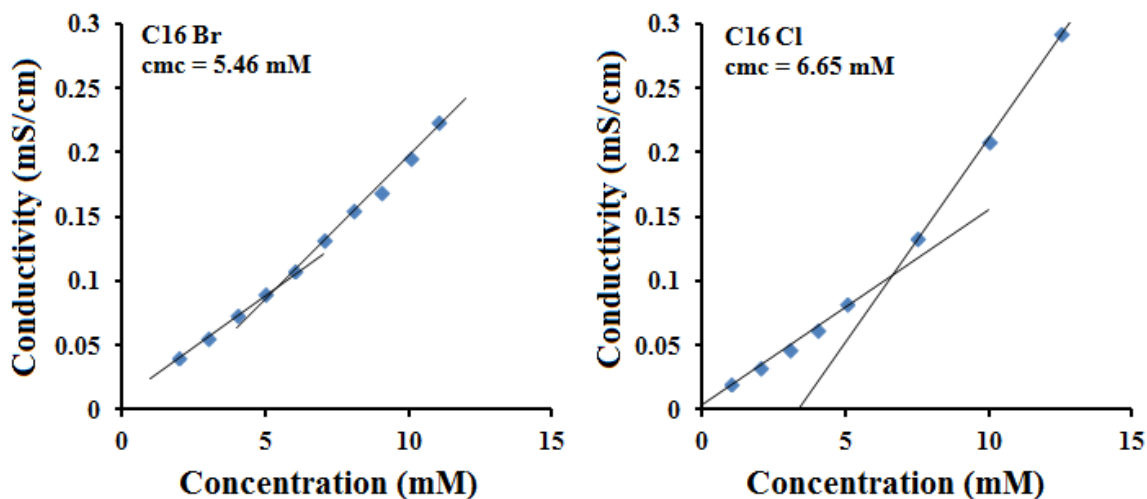


Figure 7. CMC graphs for C16 gemini surfactant bromide **4g** (a) and chloride **3g** (b). The lower conductivity slope above CMC observed for **4g** versus **3g** is due to increased lipophilicity of bromide, which has a higher tendency to localize in the Stern layer. The CMC of dihydrogenophosphate **5g** could not be determined due to very high conductivity of the counterion.

The counterion interaction with pyridinium polar head and its dependence on counterion lipophilicity can also be observed when evaluating the size and zeta potential of hydrated self-assemblies of C16 GSs **2g-5g** (Figure 8b, d). The strong association of very lipophilic PF_6^- counterion with pyridinium polar head in **2g** reduces the curvature of the assemblies, generating larger vesicles that display elevated zeta potentials as compared with chloride congener **3g**. Hexafluorophosphates **2** were difficult to formulate in water due to their high Krafft points. Only repeated freeze-thaw cycles on dilute (1

mg/mL) samples could achieve full hydration of these amphiphiles, and their supramolecular assemblies were unstable at low temperatures.

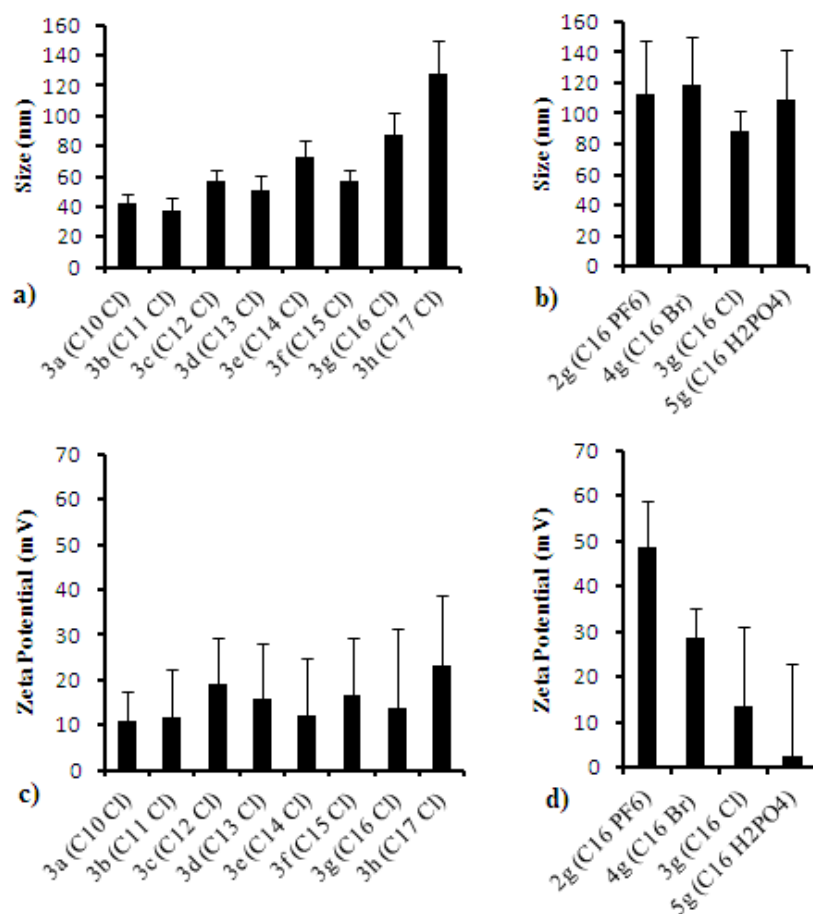


Figure 8: Impact of chain elongation and counterions on size (a, b) and zeta potential (c, d) of supramolecular assemblies generated from chloride gemini surfactants **3** (a, c) and congeners **2g-5g** having hexadecyl chains (b, d). It can be observed that chain elongation has a major impact on the size of the assemblies while counterions affect significantly the zeta potential of the supramolecular aggregates.

Stability increases with the decrease in counterion lipophilicity, generating more flexible assemblies. A slight decrease of aggregate size due to increase of curvature of the assemblies can be observed while passing from PF_6^- and Br^- to Cl^- ; bulkier hydrogenophosphate counterion increases the size of **5g** assemblies (Figure 8b). The zeta potential of the self-assemblies is significantly affected by the counterions, and it decreases monotonically from hexafluorophosphate **2g** to dihydrogenophosphate **5g**, mirroring the decrease in counterion lipophilicity. Hydrophilic counterions tend to reside more in the diffuse layer of counterions surrounding the supramolecular assembly, reducing the effective positive charge in the hydrodynamic shear boundary (Figure 8d).

The hydrated assemblies of gemini surfactants **3-5** were tested for their ability to condense DNA as a pre-requisite for acting as gene delivery systems, at 1/1, 2/1, 3/1, 4/1 and 8/1 +/- charge ratios. Unfortunately, the amphiphiles alone were not able to fully compact the DNA (data not shown). We attribute this behavior to the limited hydrophobic effect generated by these high charge/mass ratio amphiphiles, phenomenon observed also in their thermotropic behavior. In other words the self-assembly of the hydrophobic chain length is not strong enough to drive the compaction of the associated DNA. One simple solution to increase the charge/mass ratio is the addition of neutral co-lipids such as cholesterol or DOPE. The added co-lipids are increasing the hydrophobic effect and are helping the cationic species in DNA compaction (hence their denomination as “helper” lipids). The association between one molecule of gemini surfactant and one or more molecules of co-lipids also dilutes the positive charge of the cationic amphiphile and stabilize the resultant supra-molecular assemblies via reduction of electrostatic

charge repulsion between cationic gemini surfactant molecules. Moreover, DOPE was shown to facilitate endosomal escape of the lipoplex by promoting a fusogenic inverted hexagonal phase [91].

We have tested the physicochemical characteristics (size and zeta potential) for supramolecular assemblies generated from three chloride GSs with 10, 14, and 17 C atoms into the aliphatic tails **3a**, **3e**, **3h**, and cholesterol or DOPE, co-formulated at 1/1, 1/2, and 1/4 molar ratio cationic/neutral amphile (Figure 9). An examination of data from Figure 9a reveals that association of cationic amphiphile with co-lipids dramatically changed the packing parameter, shifting it towards formation of liposomes with different curvatures. The size and shape matching between amphiphilic components was essential, being influenced by the size of the individual molecules and on their molar ratio, as expected. Thus, the high curvature (low packing parameter) and smaller size of C10 representative **3a** made this gemini surfactant incompatible with cholesterol, generating unstable assemblies with a high fusion tendency at all molar ratios tested. Zwitterionic DOPE fared slightly better, with the 1/1 mixture having the smallest size and becoming larger and more unstable with the increase of colipid molar ratio. This general trend was observed also for formulations involving superior homologs **3e** and **3h** with both cholesterol and DOPE, although the stability of the mixed formulations increased considerably, probably due to better size matching. This is also the reason for the preference for DOPE vs cholesterol (at same molar ratio) of the C14 **3e**. The longest congener **3h** was compatible with both cholesterol and DOPE at 1/1 molar ratio, generating small and stable liposomes. Stability was excellent for **3h**/DOPE 1/2

liposomes, decreasing for **3h**/DOPE 1/4, **3h**/Chol 1/2, and **3h**/Chol 1/4, probably due to the lower curvature of DOPE as compared with cholesterol.

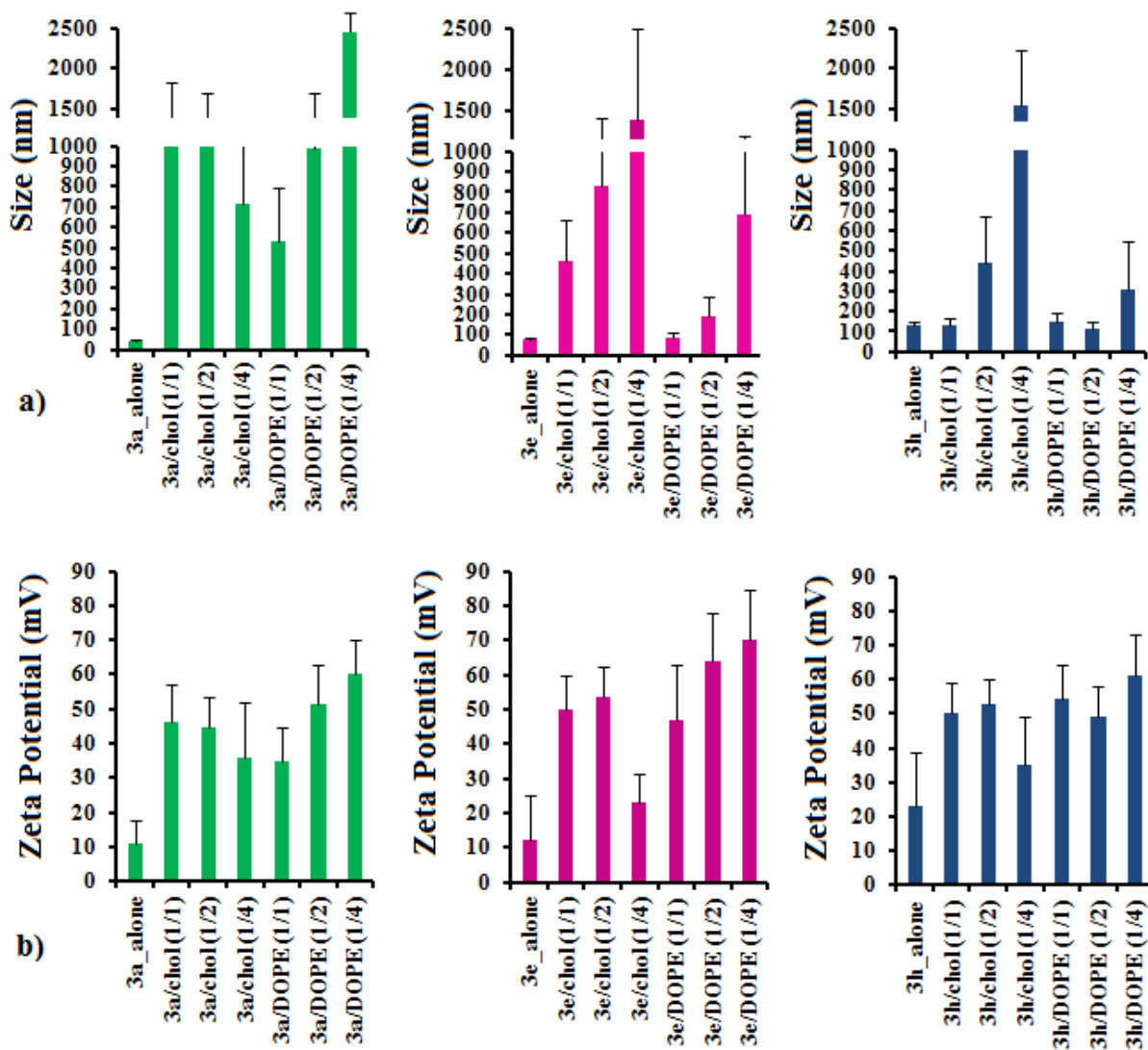


Figure 9. Size (a) and zeta potential (b) of supra-molecular assemblies generated from three cationic gemini surfactants with 10, 14, and 17 C atoms in hydrophobic tails **3a**, **3e**, **3h** and co-lipids cholesterol (chol) or DOPE at three molar ratios (1/1, 1/2, and 1/4 cationic/neutral species).

Zeta potentials (Figure 9b) were relatively homogeneous, with values around + 50 mV. The significantly higher values of the colipid mixture of geminis surfactants versus the pure cationic amphiles formulations reflect the stronger localization of the counterion in the Stern layer in colipid mixtures. For stable formulations zeta potential generally increased with the amount of co-lipid present in the formulation, thus reflecting the charge dilution and counterion localization in the close proximity of the cationic polar heads. Higher zeta potentials are benefic for interaction with DNA , lipoplex formation and stability.

We have subsequently tested the DNA compaction ability of above-mentioned gemini surfactant/colipid formulations, using only the **3e**-based formulations (**3e** is in the middle of the series in terms of chain length), generated at molar ratios of 1/1 and 1/2 charged/neutral amphiphile. The 1/4 molar ratio formulations were abandoned due to their reduced stability. The gWiz plasmid, encoding the firefly luciferase (from Aldevron) was used in all cases for reliable translation of results to future transfection experiments. The +/- charge ratios tested were 1/1, 2/1, 3/1, 4/1, 5/1 and 8/1, measuring the size and the zeta potential of the resulting lipoplexes in all DNA compaction experiments. Gel electrophoresis of lipoplexes was done in parallel in order to confirm DNA compaction (Figure 10).

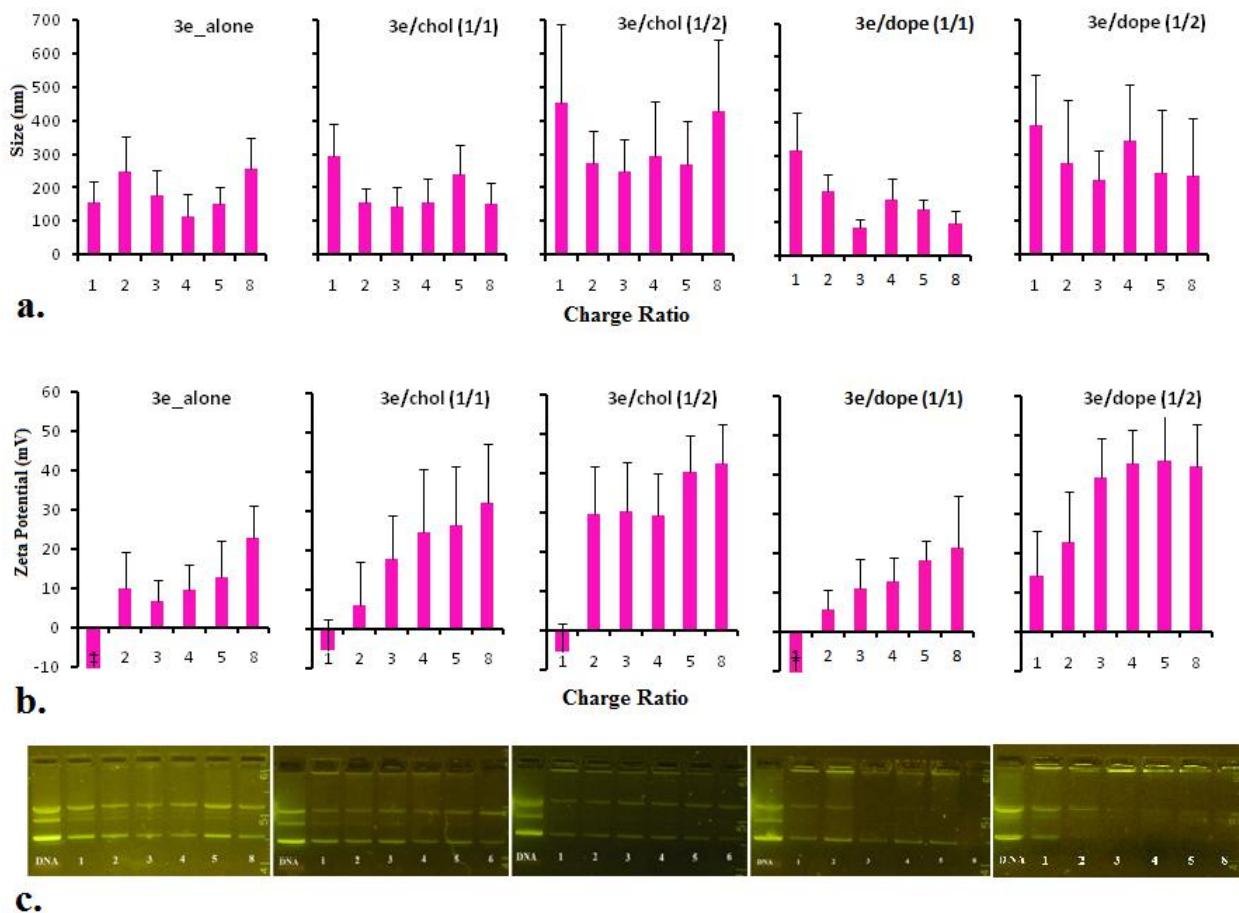


Figure 10. Size (a), zeta potential (b), and corresponding gel electrophoresis mobility (c) of lipoplexes generated from formulations based on gemini surfactant **3e**, either alone, or with cholesterol or DOPE at 1/1 and 1/2 molar ratios. Six +/- charge ratios were tested for each formulation.

Gel electrophoresis data from Figure 5c show that only DOPE-based formulations were able to efficiently compact the DNA plasmid, starting from a charge ratio +/- of 8 for formulation **3e**/DOPE (1/1) and, remarkably, from a charge ratio +/- of 3 for formulation **3e**/DOPE (1/2). The co-formulations with cholesterol, as well as the pure

gemini surfactant formulation could not efficiently compact the DNA at any charge ratio (Figure 10c), even if the negative charge of the DNA was efficiently neutralized, as revealed by the zeta potential variation (Figure 10b). For these three formulations the average size of the complex between the amphiphiles and DNA is not decreasing with the increase of charge ratio, while a significant decrease in size is visible in the case of formulations **3e**/DOPE (1/1) and **3e**/DOPE (1/2).

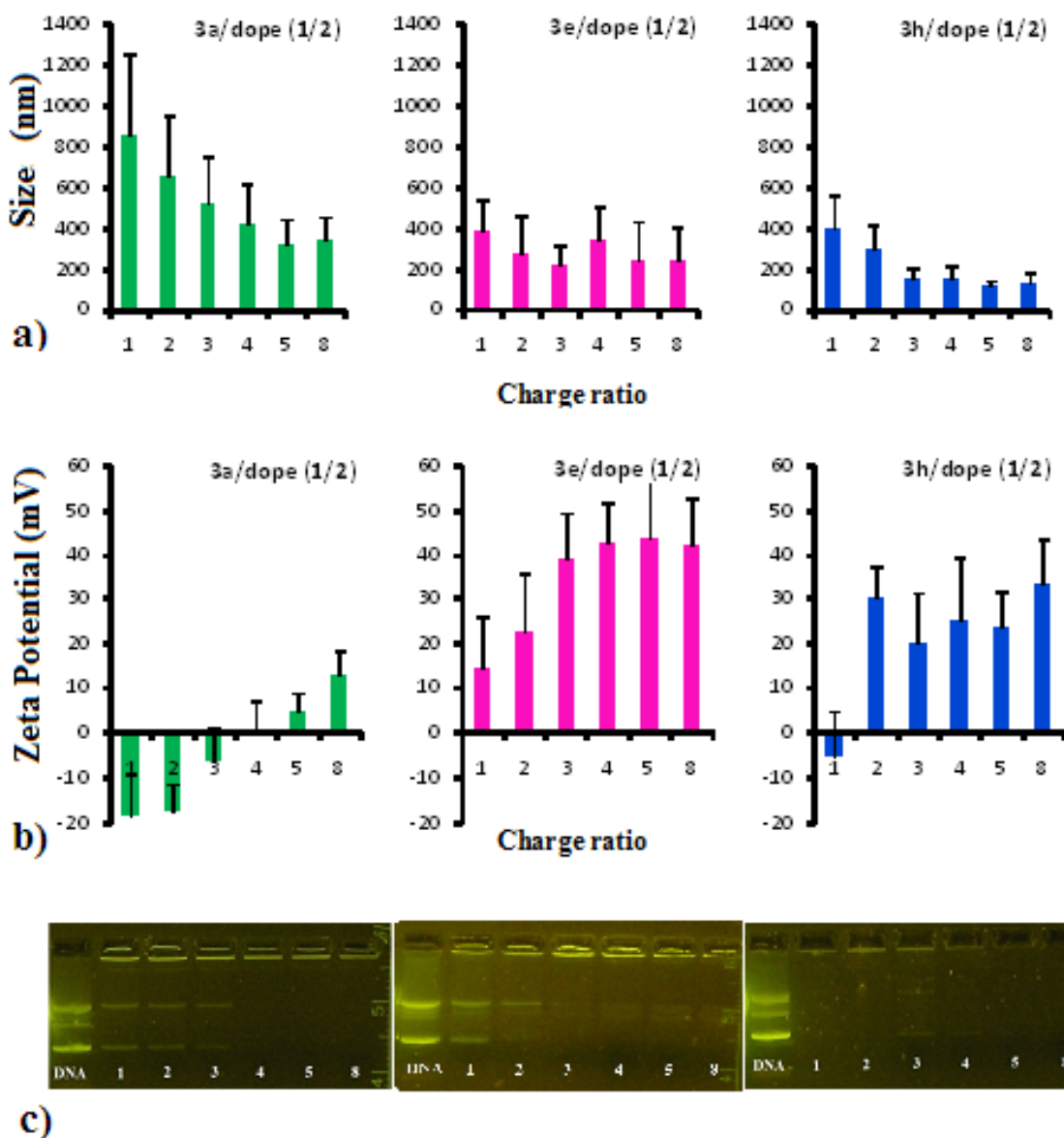


Figure 11. Validation of DNA compaction properties of liposomes containing GSs with different chain lengths. Size (a), zeta potential (b), and gel electrophoresis mobility (c) of lipoplexes generated from formulations based on GSs **3a**, **3e**, and **3h** in mixtures with DOPE at 1/2 molar ratio. Six +/- charge ratios were tested for each formulation.

Figure 10 reveals the importance of co-lipid and its molar ratio to GS for efficient compaction of functional DNA plasmids with this new cationic amphiphiles. Best results in terms of minimum charge ratio required for plasmid compaction and highest zeta potential of generated lipoplexes were obtained when **3e** was co-formulated with DOPE at 1/2 molar ratio. We have decided to validate these results on similar formulations based on its inferior and superior homologs - **3a**, and **3h**, respectively. Thus, similar DNA compaction experiments were performed on **3a**/DOPE 1/2 and **3h**/DOPE 1/2 (Figure 11). All three formulations were able to compact DNA at a charge ratio +/- around 3. The **3h**/DOPE (1/2) formulation was able to fully neutralize and condense the plasmid at a charge ratio +/- around 2. Size of the lipoplexes at same charge ratio is decreasing with the increase of chain length of the GS, revealing a better compaction of the genetic material by formulations based on GSs with longer chains. Zeta potentials of the lipoplexes at charge ratios over compaction threshold are increasing from 10-20 mV for **3a**/DOPE (1/2) to 30-40 mV for **3e**/DOPE (1/2) and **3h**/DOPE (1/2) (Figure 11).

Based on the proved ability of these liposomes to compact DNA plasmids at low charge ratios, we have extended this DOPE-based formulation to the whole series of GS chlorides **3**, as well as to the C16 representatives with other counterions **2g**, **4g**, and **5g**. The impact of chain length and counterion on the main physicochemical properties (size and zeta potential) of liposomes generated from pyridinium gemini surfactants and DOPE (1/2 molar ratio) is shown in Figure 12, together with the same parameters of their corresponding lipoplexes, generated at two cationic lipid/DNA +/- charge ratios (3/1 and 4/1).

Thus, it can be observed from the data of Figure 12 that DOPE has a levelling effect on the size of the vesicles generated from GSs **3**, with the majority of the liposomal formulations having sizes between 100 and 200 nm. This is probably due to DOPE negative curvature that efficiently compensates the positive curvature of GS molecules at the molar ratio used in the formulations. Size mismatch becomes significant for smallest homologs **3a** and **3b**, changing the packing parameter and enlarging the size of the liposomes generated from these GSs that also have the highest positive curvature within the series (Figure 12a). The levelling effect of DOPE cannot completely overcome the cohesive counterion effect, clearly visible for C16 GSs **2g-5g** based-formulations. The decrease in lipophilicity of the counterion while passing from **2g** to **4g**, **3g**, and **5g** induced a reduction of sizes of the corresponding liposomes from 300 nm to 150-200 nm (Figure 12b). However, the leveling effect of DOPE is clearly responsible for the relatively homogeneous zeta potentials (+ 50-60 mV) observed for all formulation, with the exception of very short GS **3a**, or of GS **2g** that has a highly lipophilic counterion (Figure 12c, 12d).

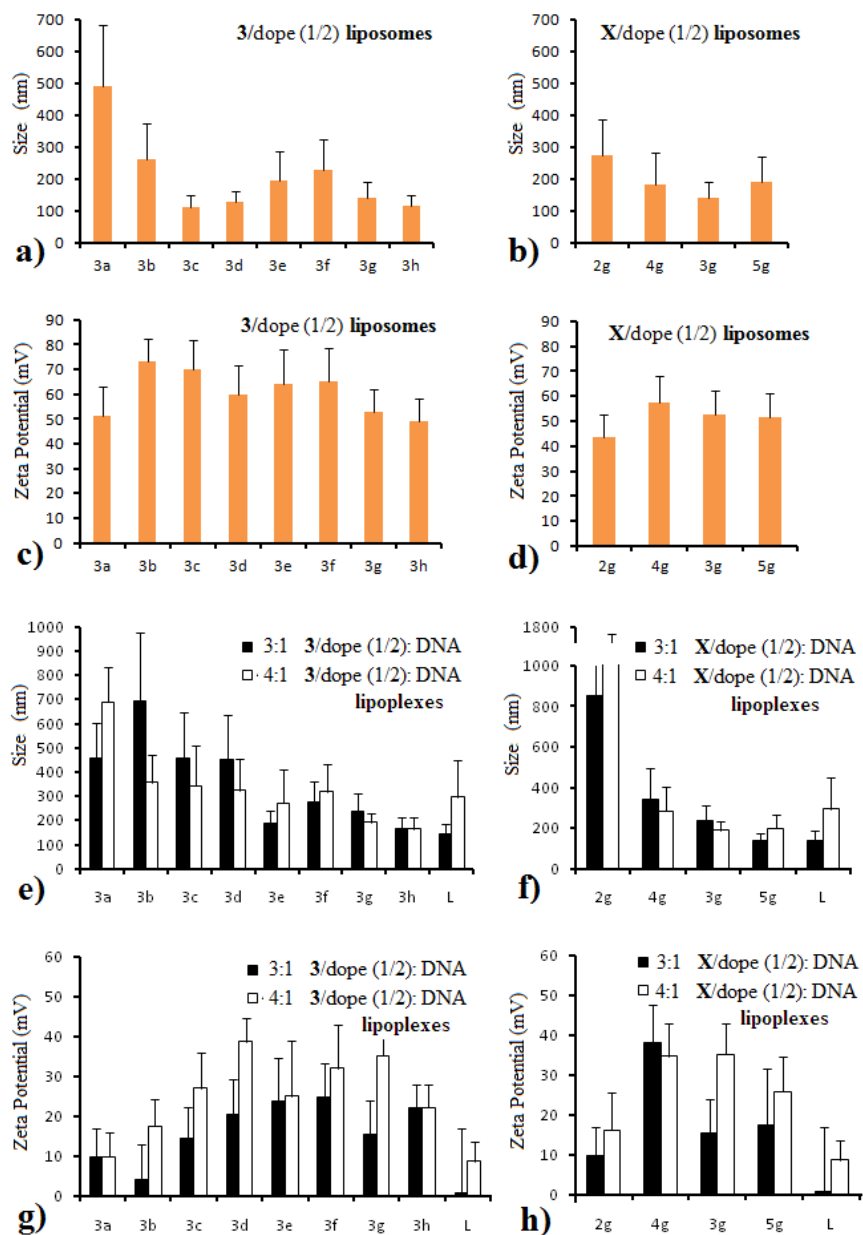


Figure 12. Size (a, b, e, f) and zeta potential (c, d, g, h) of liposomes (a-d) and corresponding DNA complexes (e-h) generated from GSs co-formulated with DOPE (1/2 molar ratio), revealing the impact of GS chain length (compounds **3a-3h**, panels a, c, e, g) and counterion (compounds **2g-5g**, panels b, d, f, h) on these physicochemical properties. For lipoplexes two +/- charge ratios were used, namely 3:1 (black bars) and 4:1 (white bars).

The ability of C16 GS **2g**, **4g** and **5g**, bearing PF_6^- , Br^- , or H_2PO_4^- counterions, to compact DNA when co-formulated with DOPE at 1/2 molar ratio was confirmed using the same methodology used for chlorides **3** (Figure 13). Lipoplex size at charge ratios above compaction decreased from 300-400 nm for lipophilic **2g** and **4g** to about 200 nm for **3g** and around 150 nm for hydrophilic representative **5g**. Zeta potentials increased with the decrease in lipophilicity of the counterion, as expected. A +/- charge ratio of at least 3 was needed in all cases (Figure 13). We have validated this ratio as the minimum DNA compaction ratio for all GS/DOPE (1/2) formulations (Figure 12e-h).

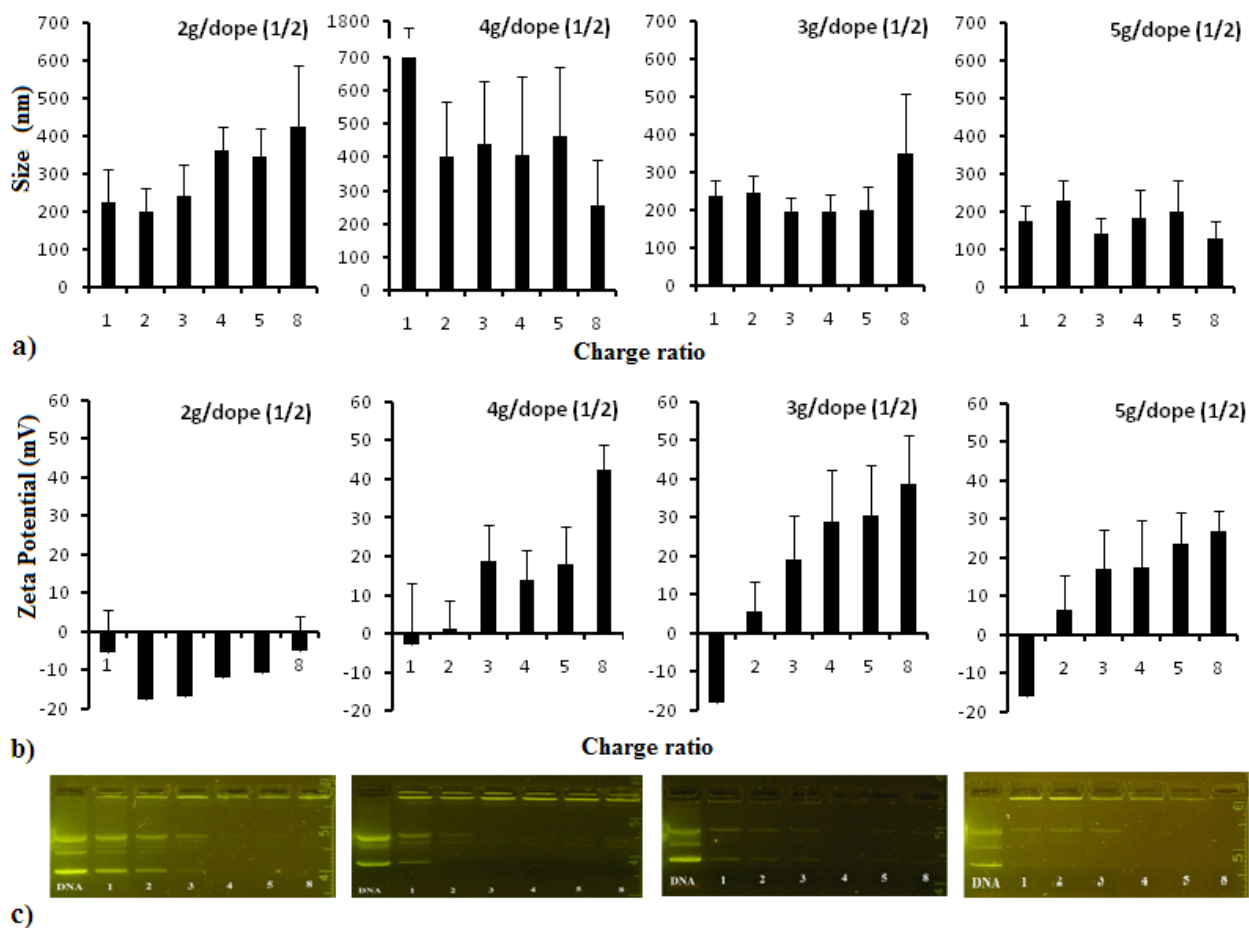


Figure 13. Size (a), zeta potential (b), and gel electrophoresis mobility (c) of lipoplexes generated from formulations based on C16 GSs **2g**, **4g**, **3g** and **5g** in mixtures with DOPE at 1/2 molar ratio. Six +/- charge ratios were tested for each formulation. Lipoplex size at charge ratios above compaction decreases with the decrease of lipophilicity of the counterion, while zeta potential increases.

Data from Figure 12 reveal that at a charge ratio +/- of 3 the sizes and zeta potentials of most lipoplexes were matching the similar parameters for which full DNA compaction was observed for individual formulations. Elevating the charge ratio to 4 further decreased the size and increased the zeta potential of lipoplexes (Figure 12e-h) but also elevated significantly the cytotoxicity of the liposomal formulations (data not shown).

Therefore the biological testings were performed at a +/- charge ratio of 3, which represents the best compromise between physicochemical parameters of lipoplexes and cytotoxicity, while still efficiently compacting the DNA plasmid. Notably, even at this lower ratio we were able to observe very small lipoplexes, in between 175-300 nm, suitable for in vivo DNA delivery [12]. The NCI-H23 lung cancer cell line was used to assess the transfection efficiency and associated cytotoxicity of all lipoplexes, using standard experimental conditions employing reduced-serum media (Optimem) [46, 77, 92]. Cells were pulse-transfected with lipoplexes for 90 min, then transfection systems were removed and cells were washed with PBS. After removal of PBS cells received standard (10 % serum) media and were incubated for 48 hours, after which they were lysed with Triton X and the content of their cytoplasm was assessed for luciferase content, normalizing the results for total protein content. Reduced-serum media (Optimem®) was used in all cases. A WST-1 cytotoxicity assay [76] was done in parallel using identical transfection parameters. The NCI-H23 cell line was selected to be used due to its sensitivity to pyridinium-based synthetic transfection systems [46, 77]. This good sensitivity, together with the high expression luciferase reporter gene used in all experiments, allows the observation of small differences in transfection efficiency and

cytotoxicity of the synthetic vectors and simplifies the evaluation process of the lipoplexes. Commercial transfection reagent Lipofectamine® was used in both experiments, as positive control reference. Results are presented in Figure 14.

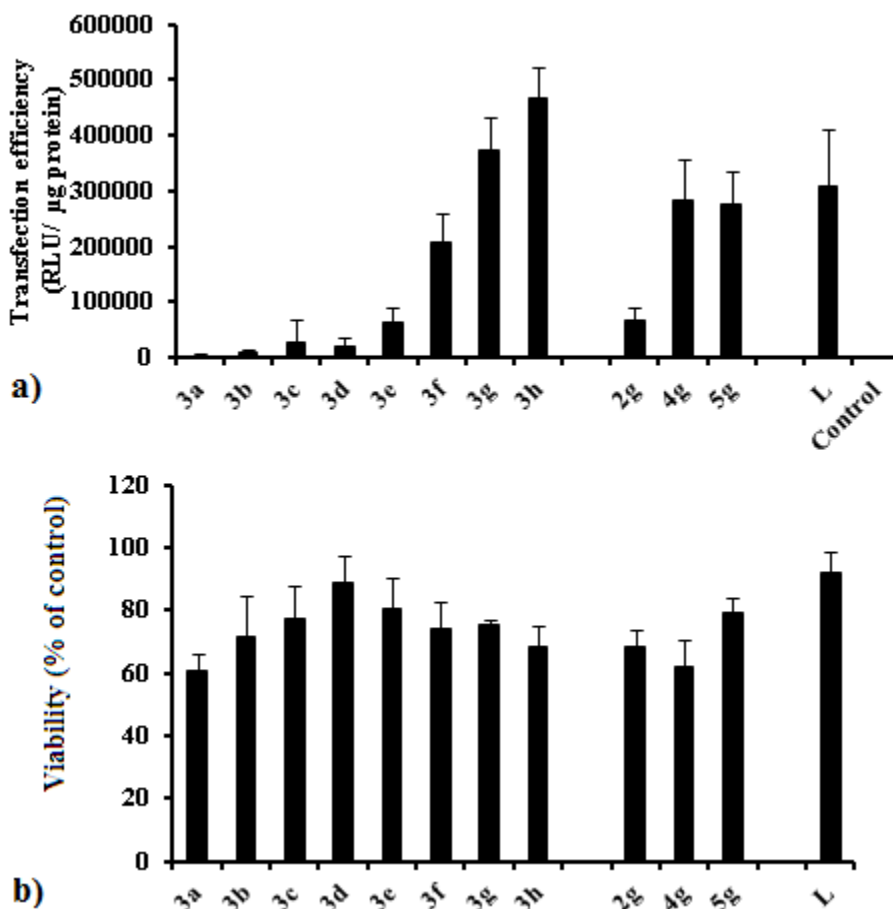


Figure 14. Transfection efficiency (a) and associated cytotoxicity (b) on NCI-H23 lung cancer cell line of lipoplexes generated from GSs co-formulated with DOPE (1/2 molar ratio) liposomes, revealing the impact of GS chain length (compounds **3a-3h**) and counterion (compounds **2g-5g**) on these biological properties. Standard transfection system Lipofectamine® was used as positive control. All lipoplexes were formed at a +/- charge ratio of 3.

Data from Figure 14 reveal a strong impact of chain length and counterion on biological properties of novel pyridinium synthetic transfection systems. Transfection efficiency increased exponentially with the increase in chain length of GS series, paralleling the decrease in size and the increase in robustness of the self-assemblies with the elongation of hydrophobic chains observed previously within chloride GS series **3** in bulk and in solution. The size match between the gemini surfactant and the DOPE helper lipid also played an essential role, with GSs **3h** (C17) and **3g** (C16) co-formulated with DOPE at 1/2 molar ratio being the most efficient formulations that surpassed Lipofectamine[®] commercial transfection system. The significant contribution of very long alkyl chains towards the self-assembling in bulk of pyridinium GSs **3g** and **3h** is translating into better transfection efficiency of the supramolecular lipoplexes generated by these GSs. The GS counterion had also a significant impact on transfection efficiency, as predicted. Chloride GS **3g** was net superior to hexafluorophosphate **2g**, and performed slightly better than bromide **4g** and dihydrogenophosphate **5g**. The superiority of chloride anion (borderline chaotropic/kosmotropic, with balanced lipophilicity) versus PF₆⁻ and Br⁻ (more chaotropic, very lipophilic) and on H₂PO₄⁻ (more kosmotropic, very hydrophilic) reveals that Cl⁻ balanced placement in between the Stern layer and the diffuse layer of anions is essential for good transfection efficiency since it can contribute to self-assembly robustness (through involvement into Stern layer) while being mobile enough to be efficiently released upon DNA compaction (Figure 14a). Notably, this behavior contrasts with physicochemical characteristics of the lipoplexes, where dihydrogenophosphate GS **5g** has generated smaller lipoplexes with slightly higher zeta potential than chloride GS **3g** (Figure 12f and 12h), thus revealing the impact of intrinsic

properties of the counterion on transfection properties of the supramolecular complexes. The dihydrogenophosphate GS **5g** displayed a slightly lower cytotoxicity, while hexafluorophosphate **2g** and especially bromide **4g**-based formulations were more cytotoxic. Within chloride GS series **3** the cytotoxic effect decreased monotonically while passing from C10 GS **3a** to C13 GS **3d**. Since the transfection efficiency was low for all these members, we can conclude that the high curvature of the cationic GS is responsible for the observed toxicity, similar to toxicity mechanism via membrane poration observed for simple surfactants [93]. For superior homologs of C13 the increase in cytotoxicity paralleled the increase in transfection efficiency, being probably related to the fact that these GSs are not degraded fast within cells. Future designs evolved from present ones and containing biodegradable groups (ester, amides, etc) will alleviate completely this problem.

An important delivery barrier against synthetic transfection systems in vivo is constituted by the presence of serum proteins and other factors, which can interact with lipoplexes and interfere with the transfection process [11, 22, 94]. These interactions are responsible for lipoplex premature inactivation in vivo and account in part for the in vitro-in vivo translational problems encountered by many groups. Therefore, we have decided to test the transfection efficiency of C16 and C17 GS **3g** and **3h**/DOPE (1/2 molar ratio) formulations, together with standard transfection system Lipofectamine[®], on NCI-H23 lung cancer cell line in regular cell media containing different serum concentrations. The percent of serum in the culture media was adjusted in between 0% and 40% to mimic the conditions encountered by lipoplexes during in vivo transfections (Figure 15).

Examination of data from Figure 15a reveals that transfection efficiency of all formulations diminishes monotonically when serum concentration is increased, as expected. However, one can observe big differences between formulations in their resistance to serum action. Thus, standard transfection system Lipofectamine®, although very efficient in the absence of serum, is inactivated rapidly by increased levels of serum in the transfection media, probably due to the instability of the lipoplex structure in the presence of serum proteins and other constitutive elements. In contrast, C16 and C17 GS **3g** and **3h**/DOPE (1/2 molar ratio) – based lipoplexes were much more robust and were able to transfect NCI-H23 lung cancer cell line with high efficiency even at relatively high serum concentrations (10% - 20%). The C17 GS **3h** constantly performed better than its inferior homolog **3g**, thus confirming previous findings (Figure 15a, Figure 14a).

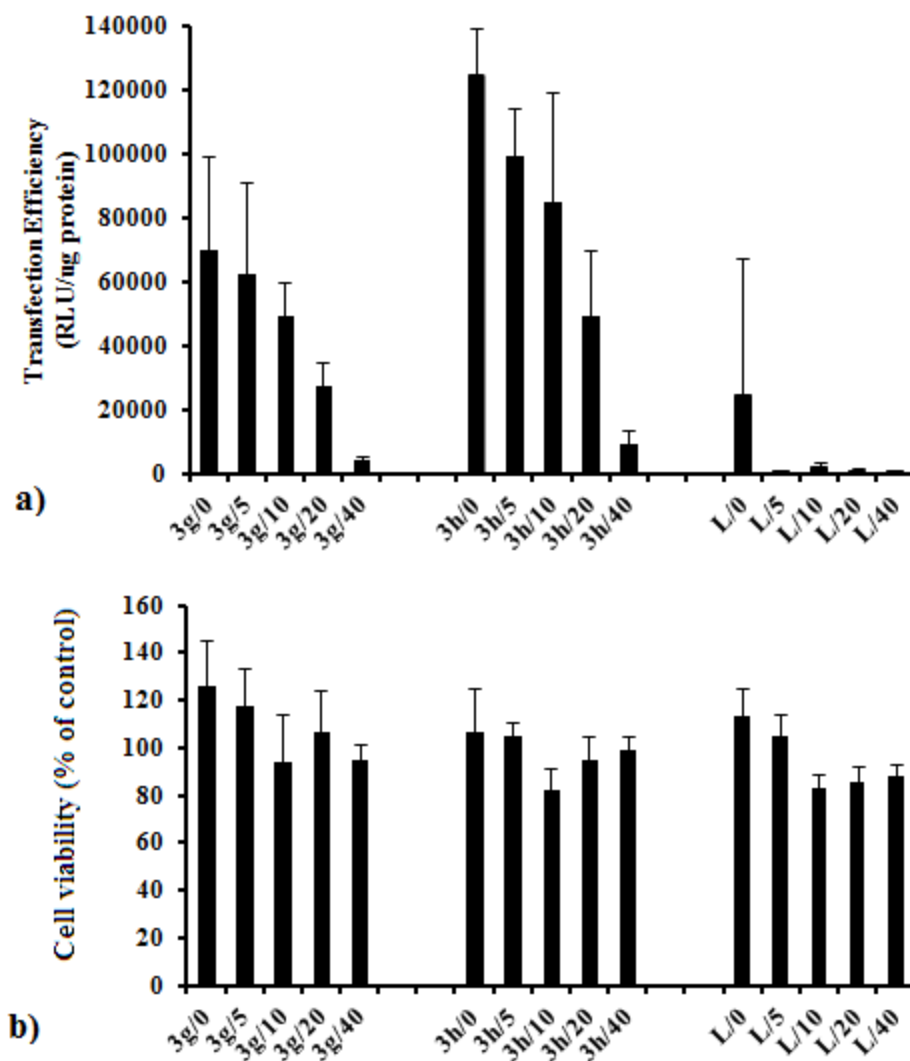


Figure 15. Transfection efficiency (a) and associated cytotoxicity (b) of lipoplexes generated from GSs **3g** and **3h** co-formulated with DOPE (1/2 molar ratio), on NCI-H23 lung cancer cell line, in standard media containing 0%, 5%, 10%, 20% and 40% serum. Standard transfection system Lipofectamine[®] was used as positive control. All lipoplexes were generated at a +/- charge ratio of 3.

Interestingly, in terms of cytotoxicity formulations based on GS **3g** and **3h** were found to be slightly less cytotoxic than Lipofectamine® in these novel conditions, confirming literature observations [89]. Cytotoxicity increased with the increase in serum concentration in all cases, probably due to lipoplex disassembling by serum protein (Figure 15b).

Conclusions

Efficient gene delivery systems based on small molecular weight amphiphiles (lipoplexes) have to overcome many internal and external delivery barriers, either general (e.g. interaction with proteins and other elements of serum, endosomal escape) or specific to the cells/tissues to be transfected[11]. These self-assembled systems have to maintain their structural integrity from the point of administration until they reach the target cells, where optimum charge density is needed for efficient internalization, endosomal escape and nucleic acid cargo release [63]. These antagonistic processes can be managed efficiently by using pyridinium amphiphiles, which possess a delocalized soft positive charge that can render an optimum binding/release profile for nucleic acid delivery [46, 51, 65, 77, 78, 95]. We have exploited the advantages of pyridinium polar head in a gemini surfactant design, which also offers besides a high charge density an optimum elastic modulus required for efficient endosomal lysis and DNA release in cytoplasm [44, 63]. A comprehensive optimization and fine tuning of the self-assembling process at the level of counterion, hydrophobic chain, added co-lipids, their nature and molar ratio, has generated efficient and robust self-assembled formulations with optimum charge density for efficient DNA delivery in conditions mimicking in vivo environment. Experiments are underway to fully assess these synthetic transfection systems for in vivo gene delivery, towards the goal to provide efficient and safe gene delivery systems for gene therapy in humans.

CHAPTER 3

MODULATION OF PYRIDINIUM CATIONIC LIPID-DNA COMPLEX PROPERTIES BY PYRIDINIUM GEMINI SURFACTANTS AND ITS IMPACT ON LIPOPLEX TRANSFECTION PROPERTIES

In this chapter, which is the continuation of chapter 2, our goal was to correlate the structural elements and the physicochemical properties of blends of pyridinium GS with pyridinium lipids and of their lipoplexes with transfection efficiency and cytotoxicity. The working hypothesis of this chapter is that the pyridinium cationic GS/lipid blends were expected to have a higher charge density than corresponding pure cationic lipid-based formulations, while displaying reduced cytotoxicity, thus synergistically combining the properties of the two classes of cationic amphiphiles.

Background and Rationale

Gene therapy has the potential to be a widespread cure for diseases caused by hereditary or acquired genetic defects, treating the source of the disease rather than its symptoms. It relies on the transfer and expression (transfection) of foreign genetic material into affected cells of a patient, either to correct a defective gene or to introduce a new function to the targeted cells. Within this new therapy, DNA, small interfering RNA (siRNA), and other nucleic acids are used as “drugs”, but even more important than the drug itself becomes its efficient and selective delivery to the target cells, and the side effects associated with the delivery process [12, 14, 96]. Thus, viruses are very efficient

gene delivery vectors but their use is associated with immunogenicity, mutagenicity and safety concerns that make their repeated administration problematic. A top-down approach is currently underway attempting to delete or replace the immunogenic structural elements [12]. In contrast, chemical methods relying on the use of self-assembled systems designed bottom up are safer and allow the delivery of DNA plasmids of practically unlimited size [18]. However, their efficiency is relatively low due to an incomplete adaptation of the structure of the synthetic delivery system to the transfection barriers in vitro and in vivo [11, 97].

Synthetic transfection systems rely on the use of cationic amphiphiles (surfactants [23, 25], gemini-[42, 47, 51, 98], trimeric- and oligomeric surfactants[46], lipids[29], dendrons, dendrimers and polymers[32]) with different sizes, shapes, and self-assembling properties. Small MW cationic amphiphiles cooperatively associate and compact nucleic acids through a major structural rearrangement process entropically-driven by the release of counterions and hydration water of both species. Safinya's group revealed the existence of lamellar (L_α^C)[99] and inverted hexagonal (H_{II}^C)[91] structures for the lipoplexes, with the later one being more transfection-efficient than the first one. The preferential formation of one of these structures depends on the overall packing parameter of the amphiphile (or mixture of amphiphiles) used to compact the DNA[53, 61, 62]. Since most of cationic lipids have packing parameters lower than 1, co-lipids with $P > 1$ such as DOPE or cholesterol (Chol, C) are blended with cationic lipids in order to induce an average packing parameter around 1 (and thus generate a lamellar structure for the lipoplex) or over 1 (when the inverted hexagonal structure is obtained, usually requiring a larger amount of colipid). The co-lipid also reduces the electrostatic

repulsions between adjacent cationic polar heads and ensures the robustness of the lipoplex through the strong hydrophobic effect that keeps the individual amphiphiles together. The ability of lipoplexes to resist the disruptive interaction with serum proteins and figurative elements of the blood is essential for the success of nucleic acid delivery via IV administration route. Once the target tissue is reached, the lipoplexes interact with the cells via multiple mechanisms (clathrin, caveolin, endocytosis/pinocytosis), being internalized and ending into internal vesicles of various structures and dynamics (clathrin coated pits, caveolae, endosomes). Once inside the cell, the supramolecular delivery system must be able to rupture the internal vesicle, disassemble fast and release its nucleic acid cargo into the cytoplasm, from where it can relocate to the nucleus and be internalized, transcribed and later translated into encoding proteins. For lipoplexes internalized via endocytosis/pinocytosis Safinya's group revealed that endosomal escape is favored by a high charge density of the lipoplex and a high elastic modulus of the lipoplex membrane-forming amphiphiles [63]. Other studies emphasized the importance of co-lipid used in liposome and lipoplex formulation, showing the stabilizing effect of cholesterol on the lipoplex transfection efficiency even at high cationic lipid/DNA charge ratios and in the presence of large amounts of serum [100, 101].

It is thus obvious that for efficient nucleic acid delivery the cationic lipid mixture must be able to accommodate both processes of DNA compaction and release. Cationic amphiphiles with a soft cationic charge are particularly suited for accommodating these antagonistic processes. They also display a reduced interaction with serum proteins which makes them well suited for in vivo use [102, 103]. The softer charge can be generated through the use of large positively charged atoms (e.g. phosphonium, arsonium instead of

ammonium [103-105]) or through the use of heterocyclic systems where the positive charge is delocalized on several atoms. Among the heterocyclic representatives the imidazolium [36] and pyridinium cationic lipids have proven their efficiency both in vitro and in vivo for the delivery of DNA and siRNA[25, 46, 64, 65, 77, 95]. Our team successfully generated pyridinium amphiphiles through the reaction of pyrylium salts with primary amines under Bayer-Piccard reaction conditions [46, 77, 78]. The procedure is versatile and allows the access to pyridinium lipids, surfactants, gemini surfactants, and oligomeric amphiphiles [46]. Extensive structure-activity relationship (SAR) studies conducted in recent years allowed us to identify efficient members within each class of above-mentioned pyridinium amphiphiles, such as lipids SPYRIT-7 [77] and gemini surfactants SPYRIT-35 and SPYRIT-68[25, 46, 106, 107] (Chart 2), together with their most efficient formulations.

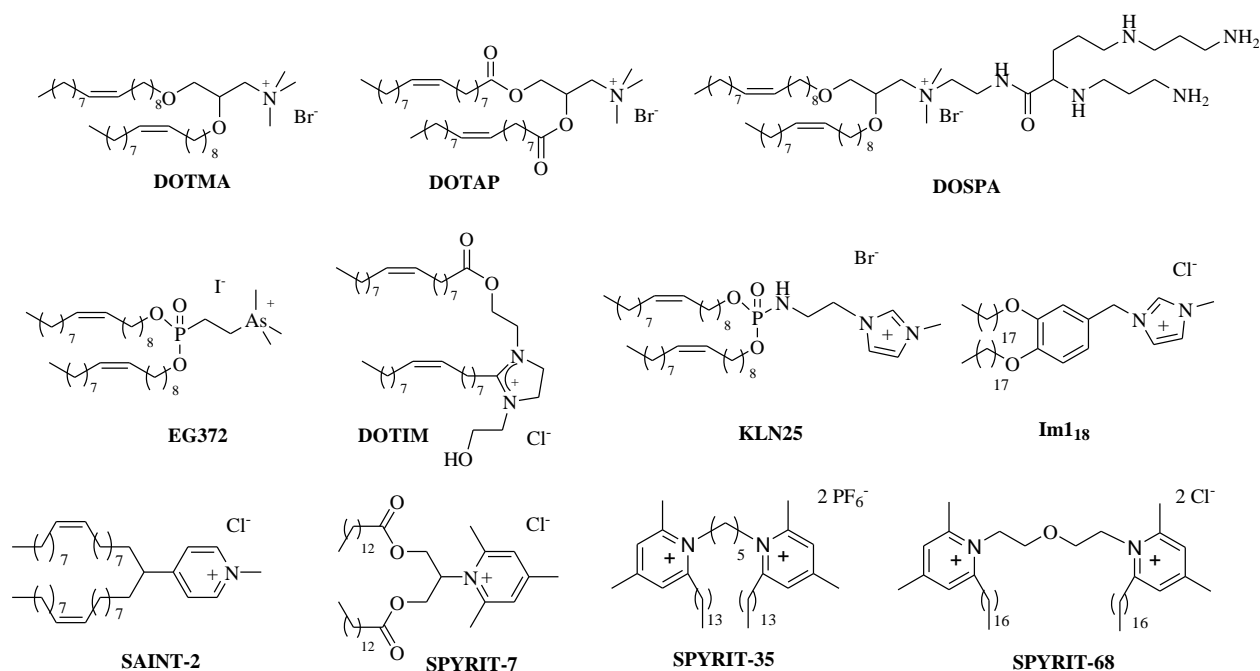


Chart 2. Representative cationic lipids used in synthetic gene delivery systems

Thus, cationic lipid SPYRIT-7 co-formulated with cholesterol at 1:1 molar ratio proved efficient in transfecting reported gene plasmids in several malignant cell lines while displaying negligible cytotoxicity[77]. An even better transfection profile was displayed by gemini surfactant SPYRIT-68, evolved throughout our synthetic program and SAR studies within this class of amphiphiles[107]. Importantly, lipoplexes based on SPYRIT-68/DOPE (1/2 molar ratio) formulation were able to retain their transfection efficiency even in the presence of elevated levels of serum in the transfection media, mimicking the in vivo conditions[107]. However, the cytotoxicity of these lipoplexes was higher, probably due to the efficient membrane destabilization properties of this class of amphiphiles, which is related with their higher charge/mass ratio, higher curvature and molecular flexibility and lower packing parameter as compared with their lipid congeners[51, 107]. Therefore we decided to investigate the use of gemini surfactant SPYRIT-68 in mixture with pyridinium lipid SPYRIT-7 seeking to combine the membrane-destabilization properties of the gemini surfactant, its high charge/mass ratio and its excellent transfection properties with the good transfection/cytotoxic profile of SPYRIT-7 based formulations. The cationic gemini surfactant/lipid blends were expected to have a higher charge density than corresponding pure cationic lipid-based formulations, while displaying reduced cytotoxicity, thus synergistically combining the properties of the two classes of cationic amphiphiles.

Materials and methods

Materials. The pyridinium cationic lipid SPYRIT-7, and the gemini surfactant SPYRIT-68 were synthesized and purified as previously reported [46, 77, 108]. Cholesterol, DOTAP, DOPE were from Avanti Polar Lipids (Alabaster, AL) and were used as received. Solvents (HPLC quality) were from Fisher Scientific (Pittsburgh, PA), EMD (Gibbstown, NJ), and VWR International (West Chester, PA). Chlorpromazine hydrochloride, genistein and EIPA were from Enzo Life Sciences (Farmingdale, NY). Tris Acetate EDTA (TAE) buffer, Lambda DNA/*Hind* III markers, Blue juice – Blue/Orange Loading dye were from Promega (Madison, WI). DNA plasmids - gWiz™ Luc plasmid encoding the firefly luciferase gene and gWiz™ GFP encoding the green fluorescent protein were from Aldevron (Fargo, ND). The GelStar Nucleic acid gel stain was from Lonza (Rockland, ME). Agarose (ultrapure) and Optimem media were from Invitrogen (Carlsbad, CA).

Methods

Preparation of hydrated lipid bilayers. Stock solutions (3 mM) of the cationic lipid SPYRIT-7 and of gemini surfactant SPYRIT-68 (0.3 mM) were prepared from powder in glass vials using CHCl₃/MeOH (2/1) as solvent (organic stock). For DOPE and cholesterol, solutions of the same concentration (3 mM) were made in CHCl₃/MeOH (2/1) as well. All solutions were swirled, purged with nitrogen, and capped securely; when not in use they were stored in the freezer at -20 °C.

Thirteen preparations were done, namely cationic lipid alone, cationic lipid mixed with cholesterol at 1:1 and 1:2 molar ratio, cationic lipid mixed with DOPE at 1:1 and 1:2 molar ratio, cationic lipid/gemini surfactant (95/2.5 molar ratio) with cholesterol at 1:1 and 1:2 molar ratio, and cationic lipid/gemini surfactant (95/2.5 molar ratio) with DOPE at 1:1 and 1:2 molar ratio, cationic lipid/gemini surfactant (90/5 molar ratio) with cholesterol at 1:1 and 1:2 molar ratio, and cationic lipid/gemini surfactant (90/5 molar ratio) with DOPE at 1:1 and 1:2 molar ratio. Thus 20 μ L of the SPYRIT-7 organic stock (3 mM) was transferred into a glass vial (total cationic lipid was 60 nmol). An amount of 20 or 40 μ L cholesterol or DOPE organic stock (3mM) was added to the vial for formulations containing colipids. In the case of gemini surfactant blends, 18 or 19 μ L of SPYRIT-7 cationic lipid organic stock (3 mM) were combined with either 10 or 5 μ L of SPYRIT-68 gemini surfactant organic stock (0.3 mM) and 20 or 40 μ L of cholesterol or DOPE (3 mM stock) respectively. Each sample was diluted with $\text{CHCl}_3/\text{MeOH}$ (2/1) to a final volume of 500 μ L. The organic solvent was evaporated to dryness in the SpeedVac for 1 h, and then the samples were further dried under vacuum in a dessicator for another hour. The dry lipid films were hydrated with 0.6 mL of deionised water yielding a 0.1 mM positive charge-containing suspension. The vials were purged with sterile nitrogen passed through a 0.22 μ m filter, sonicated at room temperature for 1 min, and then left overnight at room temperature to hydrate. The next day, each vial was freeze-thawed 10 times (-70°C/65°C).

Nano-differential scanning calorimetry. For the nanoDSC experiments the same protocol was followed except specified amounts of organic stock aliquoted out were

amplified 33.3X and the lipid films were hydrated with 1 mL deionized water. DSC measurements of the hydrates samples were obtained on a TA Instruments (New Castle, DE) NanoDSC-6300, between 5 and 95 °C, using a heating/cooling rate of 1 °C/min on 0.75 mL sample (working cell volume). No other transition temperatures except the ones represented in Figure 16 were observed. Experimental data was worked out using CpCalc software version 2.2 (Calorimetry Sciences Corp).

Liposome Preparation. The hydrated samples (0.1 mM total positive charge) prepared as described above were subsequently sonicated twice for 15 minutes at 65°C with a 15 minute pause between cycles yielding homogeneous liposomal formulations.

Liposome Characterization. A volume of 500 µL of each liposomal preparation was introduced into a disposable Malvern DTS 1060 measurement cell. The size and zeta potential of the liposomes were measured using a Zetasizer Nano (Malvern Instruments). The readings were all made at 25°C at normal resolution, using the instrument's automated feature. For the size measurements, the volume results were used in all cases, and the results were reported as the average of 10-20 runs. Zeta potentials were measured in millivolts (mV) and were the average of 10-20 runs.

Lipoplex preparation and characterization. Solutions of plasmid DNA (gWiz™ Luc plasmid, Aldevron, 6732 bp), and ladder Lambda DNA/*Hind* III (Promega), both 0.05 µg/µL, were prepared in sterile conditions, using nuclease-free water.

In six eppendorff tubes, 5 μ L of diluted DNA stock were treated with 8 μ L, 16 μ L, 24 μ L, 32 μ L, 40 μ L, and 64 μ L of diluted liposomal preparation (lipid/DNA ratios of 1/1, 2/1, 3/1, 4/1, 5/1, and 8/1). The vials were tapped gently for 1 min to ensure proper mixing, and then allowed to rest at room temperature for 30 min for proper lipoplex compaction. The volume of all lipoplex suspensions was adjusted with nuclease-free water to 150 μ L. This lipoplex stock solution was used for both gel electrophoresis and size/zeta potential measurements.

Gel electrophoresis of lipoplexes. In the gel electrophoresis experiment an amount of 15 μ L of each lipoplex formulation was aliquoted out in small eppendorf vials and each vial subsequently received 3 μ L of Blue/Orange Loading dye (Promega). A DNA standard was made by mixing 2 μ L of diluted DNA stock with 13 μ L nuclease free water and 3 μ L of Blue/Orange Loading dye. The same procedure was used to make a ladder reference standard using the Lambda DNA/*Hind* III marker. The final volume in all vials was 18 μ L. The lipoplex/dye mixtures were loaded into a 1% Agarose gel in 1X TAE buffer, pre-stained with GelStar® (Lonza) nucleic acid stain (10 μ L in 50 mL gel suspension). Gel electrophoresis was carried out at 75 mV for 75 min. DNA bands were visualized with a Mighty Bright transilluminator (Hoefer), and the gel was photographed with an Olympus C-5060 digital camera.

Lipoplex characterization. The remaining 135 μ L from each lipoplex preparation was diluted to a final volume of 600 μ L with nuclease-free water and transferred into a disposable Malvern DTS 1060 measurement cell. The size and zeta potential of the lipoplexes were measured using a Zetasizer Nano (Malvern Instruments) at 25°C at normal resolution. Volume results were used for size data, and results were reported as

the average of 10-20 runs. Zeta potentials were measured in millivolts (mV) and the average was taken of 10-20 runs.

General procedure for transfection and cytotoxicity experiments

Preparation of lipoplexes. In a typical experiment, for each cationic liposomal formulation to be tested an amount of 3 μL of a 0.5 mg/mL gWiz™ Luc plasmid DNA solution was aliquoted out in a sterile eppendorf tubes and was diluted with 13 μL nuclease-free water. The diluted DNA was then treated with 144 μL of the liposomal formulation (0.1 mM total cationic charge), prepared as indicated above. The vials were tapped gently to ensure proper mixing, and then allowed to rest at room temperature for 30 min for complete lipoplex compaction. This lipoplex stock solution was used for transfection, cytotoxicity, size, and zeta potential measurements.

Transfection and viability experiments. From the lipoplex stock solution, an amount of 135 μL was aliquoted out for each cationic lipid formulation to be tested, and was diluted with 765 μL Optimem (GibcoBRL).

The lipoplexes were tested for their ability to transfect NCI-H23 cancer cell lines. The cells were maintained in 10% fetal bovine serum (FBS) enriched medium at 37 °C in a humidified atmosphere of 95% air/5% CO₂. The media RPMI 1640 (CellGro, Houston, TX) was used for NCI-H23. Twenty-four hours prior to transfection, cells were transferred to 96-well microtiter plates (Cellstar 655180, Greiner Bio-One) at a density of 20,000 cells/well. Each well received 100 μL of appropriate medium, and the plate was

incubated in the same conditions as above. All experiments were done in quadruplicate. Two plates were made for each experiment: one for transfection and one for cytotoxicity. The error bars in figures represent one standard deviation from the average value.

Immediately before transfection the medium was removed and the cells from each well were briefly washed with 200 μ L sterile PBS. After removal of the PBS solution each well received 100 μ L of lipoplex stock solution, and the plates were returned to the incubator. After 90 min incubation time with cells the lipoplex suspension was removed, cells were washed with sterile PBS and then each well received 200 μ L of medium. Cell plates were incubated for further 48 hours, after which the transfection efficacy was determined using the first cell plate and the associated cytotoxicity was assessed using the second cell plate, transfected in similar conditions as the first one.

Transfection efficiency: luciferase and protein content assay. Forty-eight hours after transfection, the medium was aspirated and the wells were washed briefly with 200 μ L PBS. After removal of PBS the cells were lysed by adding 100 μ L 1X reporter lysis buffer (Promega) to each well and incubating the plate at 37 °C for 15 minutes. The cell lysate was collected and used for luciferase and protein assays.

For the luciferase assay, 20 μ L of cell lysate was transferred to a test tube and assessed directly by means of BD Monolight 3010 luminometer (BD Biosciences, San Jose, CA) using a luciferase assay kit (E4030) from Promega.

The protein content was quantified using a bicinchoninic acid (BCA) assay (Thermo Scientific, Rockford, IL). The BCA assay was prepared as specified in its manufacturer's instructions; 40 μ L of cell lysate were treated with 1 mL of BCA reagent

in an acryl cuvette and the solution was incubated for 1 hour at 37 °C. The light absorption of the solution was then read at 562 nm by means of a Hach DR/4000U UV-VIS Spectrometer (Loveland, CO), and the protein content was estimated by comparison to bovine serum albumin standards. The luciferase activity was normalized by the protein content and expressed as relative luminescence units/μg of protein (RLU/μg protein).

Viability assay. In order to quantify the relative cytotoxicity of the non-viral cationic vectors, a WST-1 standard viability method[76] was performed along with the luciferase and BCA assays. Forty-eight hours post-transfection, 20 μL of WST-1 tetrazolium dye solution (Roche, Mannheim, Germany) was added to each well (still containing 200 μL of medium). A blank was prepared by mixing 200 μL of medium and 20 μL of tetrazolium dye solution, and the plate was incubated at 37 °C in the CO₂ incubator. After 3 hours the colorimetric measurement was performed at 450 nm (with a reference wavelength of 650 nm that was subtracted) by means of a SpectramaxM2 microplate reader (Molecular Devices, Sunnyvale, CA). The value corresponding to the blank was deducted from the value corresponding to each well. Viability was expressed as percentage of the control, represented by cells that underwent the same treatments but did not receive any cationic lipoplexes.

Lipoplex characterization. The remaining 25 μL from each lipoplex preparation was diluted to a final volume of 500 μL with nuclease-free water and transferred into a disposable Malvern DTS 1060 measurement cell. The size and zeta potential of the lipoplexes were measured using a Zetasizer Nano (Malvern Instruments) at 25°C at normal resolution. Volume results were used for size data, and results were reported as the average of 10-20 runs. Zeta potentials were measured in millivolts (mV).

3D Transfection

NCI-H23 lung cancer, HT29 and HCT116 colon cancer cell lines were grown in RPMI-1640 media supplemented with 10% FBS in A-U96 Lipidure® plates (NOF, Tokyo, Japan) starting with a density of 1000 cells/200 μ L. Spheroid formation was observed in about two-three days, and their growth was followed and imaged. After eighteen days each spheroid (about 0.7 mm in diameter and containing about 40000 cells) was transfected by directly adding 14 μ L lipoplex suspension prepared in the same way as described above in the well. The transfection media contained the same amount of DNA as in the monolayer transfection experiment presented above (0.14 μ g/well). Two plasmids, gWizLuc and gWizGFP were used in parallel experiments. After 3 days each spheroid was transferred into an eppendorf tube, washed with PBS and imaged for GFP expression via confocal fluorescence microscopy or lysed with reporter lysis buffer 1X overnight and assessed for luciferase content, as described above. In the case of GFP measurements the washed spheroids were placed on a coverslip and GFP expression was visualized by laser scanning confocal microscopy using a Carl Zeiss 710 two-photon confocal microscope equipped with a W Plan-Apochromat 10X air objective, using 0.9X digital zoom, with excitation at 488 nm. 3D transfection images were generated by z-stacking individual 2D images using Zen 2010 Software as previously described[109, 110].

Cell internalization experiment

Twenty-four hours prior to transfection, NCI-H23 cells were transferred to 96-well microtiter plates (Cellstar 655180, Greiner Bio-One) at a density of 20,000 cells/well. Each well received 100 μ L of RPMI-1640 containing 10% FBS, and the plate was incubated overnight in the same conditions as above. All experiments were done in quadruplicate. The next day the media was removed and cells were washed with warm PBS. After PBS removal each well received 100 μ L stock solution of either chlorpromazine hydrochloride (10 μ g/mL)[111, 112], genistein (200 μ M)[111, 113] or EIPA 100 μ M[114, 115] in serum free culture media for 1 hour at 37 °C. Subsequently, 100 μ L lipoplexes were added and typical transfection procedure was conducted as described above. The transfection values obtained in the presence of cell internalization inhibitors were divided by the transfection values obtained in the absence of inhibitors (control experiment) and reported as percentage of these control values.

In a parallel experiment, NCI-H23 cells were cultured as presented above and then trypsinized, and the cell suspension was centrifuged at 1000 rpm for 3 min; the supernatant was discarded, and cells were resuspended in Optimem at a concentration of 5×10^6 viable cells/mL. A volume of 0.8 mL cell suspension was mixed with 50 μ g of plasmid DNA encoding the GFP-tagged Rab7 protein (Addgene, Cambridge MA) and was transferred into a 4-mm gap electroporation cuvette. Cells were subsequently electroporated using a Gene Pulser II electroporator (BioRad) at 350 V, 960 microfarads, and infinite resistance. The transfected cells were allowed to recover for 3 h in Optimem, after which the cell suspension was diluted with RPMI-1640 media containing 10% FBS, and the cells were counted and transferred onto 12 mm glass coverslips in a 24 well plate

at a density of about 105 cells/well. After 48 h of incubation time (37 °C, 5% CO₂), a confluence degree of about 40–60% was obtained ($\sim 2 \times 10^5$ cells/well). Media was removed, and cells were washed with PBS and subsequently incubated with 0.5 mL of lipoplexes in Optimem generated as described above (see transfection and cytotoxicity experiments). After 90 min of incubation time with cells, the lipoplex suspension was removed, cells were washed, fixed with 4% formaldehyde in PBS, washed again with PBS, and imaged for Rab7-GFP using a Carl Zeiss 510 Meta confocal microscope (Zeiss) with a 40× oil objective using an excitation wavelength of 488 nm. Images were analyzed using Zen 2010 (Zeiss).

Statistical analysis. Statistical comparisons were performed by analysis of variance (ANOVA) using GraphPad Prism 6, where $*P < 0.05$, $**P < 0.01$, $***P < 0.001$ and $****P < 0.0001$ unless specified otherwise.

Results and Discussion

The pyridinium cationic lipid SPYRIT-7, subsequently referred to as “cationic lipid” or “lipid”, and the gemini surfactant SPYRIT-68, subsequently referred to as “gemini surfactant, GS” were synthesized and purified as previously reported[77, 107].

The cationic lipid or its blends with colipids DOPE or cholesterol at 1:1 and 1:2 lipid/colipid molar ratio were hydrated with deionized water through repeated freeze/thaw cycles and subjected to nanoDSC analysis in order to determine the gel/liquid crystalline transition temperature of the pure lipid and the impact of colipid nature and amount on this transition. Similar blends in which 5% of the cationic charge brought by SPYRIT-7 was replaced with the equivalent amount of GS SPYRIT-68 were prepared in parallel and subjected to nanoDSC analysis in order to assess the effect of GS blending on bilayer fluidity. Results are presented in Figure 16.

As one may observe in Figure 16, lipid SPYRIT-7 in hydrated form has a transition temperature around 30 °C. The transition temperature of GS SPYRIT-68 was below 0 °C (data not shown). Addition of either DOPE or cholesterol colipids to SPYRIT-7 bilayers lowers substantially the transition temperature of the resulted lipid mixture with simultaneous broadening of the thermal transition peak, as expected[116-118]. The effect is proportional with the amount of colipid used. On the other hand, replacing 5% of the positive charge brought by the cationic lipid in the cationic bilayer with the same amount of charge of the corresponding amount of GS completely wipes out the remaining (broad) thermal transition of the SPYRIT-7/colipid supramolecular assemblies. Thus, blending of GS has an additional leveling effect on the gel/liquid

crystalline thermal transition of the lipid mixture, acting synergistically with the colipid towards fluidizing (laterally) the cationic bilayer. All ternary amphiphile mixtures are perfectly fluid over a wide range of temperatures (Figure 16).

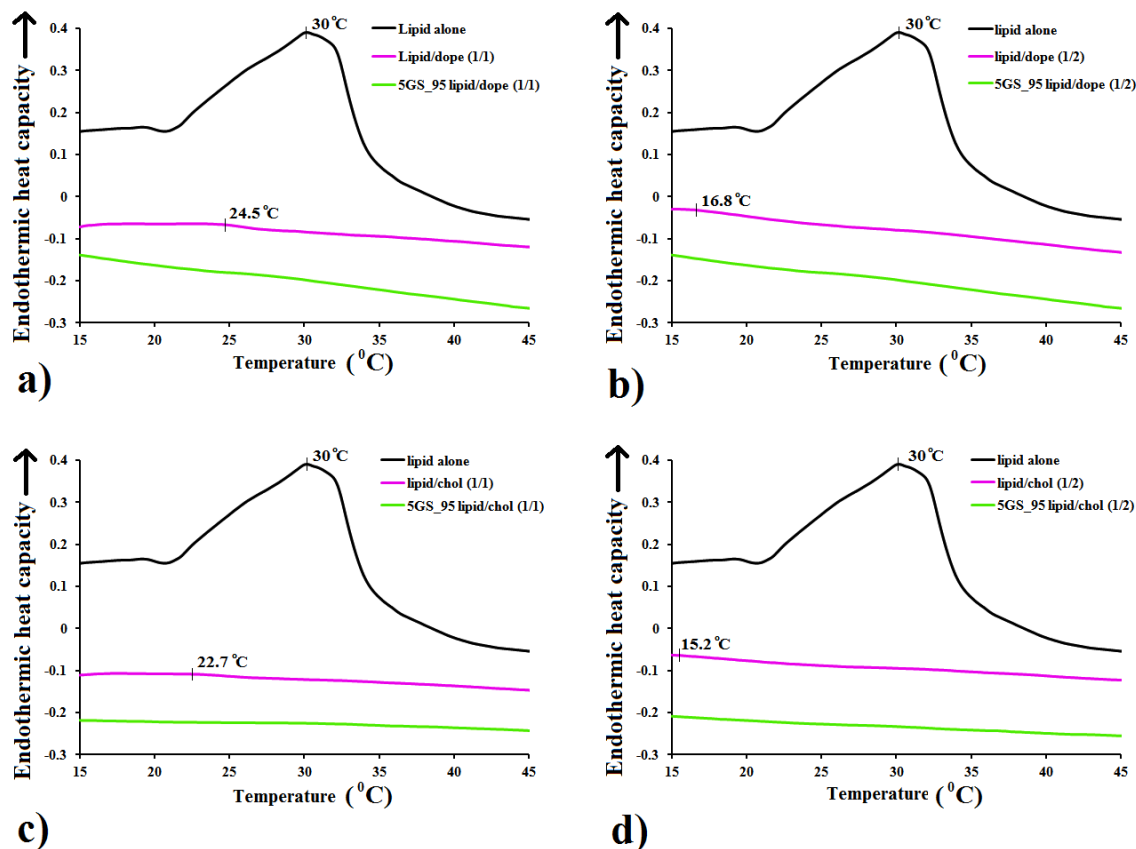


Figure 16. Comparative nanoDSC traces of cationic lipid SPYRIT-7 (“lipid”) formulated with DOPE (a, b) or cholesterol (c, d) at 1:1 (a, c) and 1:2 (b, d) molar ratios, in water, in the absence (red traces) of in the presence of 5% GS SPYRIT-68 (“GS”, green traces), against the pure cationic lipid formulation (black traces). Broadening and shifting the thermal transition of the cationic lipid to lower values by addition of colipid and subsequent complete bilayer fluidification through GS addition can be observed.

The above-mentioned hydrated cationic blends were subsequently sonicated to generate cationic liposomes. Since the gemini surfactant has a lower packing parameter (higher molecular curvature) than cationic lipid, it was expected that ternary lipid mixtures containing GS would be able to adapt higher bilayer curvatures and to yield smaller liposomes as compared with binary mixtures of SPYRIT-7 and colipids with equivalent positive charge. In order to test the effect of GS on the size/curvature of cationic liposomes, the ternary mixtures containing either 5% or 10% GS (but the same overall amount of positive charge) were made, in addition to the binary cationic lipid/colipid mixtures indicated above. The size and zeta potential of the resulted vesicles are presented in Figure 17 (panels a, c). An analysis of the data of Figure 17 reveals that the size of SPYRIT-7/Chol (1/1 and 1/2 molar ratio) liposomes was generally bigger than the size of SPYRIT-7/DOPE corresponding liposomes. Importantly, the effect of GS blending into cationic lipid/colipid formulations also depends on the nature of co-lipid used: for DOPE-based liposomes addition of 5% GS does not change significantly the size of the vesicles ($d \sim 250$ nm), while a significant decrease in size is observed for cholesterol-based liposomes (from 600 nm to about 250-300 nm). It appears that the more flexible DOPE can accommodate the small increase of the positive curvature of the bilayer induced by GS while the more rigid cholesterol cannot do that. Interestingly, doubling the amount of GS blended into bilayers *increases* the sizes of the liposomes from ~ 250 nm to 600-900 nm, with the exception of cationic amphiphiles/cholesterol 1:2 formulation, where the size of the vesicles decreases to 250 nm, as initially expected. We hypothesize that the increase in size of the supramolecular assemblies at 10 % GS after

an initial decrease at 5% GS is due either to different amphiphile distribution in the two bilayer leaflets at the two GS concentrations or to a liposome to worm micelle transition when passing from 5% to 10% GS in the cationic blend. The results of a parallel experiment of blending DOPE into a 10GS/90lipid cationic mix (Figure 17, panel b) support the first hypothesis since the size of supra-molecular aggregates increases monotonously from 400 nm to 900 nm with the increase of colipid molar fraction in the mix up to 50%, after which it decreases to about 600 nm when the amount of colipid is doubled. The possible bilayer asymmetry can explain also the variable results observed for the zeta potential of the 10GS/90lipid assemblies with variable DOPE content (Figure 17d), which increased from + 45 mV to about + 60 mV. For the other lipid blends the zeta potential decreased from ~ + 60-65 mV to + 50 mV when the amount of GS in the blend was reduced. This trend is normal since the charge density of GS SPYRIT-68 is higher than the corresponding charge density of cationic lipid SPYRIT-7 (the charge per mass ratio is in favor of GS) (Figure 17c, 17d).

The cationic formulations presented above were tested for their ability to compact plasmid DNA encoding the luciferase gene (gWizLuc, Aldevron). The compaction process was followed at different cationic amphiphile/DNA +/- charge ratios (Figure 18) by monitoring the size (Figure 18a), zeta potential (Figure 18b) and electrophoretic mobility (Figure 18c) of lipoplexes generated from each cationic amphiphile-based co-formulation used.

When the cationic lipid was formulated alone, no full compaction of the DNA could be observed (data not shown). This is probably due to the very high positive charge density in the cationic bilayer that causes strong repulsions between the cationic heads, destabilizing the bilayer and preventing the formation of stable DNA complexes.

However, efficient compaction of DNA was observed when SPYRIT-7 cationic lipid was formulated with either DOPE or cholesterol, as seen in Figure 18 (red bars, and top row of gels). The compaction process was dependent on the nature of co-lipid used (DOPE or cholesterol), on its molar ratio to cationic lipid (1:1 or 1:2), and on the cationic lipid/DNA charge ratio. For lipoplexes obtained from SPYRIT-7/ DOPE (1:1) formulation, *full compaction of DNA* occurred at cationic lipid/ DNA charge ratio between 3 and 4, as revealed by the positive shift in zeta potential and the gel electrophoresis mobility experiment. At these charge ratios a significant drop in the size of the lipoplexes from 800 nm to ~ 350 nm could also be observed in the majority of cases. At higher charge ratios, the zeta potential continued to increase to + 25 mV while the size continues to decrease, reaching a minimum average size for the complexes of 219 nm. Interestingly, the supercoiled plasmid (lower DNA band) is compacted faster than the relaxed circular DNA (Figure 18c, upper left panel). A possible explanation is

that the supercoiled DNA is compacted with a larger amount of counterions (thus requiring less cationic amphiphile) than the relaxed plasmid, similarly with the mechanism proposed recently by Aicart and Bhattacharya for the compaction of (supercoiled) plasmid DNA versus linear DNA[119]. When the molar ratio of DOPE was increased (cationic lipid/DOPE 1:2 formulation), the additional co-lipid caused full DNA compaction to occur at a cationic lipid/DNA charge ratio between 2 and 3 but the decrease in lipoplex size after compaction was less abrupt than for lipoplexes based on cationic lipid/DOPE 1:1 lipid mixtures. The zeta potential was 21.3 mV at the same charge ratio (3), significantly higher than the zeta potential for the above-mentioned lipoplexes. These results are in good agreement with the results obtained recently by Aicart and Bhattacharya for DNA compaction with cationic gemini surfactants/DOPE formulations[120].

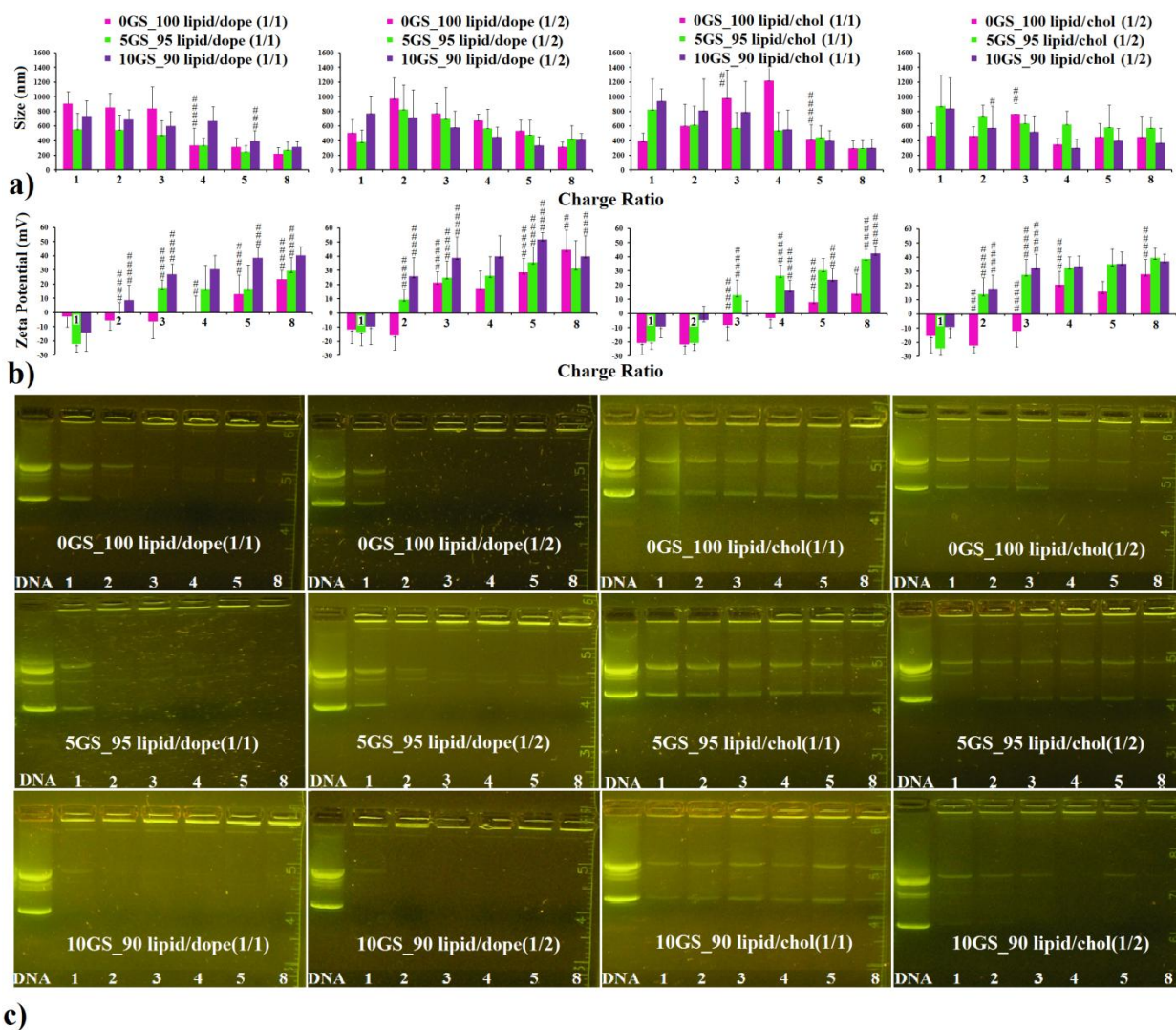


Figure 18. The compaction of DNA by pyridinium cationic amphiphiles SPYRIT-7 and SYRIT-68, co-formulated with DOPE (1:1 molar ratio, first panel column; 1:2 molar ratio, second panel column) or with cholesterol (1:1 molar ratio, third panel column; 1:2 molar ratio, fourth panel column) depicting the size (a), zeta potential (b) and electrophoretic mobility of the lipoplexes against free DNA (c), as a function of the cationic amphiphile/ DNA charge ratio. The red bars correspond to formulations in which the total positive charge is brought exclusively by SPYRIT-7 cationic lipid, while the green and violet bars represent SPYRIT-7/SPYRIT-68 blends of 95/5 and 90/10 charge

contribution respectively. Error bars represent standard deviation (n = 10-12). P values were determined by one-way ANOVA, comparing the value with the previous one in the series ($^{\#}P < 0.05$, $^{\#\#}P < 0.01$, $^{\#\#\#}P < 0.001$ and $^{\#\#\#\#}P < 0.0001$). Only the statistical significant differences were shown.

While analyzing the lipoplexes derived from SPYRIT-7/cholesterol formulation (1:1 molar ratio) one may observe that *full DNA compaction* did not occur even at high charge ratios. The zeta potential turned positive around a charge ratio of 5, when the size of lipoplexes decreases abruptly from 1218 nm to 412 nm. Doubling the amount of cholesterol in the liposomal formulation leads to (lateral) fluidization of the cationic bilayer (as presented in Figure 16) and decreases the +/- charge ratio at which DNA is compacted to 4, with a size of corresponding lipoplexes of 346 nm.

Substituting 5% of the positive charge brought by cationic lipid SPYRIT-7 in above mentioned formulations with the same amount of positive charge from gemini surfactant SPYRIT-68 had a significant effect on the corresponding lipoplex properties (Figure 18, green bars and second row of gels). Thus, DNA compaction occurred at lower charge ratios (2 for cationic lipid/DOPE 1/1 and 1/2, 3 for cationic lipid/cholesterol 1/1 and 2 for cationic lipid/cholesterol 1/2) as indicated by zeta potential shifts to positive values and confirmed by lipoplex electrophoretic mobility. The size of lipoplexes at full DNA compaction decreased for all formulations, revealing a more compact structure. In the case of lipoplexes generated from SPYRIT-7/DOPE 1/2 and SPYRIT-7/cholesterol 1/2 the supercoiled DNA was compacted faster than the relaxed one. We hypothesize that

lateral movement of gemini surfactant in the fluid bilayers allows its concentration in areas where the DNA makes high curvature loops otherwise difficult to accommodate by the less flexible cationic lipid congener. This mechanism is probably responsible for the monotonous decrease in size of lipoplexes while increasing the charge ratio observed for GS-containing lipoplexes, as opposed to dramatic size contractions observed in the case of lipoplexes derived from formulations containing exclusively cationic lipid SPYRIT-7.

Increasing the percentage of positive charge brought by gemini surfactant into the cationic amphiphile blend to 10% has a further beneficial effect: the minimum charge ratio required for DNA compaction continues to decrease, the lipoplex zeta potential is most of the times higher as compared with GS/lipid 5/95 blends and the DNA is better compacted (Figure 18 violet bars and third row of gels). DNA in DOPE-containing lipoplexes 10GS_90lipid/DOPE 1/1 is fully compacted at a +/- charge ratio of 1 for lipoplexes derived from 10GS_90lipid/DOPE 1/1) a feature that is a rather rare in cationic lipid-mediated transfection. For lipoplexes derived from 10GS_90lipid/DOPE 1/2 the supercoiled DNA is fully compacted at +/- charge ratio of 1, while a small amount of free circular plasmid still can be observed at this charge ratio. The same observations are also valid for cholesterol-containing lipoplexes, where the percent of uncompact DNA is dramatically reduced when 10% GS is blended into the cationic amphiphile mixture.

In order to test the effect of GS blending towards the transfection efficiency of the lipoplexes, we assessed the above-mentioned DNA complexes prepared at the +/- charge ratio of 3 against the NCI-H23 cell line. This cell line proved very susceptible to be transfected by pyridinium amphiphiles[46, 77] thus allowing the fine quantization of the

differences in transfection efficiency of different formulations. The cytotoxic effect associated with transfection process was quantified in parallel using a WST-1 viability assay (Figure 19). Lipoplexes generated from commercial transfection agent Lipofectamine[®] at the same charge ratio of 3 were added as reference. The size and zeta potentials of the lipoplexes were in good agreement with the ones found in the optimization study (Figure 18) with DOPE-containing lipoplexes having slightly smaller sizes as compared to cholesterol containing ones (Figure 19a). The zeta potential of all formulations was positive at this charge ratio within experimental errors (Figure 19c) and in good agreement with the values obtained in the optimization study (Figure 18). The standard transfection agent Lipofectamine generated lipoplexes with a size of 250 nm and a zeta potential of 2 mV.

In terms of transfection efficiency it can be observed that cholesterol-based lipoplexes were more efficient than DOPE-based ones at similar cationic species composition. The molar ratio of colipid in the formulation proved also important. Increasing the DOPE content of the DOPE-based lipoplexes had a beneficial effect on transfection efficiency while an increase of cholesterol molar ratio in the cholesterol-based lipoplexes decreased the transfection efficiency of corresponding DNA complexes. Lipoplexes derived from SPYRIT-7/chol 1/1 formulation were found to be equal or more efficient than Lipofectamine, confirming the conclusions of previous studies[77]. Importantly, lipoplexes derived from cationic blends containing 5 % positive charge brought by gemini surfactant SPYRIT-68 were 2-3 times more efficient than the corresponding lipoplexes generated from 100% cationic lipid, revealing a significant impact of the gemini surfactant on transfection efficiency. Lipoplexes derived from

5GS_95lipid/chol 1/1 and 1/2 were several times more efficient than Lipofectamine, while lipoplexes derived from 5GS_95lipid/DOPE 1/1 and 1/2 matched the efficiency of this standard transfection system. Interestingly, doubling the charge contribution of the gemini surfactant in the lipoplexes did not increase further the transfection efficiency; in fact the efficiency of the lipoplexes containing 10% positive charge from GS was inferior to the efficiency of lipoplexes derived only from SPYRIT-68 (Figure 19e), with the 10/90 GS/lipid : DOPE formulations being practically devoid of transfection efficiency. We hypothesize that the GS is favoring the fusion of the lipoplex with the endosomal membrane due to its high curvature and elastic modulus and high charge density, as presented by Safinya's group [100]. Similar fusogenic properties are induced into lipoplexes by DOPE through its ability to adopt an inverted hexagonal phase. However, the packing parameters of GS SPYRIT-68 and DOPE are quite opposite and we suspected that the two amphiphiles may cancel each other in terms of fusogenicity. Therefore we tested the effect of reducing the DOPE amount in the 10/90 GS/lipid blends (Figure 19b, 19d, 19f, 19h). Data from Figure 4f reveals that the transfection efficiency of 10/90 GS/lipid blends can be regained by reducing the DOPE amount. Interestingly, the 10/90 cationic GS/lipid blends were efficient in the absence of any colipid, being able to condense DNA into 400 nm lipoplexes with positive zeta potential (Figure 19b, 19d, 19f). One may also observe the excellent cytotoxic profile of the lipoplexes, irrespective of their composition. The experiment reveals the ability of gemini surfactant SPYRIT-68 to potentiate transfection without raising the cytotoxicity of the formulation, thus validating the working hypothesis.

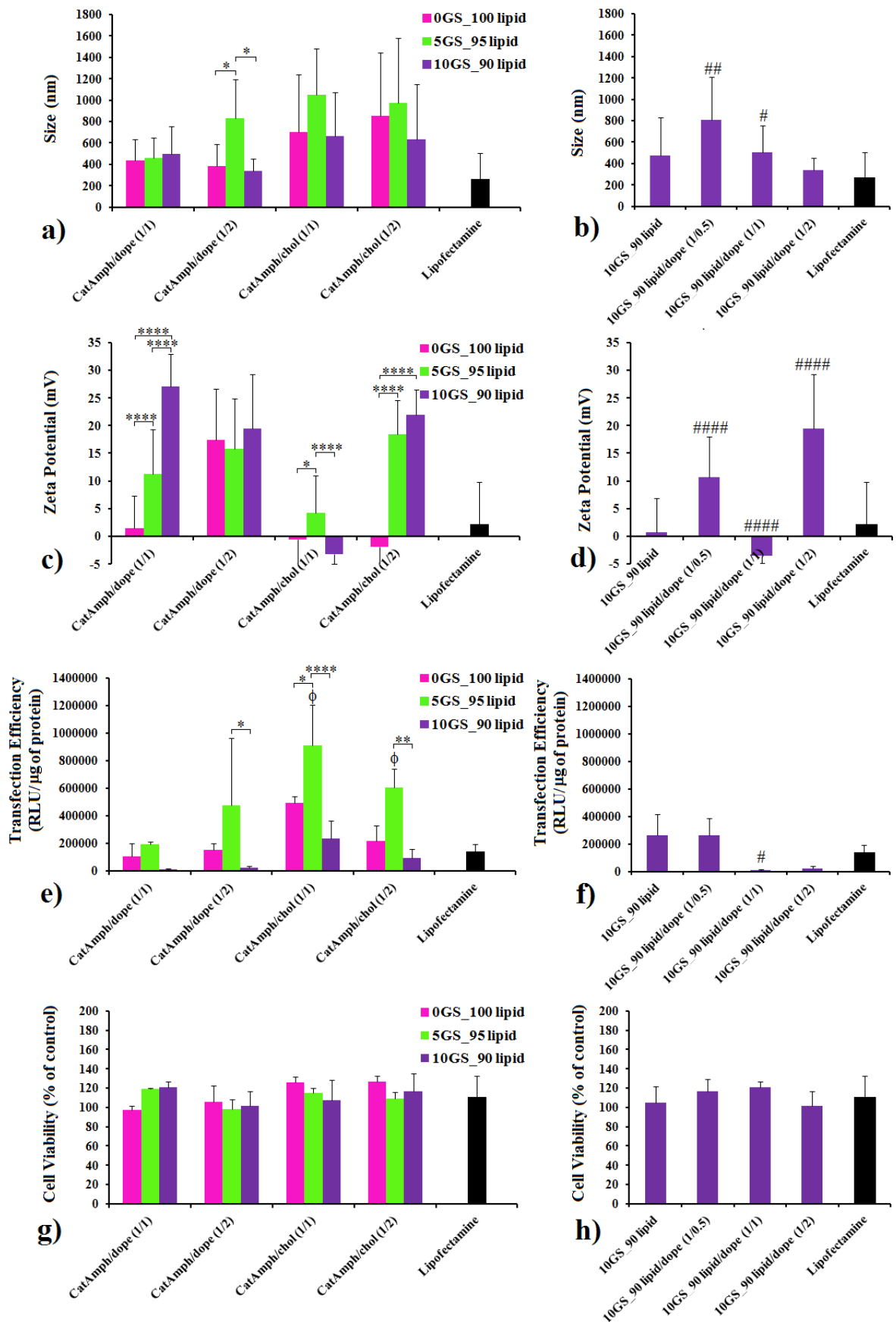


Figure 19. Size (panels a, b), zeta potential (panels c, d), transfection efficiency (panels e, f) and cytotoxicity (panels g, h) against NCI-H23 cell line of lipoplexes formed at a +/- charge ratio of 3 from SPYRIT-68/SPYRIT-7 (0/100 red bars, 5/95 green bars, 10/90 violet bars) cationic amphiphiles coformulated with either DOPE or cholesterol at 1:1 and 1:2 molar ratios. P values were determined by two-way ANOVA within one set of formulations (* $P < 0.05$, ** $P < 0.01$, *** $P < 0.001$ and **** $P < 0.0001$) or one-way ANOVA, comparing the value with the previous one ([#] $P < 0.05$, ^{##} $P < 0.01$, ^{###} $P < 0.001$ and ^{####} $P < 0.0001$). In the transfection efficiency experiment (e, f) one-way ANOVA was performed relative to Lipofectamine formulation (^Φ $P < 0.05$). Only the statistical significant differences were shown.

We also assessed the ability of the most efficient formulations towards transfecting tumor spheroids in vitro. Spheroids derived from lung carcinoma cell line NCI-H23 and from two colon carcinomas – HT-29 and HCT-116 were grown to ~ 0.7 mm diameter, when they are thought to contain about 40000 cells (the same amount of cells transfected in a well in the 96-well plate format). We incubated the individual spheroids with lipoplexes generated under the same conditions as in the 2D experiment and containing the same amount of DNA/cell. Besides luciferase we also used the gWizGFP plasmid, which allows a better visualization of the transfected cells in 3D after confocal imaging and reconstruction of the three-dimensional image from sequential 2D ones (Figure 20). Data from Figure 20 revealed an interesting trend, with the DOPE-based formulation superior to the cholesterol-based ones irrespective of the reporter gene plasmid used. Luciferase data (Figure 20b) mirrored the results obtained with GFP

plasmid. The transfection was cell-type dependent, with the NCI-H23 spheroids being the most susceptible to be transfected and showing the most significant transfection differences, followed by HCT-116 and HT-29.

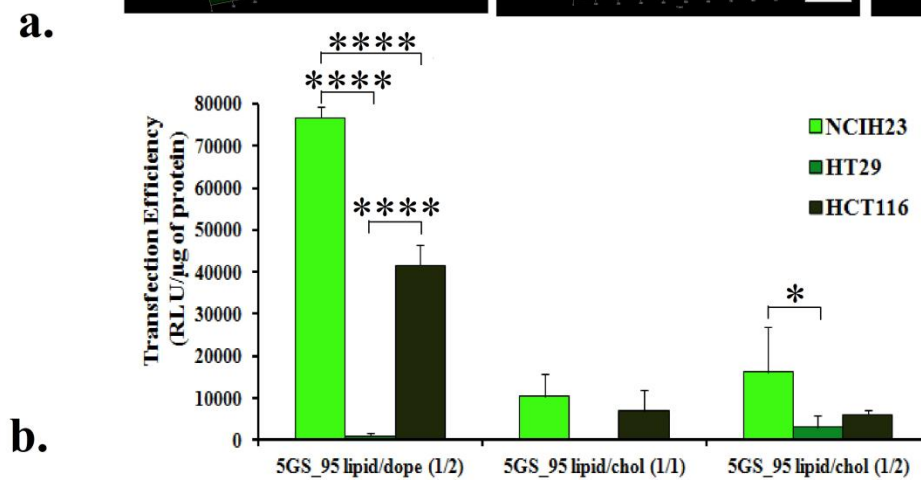
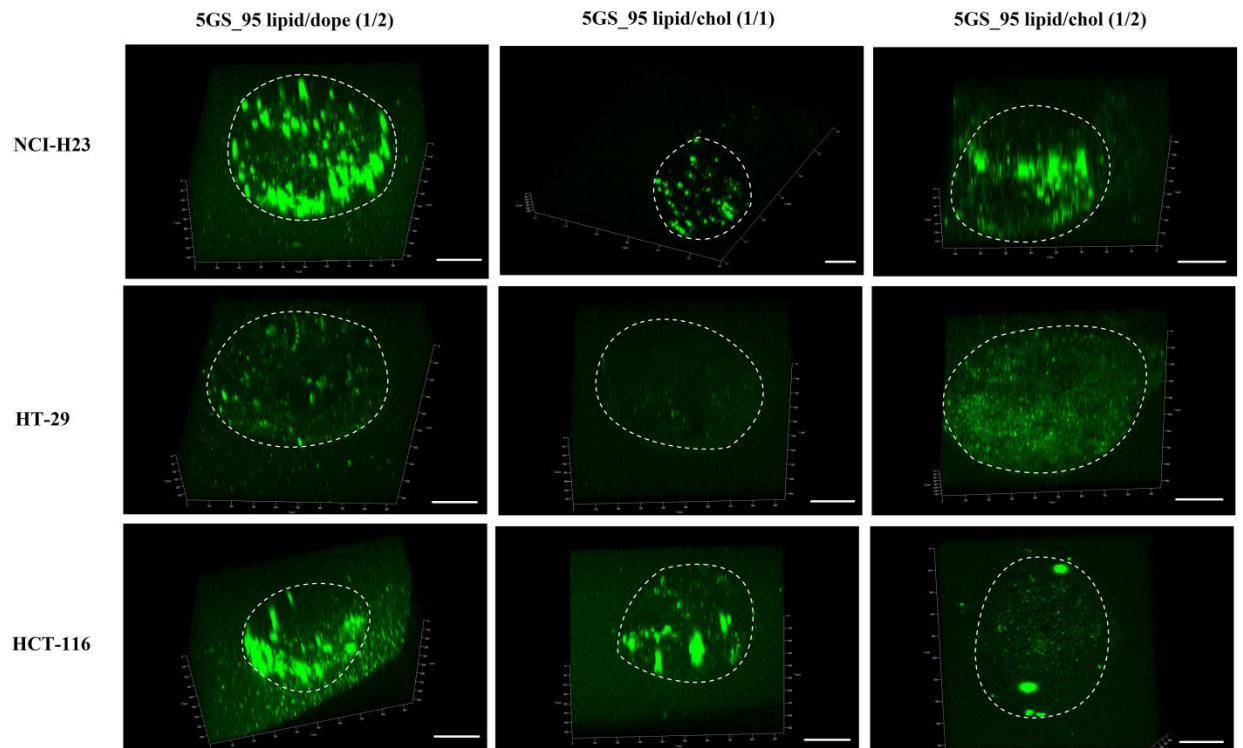


Figure 20. Transfection of NCI-H23, HT-29, HCT-116 tumor spheroids by select pyridinium cationic amphiphiles formulations, as revealed by 3D images of GFP expression (a) and luciferase quantitation (b). Boundaries of spheroids are indicated by a dotted white line. Bar represents 200 μ m. Note the strong cell dependence of transfection efficiency on cell type. P values were determined by two-way ANOVA within one set of formulations (* $P < 0.05$, ** $P < 0.01$, *** $P < 0.001$ and **** $P < 0.0001$).

The major transfection differences observed between lipoplexes containing variable amounts of GS SPYRIT-68 and between the 2D and 3D transfection experiments prompted us to assess the implication of GS in another delivery barrier, namely the cellular internalization of the lipoplexes. Several mechanism of lipoplex internalization are known, including clathrin- and caveolae-mediated endocytosis and (macro)pinocytosis, which can be selectively blocked by chlorpromazine, genistein, and 5-(N-ethyl-N-isopropyl)amiloride (EIPA)[111, 113, 121-123]. We tested the internalization mechanism used by the most efficient pyridinium lipoplexes using the same NCI-H23 lung cancer cell line and the three above-mentioned selective inhibitors. Specifically, transfection efficiency of lipoplexes generated from cationic amphiphile(s)/DOPE (1/2 molar ratio) and cationic amphiphile(s)/cholesterol (1/1 and 1/2 molar ratios) formulations, containing 0%, 5% and 10% positive charge contributed by GS SPYRIT-68, prepared at a charge ratio of 3 as previously done, was assessed in the absence and in the presence of (i) chlorpromazine (10 μ g/mL), (ii) genistein (200 μ M), and (iii) EIPA(100 μ M) (Figure 21). Data from Figure 21 revealed that the cellular uptake, measured as the ratio between the transfection efficiency in the presence of

internalization inhibitors over the transfection efficiency in normal conditions (control experiment), was strongly dependent on the composition of the lipoplexes. Thus, the DOPE-containing lipoplexes are internalized primarily through pinocytosis (inhibited by EIPA). Addition of GS SPYRIT-68 does not change the primary mechanism of internalization, but it may open an alternative caveolae-mediated endocytosis pathway (inhibited by genistein) which is dependent on the amount of GS in the formulation (Figure 6A). This availability of this pathway is controlled by the amount of fusogenic component (either GS or DOPE) in the lipoplex. On the other hand, cholesterol-containing lipoplexes derived from SPYRIT-7 use all three internalization pathways. For lipoplexes rich in cholesterol (cationic amphiphile/cholesterol molar ratio of 1:2) the blending of GS SPYRIT-68 does not have a significant effect.

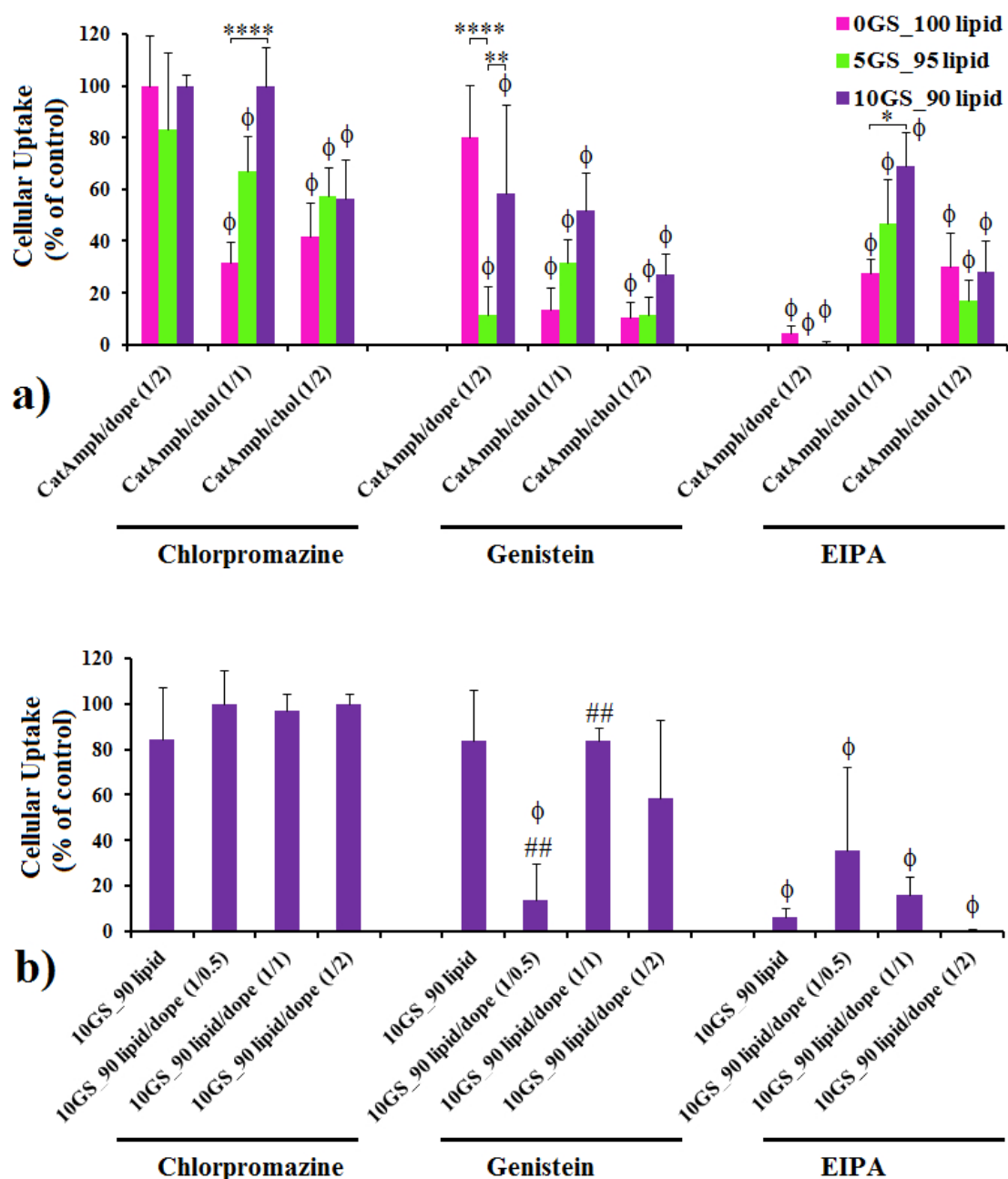


Figure 21. Cellular uptake (NCI-H23 cell line) of lipoplexes formed from SPYRIT-7/SPYRIT-68 (0/100 red bars, 5/95 green bars, 10/90 violet bars) cationic amphiphiles coformulated with either DOPE or cholesterol at 1:1 and 1:2 molar ratios (a) or from SPYRIT-7/SPYRIT-68 (10/90) cationic amphiphiles formulated alone or with DOPE at different molar ratios (b) in the presence of specific internalization inhibitors

chloropromazine, genistein and EIPA. P values were determined by one-way ANOVA, comparing the values with the control set ($^{\Phi}P < 0.05$) in panels a) and b), by two-way ANOVA within one set of formulations ($*P < 0.05$, $**P < 0.01$, $***P < 0.001$ and $****P < 0.0001$) in panel a) and by one-way ANOVA, comparing the value within a series with the previous one ($^{\#}P < 0.05$, $^{\#\#}P < 0.01$, $^{\#\#\#}P < 0.001$ and $^{\#\#\#\#}P < 0.0001$) in panel b). Only the statistical significant differences were shown.

However, a very different trend emerges for lipoplexes derived from cationic amphiphile/cholesterol formulated at 1:1 molar ratio: blending of GS SPYRIT-68 causes the simultaneous suppression of cellular uptake throughout all three pathways, in a dose-dependent manner (Figure 21a). Taking into account that these formulations were the most efficient in 2D transfection experiments, we can conclude that addition of the GS SPYRIT-68 into the lipoplexes triggers their internalization through another mechanism. A possible mechanism is through temporary poration of external membranes by the GS[63]. This fact might explain the different transfection trends observed between two-dimensional and three-dimensional transfection experiments.

Consequently, the internal membranes of endolysosomes should be affected in the same way by the GS-containing lipoplexes still internalized through the classical pathways investigated above. In order to test this hypothesis, we transfected NCI-H23 cells with Rab-7 protein labeled with GFP using the electroporation technique. This protein (a small GTPase) is specific for endolysosomes and does not exist in caveolae and in the vesicles internalized from plasmalemma[124, 125]. Forty-eight hours post-

transfection with Rab-7, the cells were incubated for 2 h with lipoplexes that did not contain GS and that contained 5% charge brought by GS, after which they were washed, fixed with 4% paraformaldehyde, washed, and imaged immediately via confocal microscopy for Rab-7 intracellular distribution against control cells that did not receive lipoplexes (Figure 22). Analyzing the data from Figure 22, one can observe that NCIH23 cells that did not have the lipoplexes display a Rab-7 intracellular distribution limited to endolysosomes (left panels) and that the transfection with lipoplexes that do not contain GS SPYRIT-68 does not alter significantly the Rab-7 intracellular distribution. However, the lipoplexes containing 5% GS promote endolysosomal membrane rupture and release of Rab-7 (and of DNA cargo) into the cytoplasm (Figure 22, right panels). The diffuse cytoplasm distribution of Rab-7 supports the proposed temporary poration of external and internal membrane by GS-containing formulations.

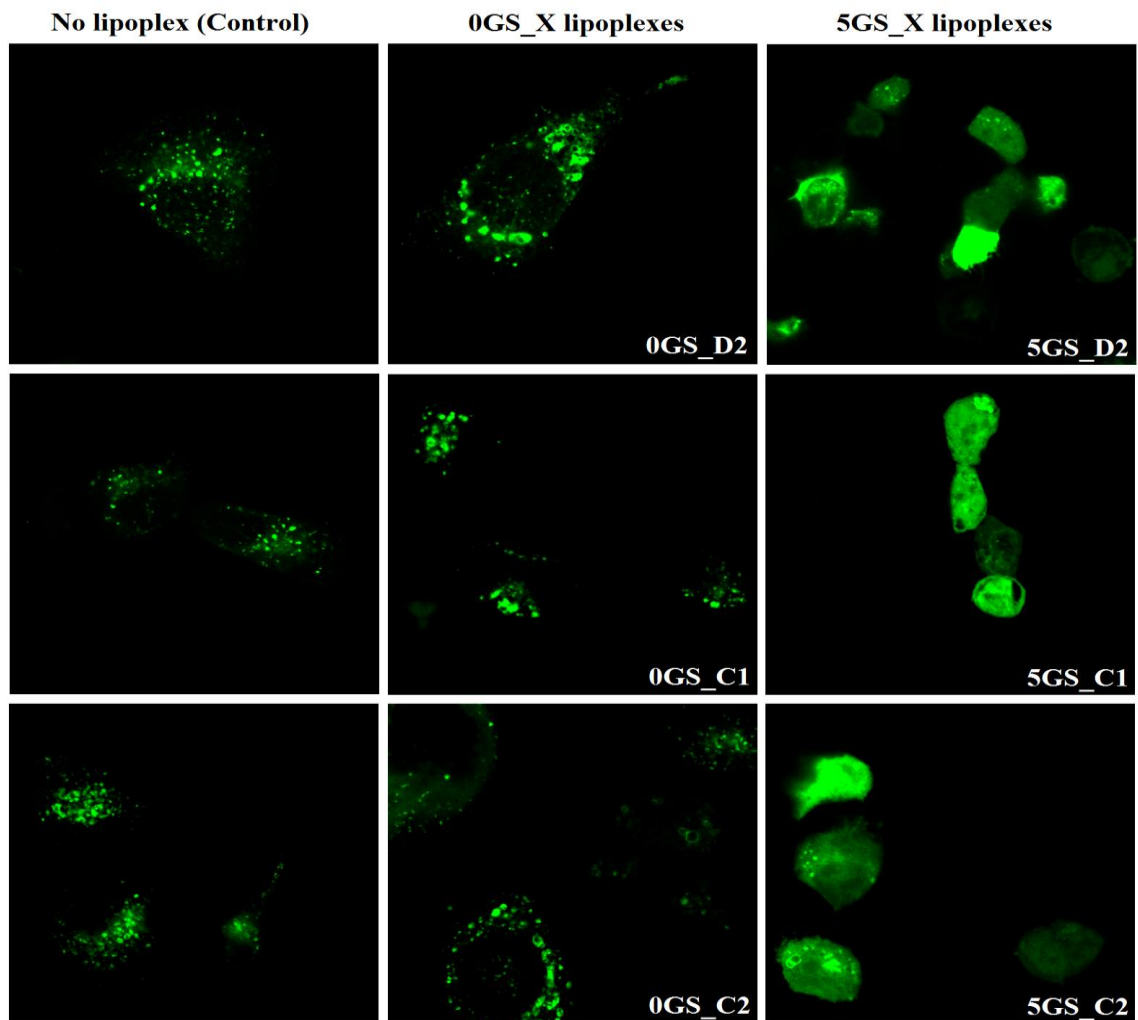


Figure 22. Pyridinium GS promotes endolysosomal escape of the GS-containing lipoplexes: confocal images of NCI- 23 cells (excitation 488 nm) expressing the endolysosomal protein GFP-Rab 7 transfected with select lipoplex formulations indicated in each case; Rab-7 protein is specific for endolysosomes [57,58] as its specific distribution can be observed in control NCI-H23 cells that did not receive lipoplexes (left panels). Lipoplexes that do not contain GS do not significantly change Rab-7 intracellular distribution (central panels), while introduction of GS in the structure of lipoplexes promotes endolysosomal membrane rupture and consequently a diffuse distribution of

Rab-7 in the cytoplasm, irrespective of the colipid used and its molar ratio in lipoplex formulations (right panels).

Conclusion

This study demonstrated that the addition of pyridinium gemini surfactant SPYRIT-68 to cationic bilayers formed by pyridinium cationic lipid SPYRIT-7 acts synergistically with co-lipids DOPE or cholesterol towards fluidizing completely the supramolecular amphiphile assembly. Blending of gemini surfactant into the cationic lipid-based bilayers can impact substantially the size and, to some extent, the zeta potential of the vesicles formed from these hydrated bilayers upon sonication. The mixed cationic amphiphile assemblies were able to fully compact plasmid DNA at lower +/- charge ratios, generate lipoplexes of smaller size and higher zeta potential as compared with corresponding cationic bilayers of equivalent positive charge containing only cationic lipid SPYRIT-7. These observations, in concert with the fluctuation observed for the size of resulting lipoplexes while increasing the cationic amphiphile/DNA charge ratio in the absence and in the presence of gemini surfactant, strongly indicate a different compaction mechanism in which the gemini surfactant concentrates in areas where DNA makes high curvature loops otherwise difficult to accommodate by the less flexible cationic lipid congener at the same +/- charge ratio. Moreover, the addition of pyridinium GS can enhance dramatically the transfection efficiency of SPYRIT-7 cationic lipid-based formulations, surpassing standard commercial transfection systems while displaying negligible cytotoxicity, as revealed by 2D- and 3-D transfection experiments.

Blending of gemini surfactant SPYRIT-68 into cationic lipid SPYRIT-7-based lipoplexes can also change substantially the internalization mechanism of the lipoplexes. The overall impact depends heavily on the presence of co-lipids, their nature and amount present into the lipoplexes, with most susceptible formulations being the ones containing cholesterol in equimolar amount to cationic lipids. The study confirmed the possibility of combining the specific properties of pyridinium gemini surfactants and cationic lipids synergistically for obtaining synthetic transfection systems with improved transfection efficiency and negligible cytotoxicity useful for therapeutic gene delivery.

CHAPTER 4

INTERFACIAL-ENGINEERED PEG₄₅-PBO_{0,6,9}-PCL_{64,58,53} AMPHIPHILIC BLOCK COPOLYMERS AS DRUG DELIVERY SYSTEMS

In this chapter, we assessed comparatively the interfacial engineering of PEG-PCL diblock copolymers into PEG-PBO-PCL triblock copolymers and its impact on self assembled supramolecular micelles in terms of hydrolytic and shelf stability, drug loading capacity, drug release profile and toxicity.

Based on literature data, our working hypothesis is that the insertion of a short hydrophobic non-hydrolyzable poly (1,2-butylene oxide) (PBO) segment between the PEG and PCL blocks will prevent water to reach the interface ester group linking the PEG to PCL block. This interface engineering will in turn increase the resilience of the polymeric material and its self-assemblies in aqueous medium, will improve circulation time and shelf stability of polymeric DDS together with their drug loading and release properties, and will also reduce the toxicity of these new polymeric DDSs.

Background and Rationale:

Cancer is currently the second most common cause of death in the US and worldwide. Among different types of cancer, lung cancer is the leading cause of cancer related mortality in U.S. and worldwide [1]. Chemotherapy is a first-line treatment and usually includes platinum cytotoxic agents, taxanes and pemetrexed [126, 127]. Unfortunately, these chemotherapeutic drugs used in the treatment of various forms of

lung cancer generally lack selectivity between normal and malignant cells and consequently are associated with significant adverse effects, many of them life-threatening. Moreover, many representatives do not have good water solubility and require delivery vehicles. The formulation vehicles used for water insoluble drugs are not inert and in fact are responsible for additional side effects, which raise the toxicity of the formulations and limit their therapeutic index. Cremophor EL (CrEL) is a formulation vehicle used for various lipophilic drugs, including paclitaxel (Taxol®). CrEL is not an inert vehicle, and exerts a range of detrimental pharmacokinetic and biological effects, including severe anaphylactoid hypersensitivity reactions, hyperlipidaemia, abnormal lipoprotein patterns, peripheral neuropathy etc [128]. Polysorbate 80 is another formulation vehicle widely used for solubilization of lipophilic drugs. In fact, Taxotere® anticancer formulation consists of docetaxel formulated in polysorbate 80. It is administered IV, as ethanol solution. The adverse effects of Taxotere® are similar to those reported for Taxol®, with hypersensitivity to the formulation and peripheral neuropathy observed in up to 40% of the treated patients [129, 130]. Other reported side effects for Taxotere® included dyspnea, hypotension, neutropenia, neurotoxicity, musculoskeletal toxicity and cumulative fluid retention [131, 132]. Albumin was also proposed as a less toxic vehicle for chemotherapeutic agents belonging to taxane family, with the introduction of Abraxane® for the treatment of breast cancer. The formulation contains 100 mg of paclitaxel absorbed into 900 mg of stabilized human albumin as a sterile lyophilized powder. Abraxane® is different from simple taxols in terms of formulations, pharmacokinetics, bioavailability, administration (30 minute infusion w/o premedication vs. 3 hr infusion with premedication) [133]. Taxol® has a higher incidence

of neutropenia and hypersensitivity reactions, whereas Abraxane[®] has a higher incidence of peripheral neuropathy, nausea, vomiting, diarrhea and asthenia. Although Abraxane[®] was superior to other formulations for taxol delivery, the search for better delivery vehicle with reduced toxicity is still ongoing [128, 133].

On the other hand, targeted drug delivery systems (DDSs) can change the pharmacokinetics of chemotherapeutic drugs, focusing their action on the tumor site [134, 135]. These engineered systems can also improve the solubility of many poorly water-soluble anticancer drugs (e.g. paclitaxel, docetaxel), can prevent their premature inactivation, and can efficiently control the amount and rate of drug delivered to the affected site [136-142]. Consequently, the therapeutic index of chemotherapeutic drugs can be significantly improved and the side effects associated with the use of these highly toxic agents can be substantially reduced, allowing efficient treatment of late stages cases of cancer, including lung cancer [143]. Lung receives 100% of cardiac output and constitutes a particularly good target for drug delivery due to its high surface area [144]. In fact, novel *targeted therapies* involving monoclonal antibodies such as bevacizumab and cetuximab complement above-mentioned chemotherapeutic drugs, being *particularly useful for late stages lung cancer* [127, 145-147]. Importantly, current five year survival rates for patient suffering from NSCLC is 19% - 50% in early stages (\leq IIIa) and less than 7 - 9% for late stages (IIIB and IV) where the tumor burden is very serious [8, 9]. *Novel efficient methods for the treatment of late stages lung cancer are urgently needed.*

Amphiphilic copolymers based on polyethylene glycol (PEG) and biodegradable lipophilic polymers such as polylactic acid (PLA) and polycaprolactone (PCL) [148-155] can self-assemble in water generating nanosystems extremely attractive as drug and gene

delivery systems [142, 156-162]. Depending on the packing parameter [53] one may observe spherical micelles, filomicelles, or polymerosomes, displaying a wide range of hydrodynamic properties and drug loading capacities [39, 155, 163, 164]. The dense PEG brush on the surface of these nanosystems reduces the interaction with proteins and figurative elements of the blood, conferring “stealth” properties and thus increasing the circulation time of the delivery system [142, 151, 162]. Other important advantages include the relative ease of synthesis and formulation, good control of supra-molecular shape and stiffness, an excellent biocompatibility, a large cargo loading capacity and a favorable drug release profile. They also allow many derivatization strategies for practically endless targeting possibilities [39, 164-168]. These major advantages propelled polymeric DDSs into clinical trials for treatment of several cancers [168]. Notably, PEG-PLA micelles with hydrodynamic diameter between 20-50 nm encapsulating paclitaxel (Genexol-PM) are evaluated in phase I/II for the management of pancreatic and ovarian cancer and in phase II for the treatment of non-small-cell lung cancer in combination with carboplatin [168, 169]. Genexol-PM was recently approved for the clinical treatment of breast cancer in South Korea.

The shelf stability, in vivo dynamic stability and circulation time, drug protection against degradation, as well as drug loading and drug release profiles of these DDSs depend heavily on the resilience of the building blocks against hydrolytic degradation. Also important is the extent of their interaction with various other amphiphilic compounds and entities (proteins, cells) encountered from the site of administration to the target cells/tissues [162]. These properties are directly influenced by the structure of the

two interfaces present in the block copolymers: the hydrophilic-hydrophobic interface and the interface between the chemically stable and the biodegradable polymeric blocks.

Moreover, an important premise for successful targeted drug delivery (to the lung) is a good circulation time of the DDS, in the range of days to weeks [162]. This allows efficient and selective targeting and accumulation of DDSs at tumor sites via EPR effect [141, 142, 162, 170, 171]. Presently, circulation time of biocompatible PEG-based DDSs is in the range of hours to 1-2 days at best [39, 172]. To a large extent this is due to the premature inactivation of these DDSs through substantial modification of their physicochemical properties (size, shape, zeta potential, PEG chain density) via absorption of opsonins and other amphiphilic blood proteins at the hydrophilic/hydrophobic interface. Some amphiphilic proteins such as albumin and especially endothelial lipases [173-175] have esterase activity and thus can catalyze the hydrolysis of the ester junction between the PEG block and the polyester hydrophobic core [176-178]. The result is PEG shedding and a loss of stealth properties [179, 180], with subsequent binding of other blood proteins [181, 182], uptake by macrophages of the mononuclear phagocyte system, or removal by Kupffer cells [162]. The loaded drug is either prematurely released in the bloodstream or is ending in scavenging cells, causing systemic toxicity. The use of longer PEG segments (MW > 5000 Da) [181] can partially alleviate the problem, at the expense of increasing the size and immunogenicity of the nanoparticles and of decreasing the availability of the targeting moiety.

In DDSs based on self-assembled PEG-based amphiphilic diblock copolymers such as PEG-PLA, PEG-PLGA, PEG-PCL, the boundary between the biodegradable block and the hydrolytically stable block coincides with the hydrophilic/hydrophobic

self-assembling interface. Water has free access to the interface between the stable (PEG) and the hydrolysable block (PLA, PCL), therefore hydrolysis can easily occur. Adsorption at this double interface of amphiphilic proteins with esterase activity (e. g. lipases [176, 177], albumin) can dramatically accelerate the hydrolysis process and can cause fast and complete degradation of the nanosystems within hours, as shown by literature studies [176, 177, 179, 183-185].

Modification of physicochemical properties of polymeric DDSs via hydrolytic degradation at the hydrophilic/hydrophobic interface can also be self-catalyzed by small amounts of acid monomer (lactic, 6-hydroxycaproic) released when these (loaded) nanosystems are stored before use, with negative consequences towards the shelf life and batch-to-batch consistency of these formulations. The hydrolysis is accelerated by the nanodispersion of the material, which greatly enhances the surface area exposed to solvent and by acidic products of the process. The negative impact is larger when encapsulated drugs are also hydrolytically vulnerable.

The hydrophilic/hydrophobic interface is also responsible for the control of the drug loading and drug release processes. Many DDSs, including those based on amphiphilic diblock copolymers, are characterized by a rapid initial release (“burst release”), followed by a phase with slower release kinetics [186]. Burst release is not only wasteful of drug payload but also potentially harmful for the patient. Development of novel chemical ways to finely tune these interfaces is therefore needed and constitutes our long-term goal. It should lead to the development of long circulating DDSs, with long shelf stability and tailored drug loading and release profiles, suitable for targeted delivery of drugs, including anticancer agents.

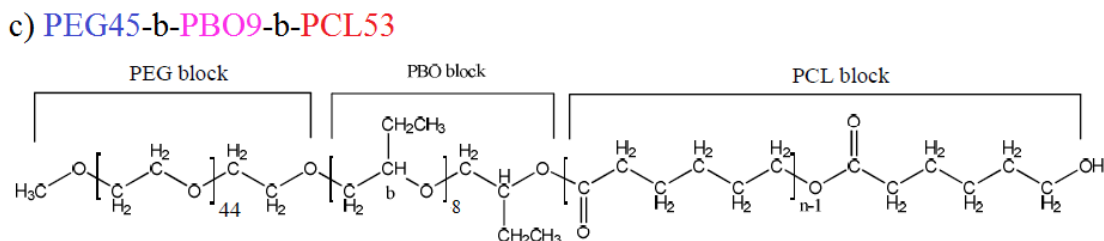
Towards this goal, it was hypothesized [184] that the separation of the hydrophilic/hydrophobic self-assembling interface of PEG-based amphiphilic diblock copolymers from the hydrolysable boundary between biodegradable and non-degradable blocks will increase the resilience of the polymeric material and its self-assemblies in aqueous medium, will improve circulation time and shelf stability of DDS, and will efficiently modulate its drug loading and release properties. PEG-PCL was selected as a model for implementing our interfacial inactivation strategy because the semi-crystalline nature of the PCL block allows a better evaluation of consequences associated with interfacial engineering of amphiphilic block copolymers [154, 187]. Thus, in the novel copolymer design (Chart 3) the hydrophilic/hydrophobic interface was separated from the boundary between the non-hydrolysable PEG and the hydrolysable PCL blocks through the insertion of a short, non-degradable oligomeric hydrophobic poly(butylene oxide) (PBO) linking segment. Preliminary studies performed on the PEG45-PCL64 diblock copolymer model and on the novel interfacial-engineered triblock copolymer congeners PEG45-PBO6-PCL58 and PEG₄₅-PBO9-PCL53 (Chart 3), self-assembled into supra-molecular micelles, pleaded for the feasibility of the concept and suggest an interfacial activation model for the degradation of amphiphilic block copolymer micelles [184]. As a consequence, more efficient drug delivery systems are expected to be generated based on our proposed interfacial polymer tuning concept. The evaluation of this working

a) **PEG45-b-PCL64**

PEG block

PCL block

$$\text{H}_3\text{C}-\text{O}-\left[\text{CH}_2-\text{CH}_2-\text{O}\right]_{44}-\text{CH}_2-\text{CH}_2-\text{O}-\left[\text{CH}_2-\text{CH}_2-\text{CH}_2-\text{CH}_2-\text{CH}_2-\text{C}(=\text{O})\right]_{n-1}-\text{CH}_2-\text{CH}_2-\text{CH}_2-\text{CH}_2-\text{CH}_2-\text{OH}$$



The anticancer drug docetaxel was selected as prototypical chemotherapeutic agent to be loaded and delivered due to its broad spectrum of antitumor activity and its approved use in the treatment of advanced non-small-cell lung cancer [188]. The availability of its current clinical formulation (Taxotere[®]) and the well-described side effects associated with its use also recommended the use of this chemotherapeutic agent.

Another reason for selecting this drug was its susceptibility against hydrolysis [189], and the limited stability of the polysorbate 80 formulation in ethanol (< 8h).

Materials and Methods

Materials. Diblock and triblock polymers were synthesized as previously described by Dr. Wayland lab [184]. Acetone and acetonitrile were from Fischer Scientific (Fair Lawn, NJ), potassium dihydrogen phosphate was from EM Science (Gibbstown, NJ), polysorbate 80 was from Sigma-Aldrich (St Louis, MO), ethanol was from Mallinckrodt Chemical (Phillipsburg, NJ), isopropanol was from Macron fine chemical (Center Valley, PA), Phosphate buffer saline tablets, butyrylcholinesterase, P. cepecia lipase, carbonic anhydrase Isozyme II and albumin were supplied by Sigma Aldrich (St Louis, MO). Docetaxel (DTX) was purchased from Alpha Aesar (Lancaster). NCI-H23 lung cancer cell line was from ATCC (Manassas, VA), RPMI 1640 was from CellGro (Houston, TX) and 96-well microtiter plates (Cellstar 655180) were from Greiner Bio-One (Germany). Millipore Di water was used for all solutions and formulations.

Methods.

Differential scanning calorimetry (DSC) was done using a TA Instruments Q200 MDSC (New Castle, DE) using a heating/cooling rate of 5 °C/min, with material loaded into normal Tzero aluminum pans.

HPLC was performed using a HP 1050 liquid chromatograph, equipped with autosampler, column oven and UV detector. An amount of 10 μ L of sample was injected in a Supercosil (1.5 cm x 4 mm, 5 μ m) LC-18 column and the analysis was performed following the method of Ostacolo et al, 2010 [190]. The sample was eluted with mobile phase consisting of potassium phosphate buffer (pH 4.5): acetonitrile 40:60 (v/v) at the flow rate of 1 mL/min. Detection of docetaxel was performed at 227 nm. Docetaxel standards were prepared in acetonitrile: water 50:50 v/v. Linearity of response for docetaxel quantitation was observed from 1 μ g/mL to 16 μ g/mL.

The size and zeta potential of the liposomes were measured using a Zetasizer Nano (Malvern Instruments) and a DTS1060 measurement cell. The readings were all made at 25°C at normal resolution, using the instrument's automated feature. For the size measurements, the volume results were used in all cases, and the results were reported as the average of 10-20 runs. Zeta potentials were measured in millivolts (mV).

PEG Assay. Two reagent stock solutions were made prior to performing the assay. The solution A contained 2.4 g barium chloride, 8 mL 6 M HCl and 32 mL deionized water while the solution B was prepared by mixing 800 mg of potassium iodide, 500 mg of iodine and 40 mL of DI water. Solution B was very concentrated and not all iodine was dissolved. A PEG2000 solution of $c = 0.2$ mg/ mL was prepared in deionized water and was used as standard. In a typical assay, a volume of 10 μ L of polymeric micelles was used for the PEG analysis and was aliquoted out in a 1 mL cuvette. Separately, aliquots of PEG standard solution were made in 7 cuvettes (0.1-10 μ g

PEG) in order to construct a calibration curve. The PEG standards and polymer dispersions were diluted to 720 μ L final volume with DI water. Subsequently, 40 μ L of solution A was added in all the cuvettes and the content was mixed thoroughly. Solution B was diluted with water in ratio of 1:5 prior to use and 40 μ L of diluted solution B was added in each cuvette. After mixing, the resulting solutions were incubated for 10 minutes at room temperature and their absorbance was recorded at 535 nm using a Hach DR/4000 UV spectrometer (Loveland, CO).

Gel Permeation Chromatography (GPC) was performed on a Shimadzu Prominence UFLC, equipped with an LC-20AD pump, vacuum degasser, column oven, and Shodex RI-71 refractive index detector, using a Phenogel column (300 x 7.8 mm, 5 micron, Phenomenex (Torrance, CA)). The samples were dissolved in DMF and were injected into the GPC circuit through a 100 μ L loop. All the samples were eluted with DMF as mobile phase at a flow rate of 1 mL/min.

UV-VIS spectroscopy. The absorbance of samples from acetone analysis, hemolysis experiment and PEG assay was recorded with a Hach DR/4000 UV-vis spectrophotometer (Loveland, CO). The wavelength used for analysis was 266 nm for acetone quantitation, 541 nm for hemolysis experiment and 535 nm for PEG calibration.

Cell culture. NCI-H23 cells were maintained in 10% fetal bovine serum (FBS) enriched RPMI medium at 37 °C in a humidified atmosphere of 95% air/5% CO₂. Twenty-four hours prior to experiment, cells were transferred to 96-well microtiter plates (Cellstar 655180, Greiner Bio-One) at a density of 5000 cells/well. All experiments were done in quadruplicate.

Preparation and characterization of drug loaded polymeric micelles. A stock solution of docetaxel (1 mg/mL, 3.5 mL) was prepared in acetone. An amount of 0.5 mL was aliquoted out in 3 vials and acetone was removed through nitrogen purging. A polymer stock solution (10 mg/mL) was also prepared in acetone and filtered through a 0.2 µm filter. An amount of 500 µL of stock solution was transferred into the docetaxel containing vial. DI water (5 mL) was added dropwise at the rate of 0.5 mL/min in each vial, under continuous stirring (600 rpm). The micelles thus prepared were sized and then dialyzed through 3500 MWCO dialysis membrane for 3 h under continuous stirring at 110 rpm. Water was changed 5 times for first 5 h and the dialysis bag was subsequently stirred overnight. A small aliquot were removed at different times to monitor the size of the micelle and their acetone content (via UV at 266 nm). When $A_{266\text{nm}}$ was less than 0.15AU, the formulation was removed from dialysis bag, filtered through 0.2 µm, sized and placed immediately in the subsequent experiment.

The yield of each formulation was determined using 10 µL of formulation via the PEG assay described above. Subsequently, a volume of 500 µL of each polymeric

micelle was introduced into a disposable Malvern DTS 1060 measurement cell and size and zeta potential was measured as described above.

For drug content analysis, one volume of micelle suspension was diluted with an equal volume of isopropanol, followed by sonication for 15 min to ensure complete micelle breakdown. Docetaxel was assessed using the HPLC method described above. Alternatively, the micelle suspension was lyophilized and the residue was dissolved into HPLC mobile phase. Drug loading and encapsulation efficiency were determined using following expression:

Drug loading = (amount of docetaxel present in the micelle/ amount of docetaxel and polymer determined)*100

Encapsulation efficiency = (actual drug loading / initial drug loaded into the micelle)*100

DSC analysis was performed as indicated above on lyophilized powder obtained from pristine and drug loaded micelles.

Docetaxel release from micelles. In vitro release of DTX from micelles was evaluated by dialysis at 37 °C in sink condition [190]. Drug loaded micelles prepared as presented above, were diluted with concentrated PBS to a final concentration 2 mg/mL polymer in PBS (0.01M phosphate, 0.027 M KCl, 0.137 M NaCl, pH = 7.4). The drug loaded micelles were placed in slide-a-lyzer mini dialysis devices (MWCO: 3500 Da, Thermo Scientific, Pierce catalog no. 88400). At least 8 micelle loaded devices were used

for each polymer. The samples were placed in 1 L of the PBS (same concentration) containing 1% albumin and thermostated at 37 °C (sink condition occurred). At scheduled time intervals (15 min, 30 min, 1 h, 2 h, 4 h, 24 h, 1 day, 4 days, 7 days, 24 days and 28 days) one device for each polymer was taken out of the external release medium and analyzed for the amount of DTX still encapsulated using HPLC as described above.

Critical aggregation concentration (CAC). The concentrated pristine (unloaded) polymeric micelle were diluted sequentially and sized at various time points using DLS. CAC is the concentration at which micelle dissemble into individual polymeric units.

Enzymatic degradation of polymeric micelles

Evaluation of enzymatic activity. The esterase activity of various enzymes including carbonic anhydrase (Isozyme II), butyrylcholinesterase, P. cepacia lipase and albumin were evaluated using UV spectrophotometry for the hydrolysis of p-nitrophenyl acetate, which was used as a substrate for all these enzymes. A substrate stock solution of 6.3 mg/mL was constituted in ethanol and 500 μ L of this stock was diluted with 50 mL of DI water prior to analysis. All the enzymes stocks were prepared at the minimal concentration of 1 mg/mL. In a typical experiment, 800 μ L of substrate, 100 μ L of concentrated (10X) PBS was introduced into 1 mL cuvettes, which were subsequently

thermostated at 37 °C. An amount of 100 µL of enzyme stock solution was added to initiate the reaction. The absorption of the mixture was recorded at 405 nm at different time intervals. A control sample with no enzyme in it was also recorded.

Enzymatic degradation of polymeric micelles. Stock solutions of Carbonic anhydrase, butyrylcholinesterase, lipase, and albumin were prepared 10X more concentrated than their physiological physiological concentration in the human body, namely 40 U/mL (1 mg/mL) for P. Cepecia lipase, 40 U/mL (2 mg/mL) for butyrylcholinesterase, 1 mg/mL for carbonic anhydrase and 500 mg/mL for human albumin. The polymeric micelles were diluted to the same concentration of 1.25 mg/mL. All these stocks are used to analyze enzymatic activity on the micelles using gel permeation chromatography (GPC) and/or dynamic light scattering (DLS).

GPC analysis was performed for P. Cepecia lipase. In a typical experiment, five vials were taken for each polymer. Each vial received 800 µL of polymeric micelles (1.25 mg/mL), 100 µL of concentrated PBS and 100 µL of enzymatic stock. All the eppendorfs were incubated at 37 ° C in a water bath. Each hour, one eppendorf containing polymeric micelles was taken out and was frozen in a dry ice/acetone bath and subsequently stored in freezer at -20 °C. After five hours, all the frozen samples were lyophilized overnight using the Speed Vac. The next day, 150 µL of dimethyl formamide (DMF) were added to the lyophilized powder in each vial and the solution was centrifuged for 5 minutes. Subsequently, 100 µL of supernatant were aliquoted out and injected into GPC system for enzymatic degradation analysis.

DLS analysis was carried out for lipase, carbonic anhydrase, butyrylcholinesterase, albumin (alone) and their binary combinations which includes lipase with albumin; carbonic anhydrase with albumin; and Butyrylcholinesterase with albumin in order to mimic the environment encountered in the blood vessels. A separate cuvette was used for each polymeric suspension. Similar to GPC, each cuvette received 800 μ L of polymeric micelles (1.25 mg/mL), 100 μ L of enzyme stock and 100 μ L of concentrated PBS (10X). All the cuvettes were incubated at 37 ° C in a water bath. For each selected points, the sample mixtures were read for size and then returned to the water bath.

Stability Studies:

Shelf stability. The drug loaded polymeric micelle were placed in di-ionized water and stored at room temperature for few weeks. The particle size of micelles was measured at various intervals after storage.

Long term Stability. Freshly prepared polymeric micelle were placed at 4 C for 7 months and then analyzed in terms of size, appearance, polymer concentration and drug loading as indicated above.

Cell viability/ proliferation assay. NCI-H23 cells were plated in 96 well plates at a density of 5000 cells/ well. After 24 h incubation at 37 °C in the incubator, the media was removed and cells were washed with 200 μ L sterile PBS. After removal of PBS, they

were treated with 200 μ L of nanocarrier suspension in media containing 10 % FBS. The concentration of docetaxel in the nanocarrier was 10^{-5} , 10^{-6} , 5.10^{-7} , 5.10^{-8} , 10^{-8} , 5.10^{-9} , 10^{-9} , 5.10^{-10} , 10^{-10} , 10^{-11} M. Each concentration was assessed in quadruplicate. Three self assembled nanocarriers from PEG45PCL64, PEG45-PBO6-PCL58, PEG45-PBO9-PCL61 were assessed, together with a polysorbate 80 / Ethanol / DTX formulation (72.8, 24.3, 2.9 wt%) equivalent Taxotere[®].

After 72 h incubation time, the media was removed and cells were washed with 200 μ L PBS. After removal of PBS, each well received 100 μ L of a WST-1 solution in media obtained by diluting 1 volume WST-1 solution (Roche) with 10 volumes of RPMI media with 10 % FBS and cells were returned to 2 hr incubation. The amount of formazan formed was readed after 3 hours via absorbance at 450 nm (A450). Absorbance at 650 nm was deducted from A450. Viability was expressed as % of control

Hemolysis test. Hemolysis studies were carried out on DTX-loaded polymeric micelles and Taxotere[®] formulation having the same amount of loaded DTX. Briefly, freshly collected mouse blood was centrifuged at 3000 rpm for 5 min to sediment the red blood cells (RBCs). The supernatant was discarded and the RBC pellets were washed five times with 150 mM NaCl followed by centrifugation at 3000 rpm for 5 min. The RBC pellet was finally diluted 1:10 with isotonic PBS. RBC suspension (80 μ L) was added to 0.72 mL of polymeric micelles or Taxotere[®] in PBS at a DTX concentration of 0.15 mg/mL. A sample containing only polysorbate 80 (same amount as in Taxotere[®]) was done in parallel to access the toxicity of the vehicle in Taxotere[®] formulation. After incubation at

37 °C for 30 min, samples were centrifuged at 3000 rpm for 5 min to remove non-lysed RBC. The supernatants were collected and analyzed for hemoglobin content by monitoring absorbance at 541 nm. Positive and negative controls were made using DI water or PBS (0.72 mL). The degree of hemolysis was determined by the following equation:

$$\%hemolysis = \frac{(absorbance\ of\ sample) - (absorbance\ of\ blank)}{highest\ absorbance\ for\ positive\ control} \times 100$$

where ABS_{100} and ABS_0 are the absorbances of the solution at 100% and 0% hemolysis, respectively. Results are reported as mean of three measurements \pm SD.

Results and Discussion

The nanoprecipitation method is a simple, efficient method for drug loading of polymeric micelles, which was used in our study. A solution of polymer and drug in acetone made at a certain polymer/drug mass ratio was diluted with water or buffer causing the self-assembling of the polymer and the simultaneous encapsulation of the drug. Acetone was subsequently removed via dialysis through semi-permeable membranes (either 10000 or 3500 MWCO) overnight. UV-Vis confirmed complete acetone removal ($A_{266} < 0.3$ AU). A control experiment (no drug) was performed in parallel and is shown in Figure 23.

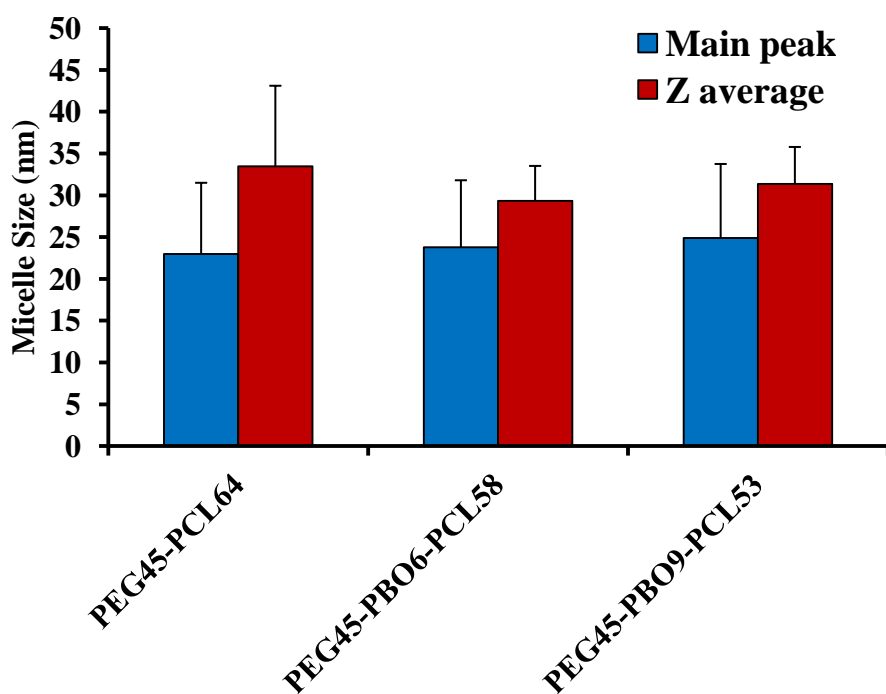


Figure 23: Size of the micelles generated from the amphiphilic block copolymers PEG₄₅PCL₆₄, PEG₄₅PBO₆PCL₅₈ and PEG₄₅PBO₉PCL₅₃ in water using nanoprecipitation from acetone, followed by dialysis.

Data from Figure 23 reveals that there is a difference between the Z_{avg} of the formulations and the main peak read by the instrument. The Z_{avg} parameter is defined as the hydrodynamic diameter of a monodispersed system equivalent to the polydispersed system analyzed. This difference reflects the degree of polydispersity of the formulation. One can observe that the micelles generated from the diblock copolymer are more polydisperse than the ones generated from the triblock copolymers. The size of the PBO block does not influence the micelle polydispersity in a significant way. Interestingly, the main peak observed in each micelle formulation is identical across the formulation. This was as expected since the two triblock copolymers were engineered to have a hydrophobic segment about the same size as the one in the diblock congener. In other words, the PBO segment does not influence the main peak of the formulation but significantly influences the polydispersity of the formulation. Two triblock copolymers generate more homogenous formulations, fact that can be also observed if one considers the Z_{av} fluctuation interval.

For loading the polymeric micelles, docetaxel was added to the polymer acetone solution in a mass ratio of 9/1 polymer/DTX (10% drug) or 3/1 (polymer/DTX (25% drug) keeping the rest of the formulation procedure and parameters identical. The size of the DTX loaded micelles is shown in Figure 24.

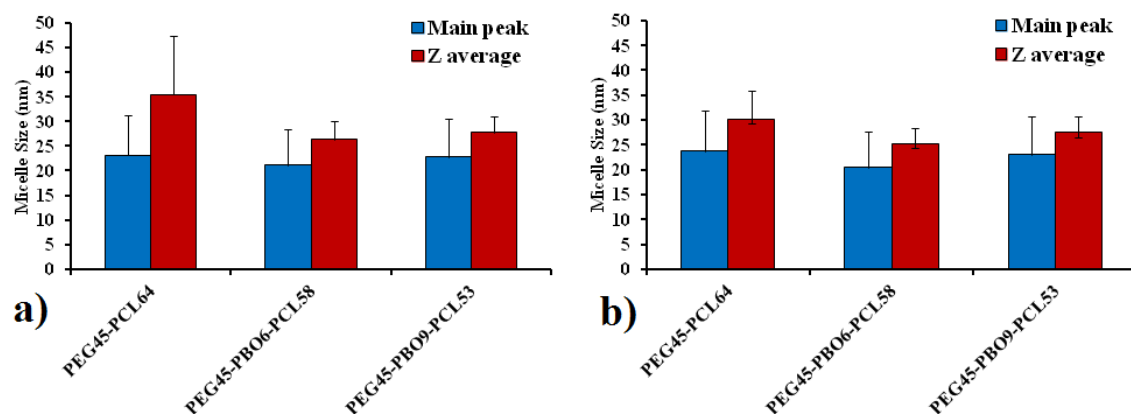


Figure 24: Size of the micelles generated from the amphiphilic block copolymer PEG₄₅PCL₆₄, PEG₄₅PBO₆PCL₅₈, PEG₄₅PBO₉PCL₅₃ and doctexel (mass ratio polymer/drug = 9/1 (a) and mass ratio polymer/drug = 3/1 (b)) in water using nanoprecipitation from acetone, followed by dialysis.

Analyzing the data in Figure 24, one can observe that drug loading did not change significantly the micelle size irrespective of initial loading ratio polymer/drug. The main peak of the formulations remained at around 24 nm. In terms of polydispersity of formulations, it can be observed that DTX loading leveled the differences between different formulations and the leveling effect is more pronounced when more drug was present (compare Figure 24a and 24b). This was expected since the loading of the drug in between the hydrophobic polymer chains (driven only by hydrophobic interactions) effectively alleviates any effects of the modified interface.

We subsequently analyzed the drug loading and the encapsulation efficiency for the polymeric micelles at the two initial polymer/DTX ratio mass ratio (9/1 and 3/1). This was achieved via lyophilization of the formulations, dissolution of the solid materials in MeCN/H₂O followed by HPLC analysis. The results are shown in Table 3.

Table 3: Docetaxel loading and encapsulation efficiency of PEG₄₅PCL₆₄, PEG₄₅PBO₆PCL₅₈, PEG₄₅PBO₉PCL₅₃ micelles at two different initial loadings ratio polymer/drug (9/1 and 3/1).

Polymer used for drug encapsulation	Actual drug loading (%) of polymeric micelle		Encapsulation efficiency (%) of polymeric micelle	
	10% DTX-loaded	25% DTX-loaded	10% DTX-loaded	25% DTX-loaded
PEG45-PCL64	5.8	10.9	58.09	43.8
PEG45-PBO6-PCL58	8.75	8.5	87.5	34.1
PEG45-PBO9-PCL53	9.12	11.45	91.2	45.8

Data from Table 3 revealed that the amount of drug loaded and the encapsulation efficiency depended on the nature of block copolymer used and especially on the polymer/drug ratio, as observed also by others [190]. The encapsulation efficiency at high polymer/drug ratio (3/1) was quite low and can be explained by the micelle destabilization due to drug overloading. The drug overloading causes coalescence of the individual micelles in larger aggregates, which are removed in the process of filtration of formulations through 0.2 μm filter. The result is the rather uniform size of the final micellar formulation, confirming the leveling effect of drug on the modified polymeric interface.

At lower initial polymer/drug mass ratio, the encapsulation efficiency of the block copolymer is substantially improved and the effect of engineered block interface can be easily evaluated. The triblock copolymers were loaded with DTX more efficiently than the diblock cogener. The encapsulation efficiency increases with the elongation of the

PBO segments, reaching the maximum for the PEG45PBO9PCL53. We hypothesize that the PBO segment in the triblock copolymer “softens” the hydrophilic-hydrophobic interface and keeps the individual CL chains less packed than in PEG45-PCL64 diblock, thus allowing a better loading and a greater (loaded) micelle stability (see Figure 25a for representative cartoons).

In order to confirm this hypothesis, we performed DSC analysis of lyophilized DTX loaded micellar formulations together with similar analysis of the pristine (unloaded) formulations. It is known that the thermal behavior of the amphiphilic block copolymers dictates the thermodynamic and kinetic stability of these nanosystems. In fact, the PEG-PCL amphiphilic block copolymers have attracted wide attention due to its semicrystalline, hydrophobic but hydrolytically degradable nature of PCL and “stealth” properties of the PEG brush. The DSC traces of lyophilized naked polymeric micelles upon first heating were shown in Figure 25b. PEG45-PCL64 block copolymer has a weight fraction of PEG of approximately 21%. It was previously shown that the melting of PEG block is observable for PEG weight fraction in the parent polymer bigger than 20% [191, 192]. Also, it is known that PEG block in PEG-PCL copolymers broadens the melting peak of PCL due to retardation in crystallization by PEO. Thus, the DSC trace of PEG45-PCL64 shows a small transition for PEG at 36.36 °C, followed by a bigger transition for PCL at 55.51 °C. Insertion of PBO block impedes the crystallization of PEG segments and wipes out the PEG transition for PEG45-PBO6/9-PCL58. This might also explain fast and easy formation of polymeric micelles through nanoprecipitation, since PEG is in the amorphous form and can readily hydrate. The high steric demand of the PBO segment also softens the packing of PCL at interface, resulting in shifts of CL

melting temperature to lower values (see Figure 25a for a cartoon representation). Consequently, a second peak for CL is generated at lower temperature, reflecting a diminished local crystallinity. Moreover, overall CL packing decreases with increase of PBO length, causing a shift of the transition temperature from 55.51 °C (no BO) to 55.08 °C (6 BO units) to 54.94 °C (9 BO units).

Considering the loaded polymers, one can observe that the loading of drug have smoothened the thermal transitions of amphiphilic block copolymeric micelles. Drug loading also decreased the transitions temperature and enthalpy of all loaded polymeric micelles, as compared to their unloaded micelle counterparts. This thermal behavior suggests the reduction in degree of the crystallinity of the polymeric micelles as a result of drug loading, as expected.

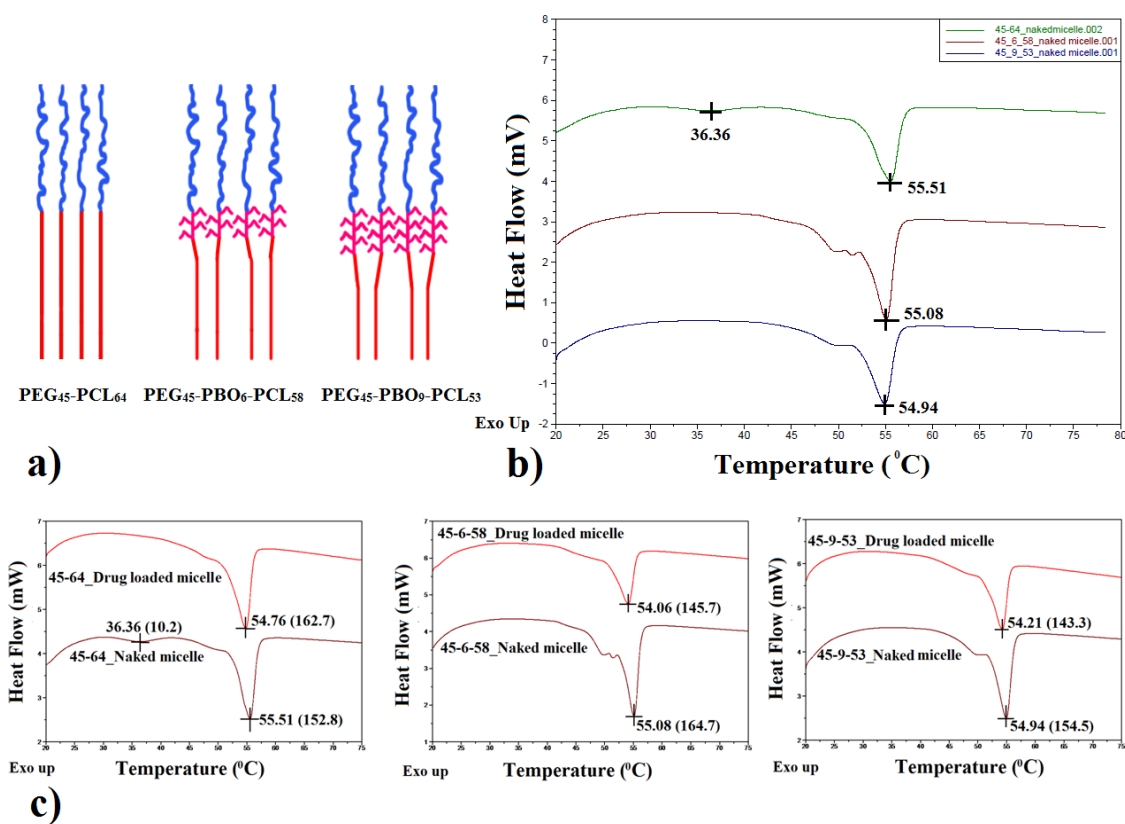


Figure 25: **(a)** Cartoon of the representative amphiphilic block copolymers showing the influence of PBO interface on the crystallinity of the CL block; **(b)** DSC traces of lyophilized naked micelles **(c)** Comparative DSC traces of docetaxel loaded (top) and unloaded (bottom) micelles of PEG₄₅-PCL₆₄, PEG₄₅-PBO₆-PCL₅₈ and PEG₄₅-PBO₉-PCL₅₃

Since DSC experiments confirmed the destabilizing effect of docetaxel on micelle formation and stability, we decided to optimize the process of drug loading. We hypothesized that the micelle destabilization is due to the overloading of polymeric micelles that can change the packing parameter of the amphiphiles and the structure of

the interface. Hence, we focused on the 9/1 polymer/drug mass ratio that gave best preliminary results and was also the most economic ratio in terms of maximizing the amount of drug and polymer components that were translate in the final formulations.

On the other hand, it is known that acetone acts as an amphiphilic solvent and helps the lipophilic DTX percolates in the hydrophilic interior of the micelle. It also helps the organization of the materials at the hydrophilic-hydrophobic interface, being slowly eliminated during the dialysis process. The removal process occurs rather fast when dialysis membranes with 10000 MWCO are use. Consequently, we decided to replace the 10000 MWCO membranes with 3500 MWCO membranes ones. This modification is expected to slow down considerably the acetone removal, with benefic effects towards micelle loading and stability. Moreover, the use of a membrane with smaller pores was expected to increase the yield of the polymeric micelles and the encapsulation efficiency by limiting the loss of material (DTX and polymer) through the dialysis bag pores. The results of this new loading experiment are presented in Table 4. All parameters were kept identical except MWCO of dialysis bag that was changed from 10000 to 3500.

Table 4: The main physicochemical characteristics, nanoparticles yield, drug loading and drug encapsulation efficiency of docetaxel loaded polymeric micelles

Polymer used for drug encapsulation	Yield (%)	Hydrodynamic size (D_H , nm)		Zeta potential (mV)		Actual drug loading (%) of polymeric micelle	Encapsulation efficiency (%) of polymeric micelle
		Unloaded	DTX-loaded	Unloaded	DTX-loaded		
PEG45-PCL64	78.11	22.98 ± 8.51	26.80 ± 5.33	-4.89	-1.52	9.7	97.9
PEG45-PBO6-PCL58	84.8	23.79 ± 8.00	25.45 ± 4.73	-5.44	-1.11	8.4	84.5
PEG45-PBO9-PCL53	91.46	24.88 ± 8.86	23.3 ± 3.28	-4.31	-5.44	10	100

Data from Table 4 confirmed the substantial impact of the dialysis bag pores in the formulation process and allowed a more detailed view on the impact of different structural parameters on polymeric drug loading. One can observe that the diblock copolymer generated the most heterogeneous formulation, which also had good encapsulation efficiency, much improved in comparison with previous experiment. The homogeneity of the DTX formulation further improved with PEG45-PBO6-PCL58 and reached the maximum for PEG45-PBO9-PCL53. The yield of micelles obtained followed the same trend, confirming the significant impact of the PBO segment on DTX- loaded micelle formation and stability. The encapsulation efficiency was somehow lower for PEG45-PBO6-PCL58, which in conjunction with the DSC data, reveals the impact of engineered PBO interface on drug encapsulation and allows the selection the optimal length for this polymer block.

The size of all polymeric micelles below 30 nm, which allow us to anticipate the achievement of a high extravasation efficacy, based on enhanced permeation and retention (EPR) effect [193, 194]. The zeta potentials of all the formulations were also quite similar with the DTX loaded micelles derived from PEG45-PBO9-PCL53 having the most negative value.

The leaky vasculature and poor lymphatic drainage of the solid tumor enables the passive accumulation of the drug loaded micelles inside the tumor (EPR effect) [193]. Ideally, the drug delivery system should have a long circulation time to fully exploit the EPR effect [195]. Maeda's group has shown that the "Area under the curve" (AUC) must be high for more than 6 h for rats and mice for optimal drug accumulation at the tumor through EPR effect [196]. Since, the long circulation life and stability of the polymeric

micelles depends upon the thermodynamic and kinetic parameters of the assembly [195], we analyzed both these parameters in detail.

Focusing on the thermodynamic aspects of self assembling, it must be emphasized that when the drug loaded polymeric micelles are administered intravenously, these micelles will be diluted in 5.5 L of human blood. The dilution can significantly restrict the thermodynamic stability of the DDSs in vivo [195]. The micelle based delivery systems should not dissemble upon dilution in order to maintain efficient delivery of drug to the target site. In this context, a key parameter to be evaluated is critical aggregation concentration (CAC), defined as the minimum concentration of the amphiphilic block copolymer needed to form a self assembled micelle. CAC has an important influence on the drug delivery capacity of the polymeric micelles. Low CAC is desirable for better drug retention in the polymeric micelle in vivo upon dilution. It has been shown that administration of the PEG-PCL micelles below the CAC results in rapid elimination of the copolymers from the circulation [195]. We have determined CAC (via DLS) for the three polymeric micelles by plotting the size of the micelles versus their concentration at 25 °C (Figure 26). Analyzing the data in Figure 26, one may observe that both diblock and triblock polymeric micelles have very low CAC, which makes them an ideal candidate for a drug delivery system. It can also be observed that the sigmoidal transition from pre-micellar phase to post-micellar phase of the PEG45-PBO6/9-PCL58/53 is not abrupt, as compared to diblocks polymeric micelles. This additional stabilization effect might be due to the PBO segment, which acts as cushion at the interface and smoothen the pre/post-micellar transition of the polymeric micelles. Lower CAC for triblocks and diblock copolymers projects better drug retention and delivering capacity of the

corresponding polymeric micelles and are consistent with the known CAC values of amphiphilic block copolymer micelles reported in the literature [152, 197].

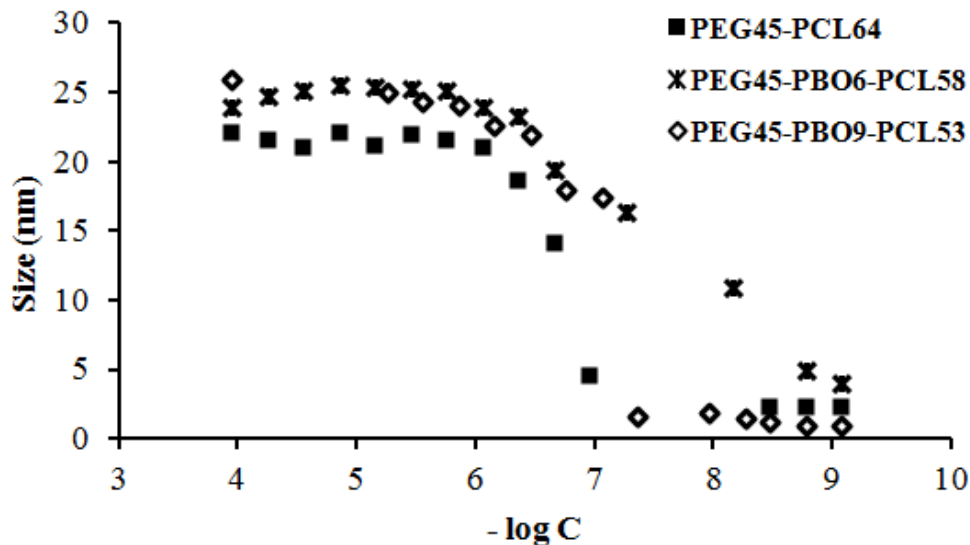
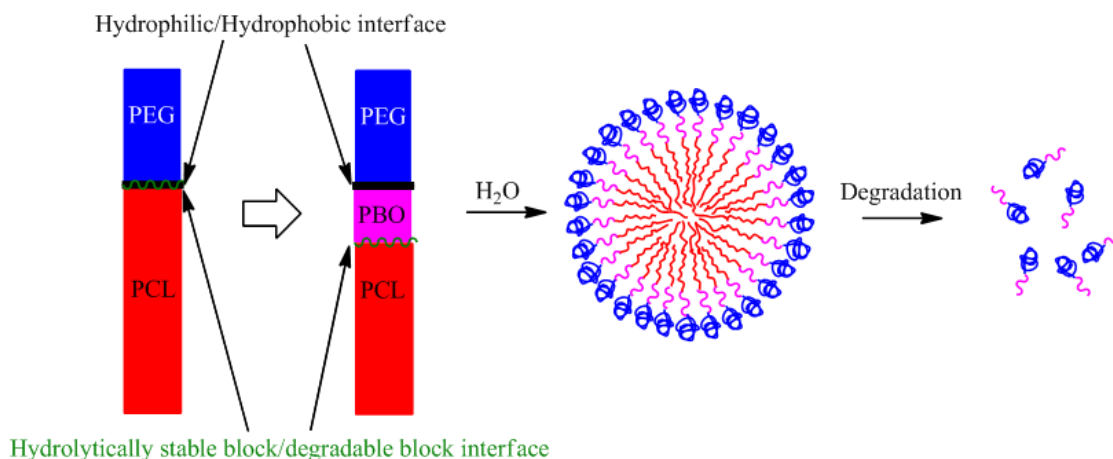


Figure 26: Self assembling of the three amphiphilic block copolymers in water at 25 °C followed by DLS, revealing the Critical Aggregation Concentration (CAC) of the polymeric micelles

The kinetic parameters of the self assembling process related to the spontaneous and enzyme catalyzed degradation of the polymer micelles, which contributes to the shortening of circulation life and to the premature drug release of the drug from the polymeric micelles in vivo. The enzymatic degradation of polymeric micelles have been studied extensively in the literature [176, 184]. It is known that polymeric micelle degradation is generally triggered by water molecules that percolate the self assembled polymeric micelles and induce the chemical degradation of the polymer core, creating oligomers and monomers [198]. The micelle degradation process occurs either passively

through hydrolysis or actively via enzymatic reactions [199]. The factors that are influencing these processes are complex and include the type of chemical bonds of the polymer, the pH, copolymer composition and water uptake [198]. The CL units in the PEG-PCL block copolymers are connected by hydrolytically cleavable ester bonds. The boundary between the non degradable (PEG) and degradable (PCL) block coincides with the hydrophilic-hydrophobic interface in PEG-PCL diblock copolymers. It is easy for water molecules and esterase enzymes to reach ester interface, and catalyze the hydrolysis of the ester bond between the PEG block and the polyester hydrophobic core. We hypothesized that the insertion of PBO will move the hydrophilic-hydrophobic junction away from the PCL interface ester group, which could prevent the access of water and esterases to this vulnerable bond, thus providing a strategy for tuning the micelle stability (Scheme 2).

In order to prove this hypothesis, we carried out the enzymatic catalyzed degradation studies of polymeric micelles using three classes of esterases found in human blood. Our objective was to evaluate the stability of PEG45-PCL64 diblock micelles, in comparison with PEG45-PBO6/9-PCL58/53 triblock polymeric micelles for esterase catalyzed micelle degradation in PBS at 37 °C.



Scheme 2: Cartoon revealing the interfacial engineering of PEG-PCL block copolymers and the structure and dynamic of the novel triblock copolymers as novel polymeric drug delivery systems

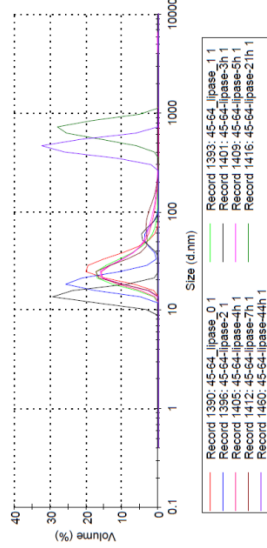
Thus, the stability of the three types of polymeric micelles was evaluated in presence of several esterases including lipase (*P. Cepacia*), butyrylcholinesterase, carbonic anhydrase, albumin and their binary combinations, through DLS and GPC. In a typical experiment, preformed polymeric micelles (1mg/mL) were incubated with enzymes (at their physiologic concentration) in PBS at 37 °C and the size of the polymeric assemblies was recorded at different time points using DLS (Figure 27).

We monitored the degradation of all three polymeric micelles in PBS at 37 °C by *P. Cepacia* lipase (Figure 27a), butyrylcholinesterase (Figure 27b), carbonic anhydrase (Figure 27c) and human albumin (Figure 27d) via DLS. Data from Figure 27 showed that the PEG45-PCL64 polymeric micelles were degraded completely after seven hours of incubation with the *P. Cepacia* lipase, as revealed from the change in the size of the

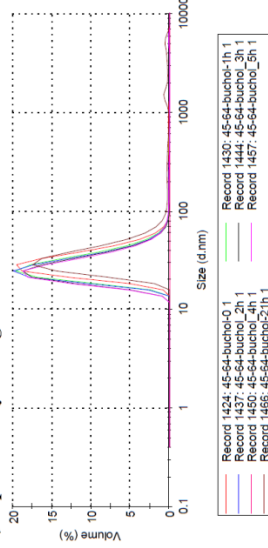
micelles over time. However, triblock micelles PEG45-PBO6-PCL58 have resisted the micelle degradation for up to 21 hours and PEG45-PBO9-PCL53 micelles displayed an even better resistance to hydrolysis, remaining unperturbed after 24 h incubation time with *P. Cepacia* lipase. The higher stability of the triblock copolymer micelles, as compared to diblock polymeric micelles is due to the separation between hydrolytically-cleavable interface (PBO-PCL) and the hydrophilic-hydrophobic (PEG-PBO) interface provided by PBO. The experiment also reveals that the longer PBO segment (9 BO units) was more efficient than the shorter one (6 BO units) (Figure 27a). Another important conclusion of this experiment is that the enzyme docks at the hydrophilic-hydrophobic interface and initiate the hydrolysis of the PCL core. NMR experiments performed by Dr. Xiaobo Zhu [184] confirmed this hypothesis.

On the other hand, butyrylcholinesterase (Figure 27b) and carbonic anhydrase (Figure 27c) were much less efficient toward the hydrolysis of the polymeric micelles, revealing the importance of the compatibility of the structure of the active site of the esterase with the structure of the substrate that is to be processed. Last but not least, albumin, an amphiphilic protein present in abundance in blood and displaying weak esterase activity [200] was able to slowly degrade the diblock copolymer (Figure 27d). The triblock copolymer micelles were significantly more resistant to hydrolysis by albumin, with the micelles derived from the PEG45-PBO9-PCL53 being the most resilient, similarly to the lipase experiment (compare Figure 27a with Figure 27d)

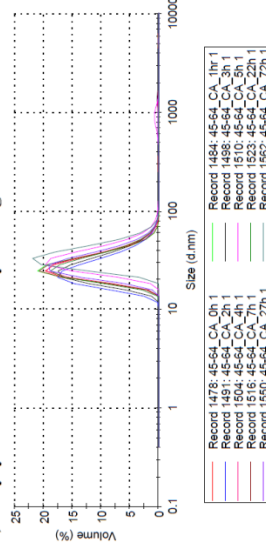
PEG45-PCL64



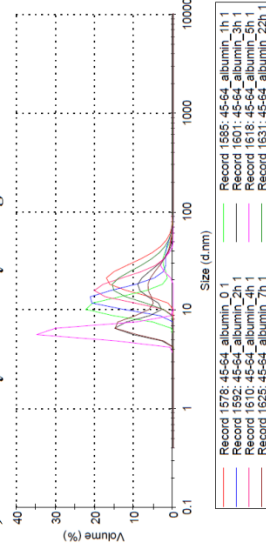
a) Lipase catalysed degradation



b) Butyrylcholinesterase catalysed degradation

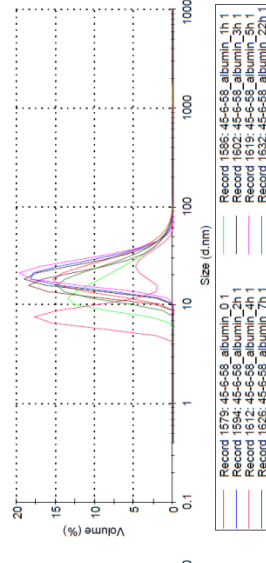
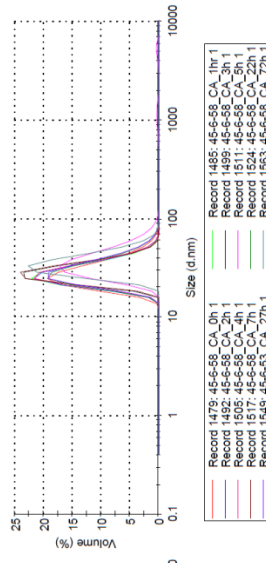
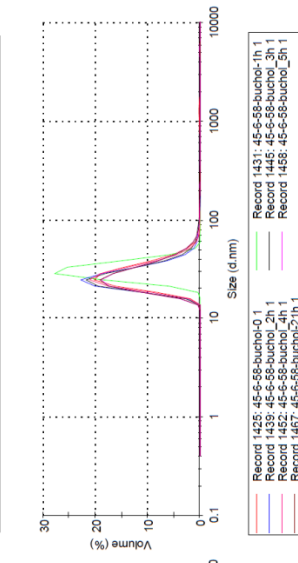
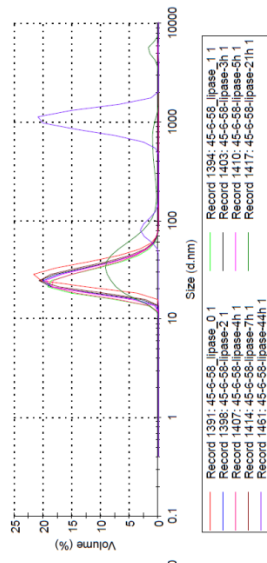


c) Carbonic Anhydrase catalysed degradation



d) Albumin catalysed Degradation

PEG45-PBO6-PCL58



PEG45-PBO9-PCL53

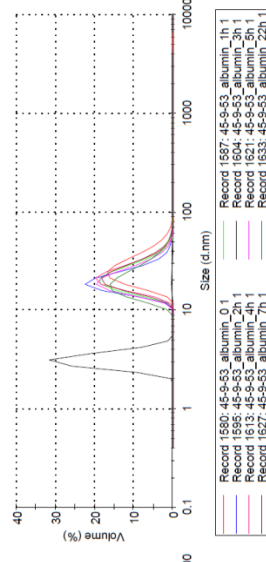
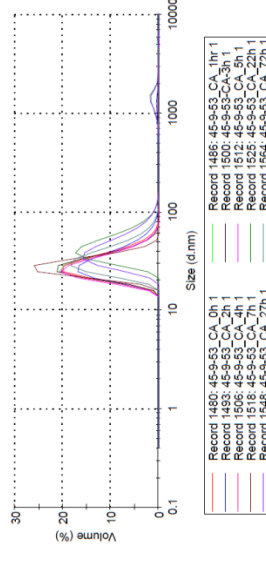
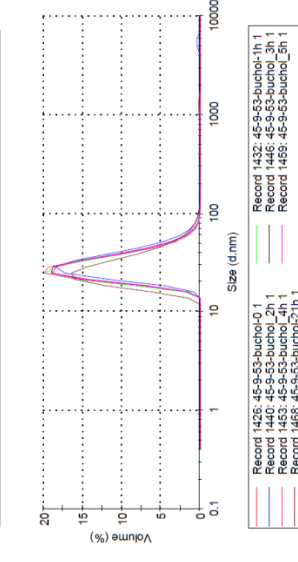
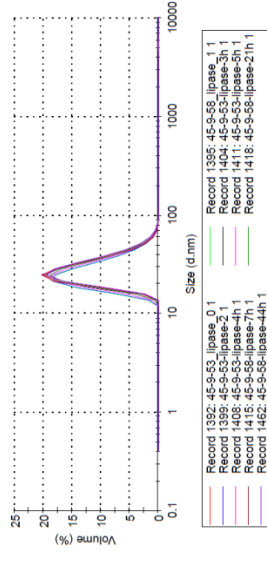


Figure 27: Time dependent degradation of polymeric micelle in PBS at 37 °C by lipase (a), butyrylcholinesterase (b), carbonic anhydrase (c) and albumin (d) monitored by DLS

The result of DLS analysis of lipase catalyzed polymeric micelles degradation (Figure 27a) was also confirmed by GPC analysis of the same process (performed by Dr. Xiaobo Zhu). In this case, the degradation of the polymeric micelles was monitored by the reduction in the area of the main peak of GPC trace corresponding to pristine (intact) copolymer and the corresponding increase in the area of the monomer/oligomers peaks (Figure 28). The GPC traces of all three micelles were compared after 4 h incubation time with lipase. One can clearly observe that the PEG45-PCL64 polymeric micelles were substantially degraded by lipase enzyme, followed by PEG45-PBO6-PCL58 and PEG45-PBO9-PCL53 micelles (Figure 28). The decreased rate of lipase catalyzed polyester hydrolysis monitored by DLS and GPC experiments proved the success of interfacial engineering of the PEG-PCL diblock copolymers and the superior resilience of triblock micelles compared to diblock ones.

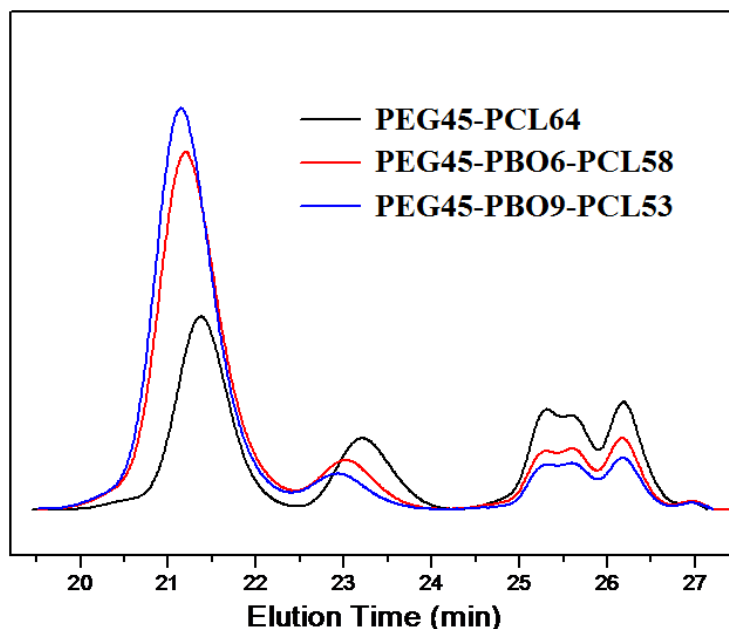


Figure 28: GPC traces for DMF solutions that contain all the products from the *P. cepacia* lipase catalyzed hydrolytic degradation of PEG₄₅-*b*-PBO_{*n*}-*b*-PCL₆₀ (*n* = 0, 6, 9)

micelles in aqueous PBS (pH = 7.4) at 37 °C and at a constant reaction time of 4.0 hours (t = 4.0 h) [184]

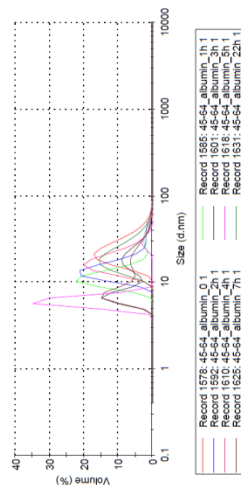
The observed degradation of polymeric micelles by lipases and albumin prompted us to perform another experiment in order to better mimic the conditions encountered by these micelles in vivo, upon I.V. administration. Human blood has 35-50 g/L of albumin protein, which is well known for its interactions with drugs due to its amphiphilic nature. Despite being a weak esterase, very high concentration of albumin in serum can significantly affect the drug delivery system. Therefore, lipase catalyzed degradation of polymeric micelles was conducted again under similar conditions but in the presence of albumin as interfacial destabilizer (and second esterase) (Figure 29). An analysis of data from Figure 29 has shown that albumin accelerates the enzymatic degradation of polymeric micelles significantly. PEG45-PCL64 polymeric micelles were degraded by lipase within one hour under the new conditions, whereas PEG45-PBO9-PCL53 resisted the enzymatic degradation for a few hours (Figure 29b). It must be noted here that the albumin concentration used in the experiment (1 g/L) was smaller than the actual concentration of albumin present in the serum (50 g/L) for the sake of experiment feasibility (high albumin concentration can mask the DLS signal of micelles). The net effect of albumin would be expected to be much stronger than the in vivo observed degradation of the polymeric micelles in this experiment. The PEG45-PBO9-PCL53 polymeric micelles have shown the resistance to enzymatic degradation even in these extreme hostile conditions, thus confirming their superiority over PEG45-PCL64 polymeric micelles. Under similar conditions, butyrylcholinesterase, carbonic anhydrase

enzymes were not able to degrade the polymeric micelles even in the presence of albumin (Compare Figure 29a with Figure 29c and Figure 29d).

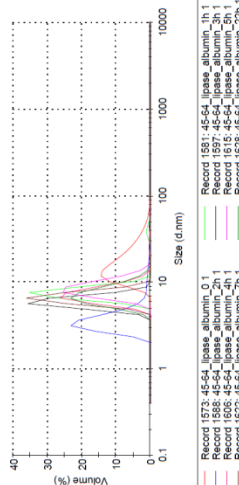
PEG45-PCL64

PEG45-PBO6-PCL58

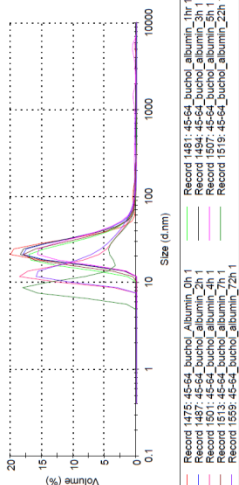
PEG45-PBO9-PCL53



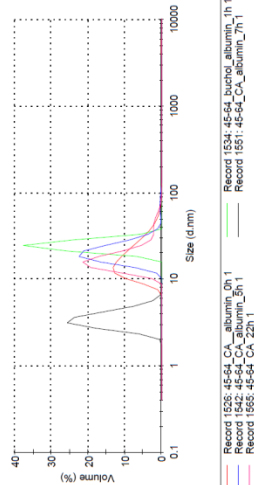
a) Albumin catalysed Degradation



b) Lipase catalysed degradation



c) Butyrylcholinesterase catalysed degradation



d) Carbonic Anhydrase catalysed degradation

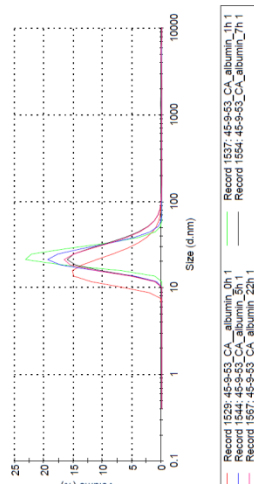
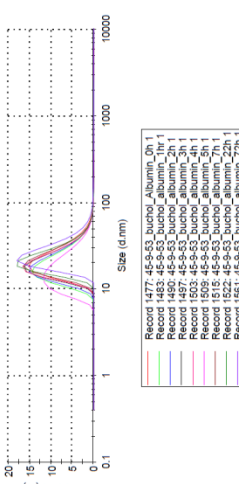
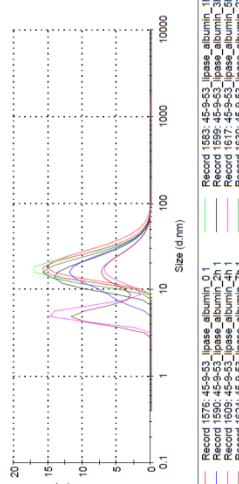
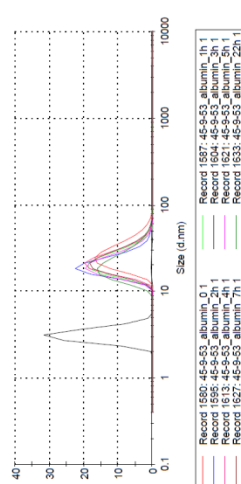
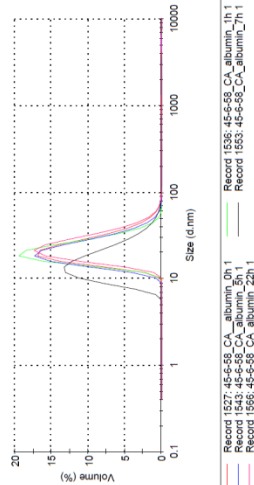
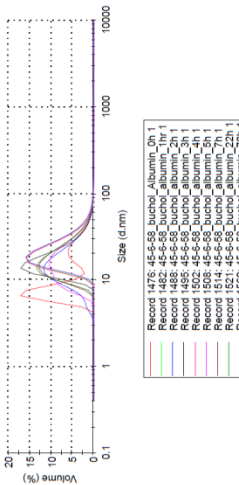
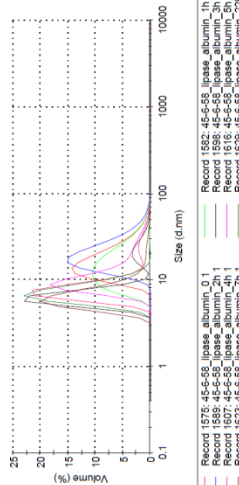
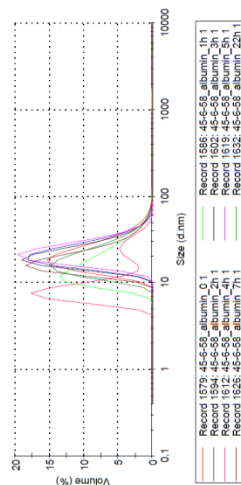


Figure 29: Effect of albumin alone (a), of a binary mixture of lipase and albumin (b), butyrylcholinesterase and albumin (c) and carbonic anhydrase and albumin (d) on degradation of polymeric micelles in PBS at 37 °C

It can be concluded that the enzymatic degradation of PEG45-PCL64 polymeric micelles in PBS at 37 °C is highly dependent on the nature of enzyme and on the presence of other amphiphilic proteins such as albumin. Only lipase enzymes are structurally adapted and have the necessary interface to dock to the micelle interface and hydrolyze the core of the polymeric micelles. Engineering the hydrophilic/hydrophobic interface in PEG-PCL via insertion of a hydrophobic non-biodegradable PBO block constitutes an efficient way to reduce the susceptibility of amphiphilic polymeric micelles towards enzymatic hydrolysis, thus increasing their circulation time.

Besides various enzymes and amphiphilic proteins, drug loaded polymeric micelles will also encounter red blood cells (RBCs) during their circulation. The ideal delivery system should not be toxic to RBCs. Consequently, the docetaxel-loaded polymeric micelles were tested for their toxicity to RBCs at a docetaxel concentration of 0.15 mg/mL. The results were compared with the commercial available docetaxel formulation (Taxotere®) and its component polysorbate 80 (Figure 30). Data from Figure 30 revealed that the RBC toxicity in Taxotere is mainly due to polysorbate 80, which justifies the search for a better delivery system. All three DTX-loaded polymeric micelles were tested at the same loaded drug concentration of 0.15 mg/mL and were found to be less toxic than commercially available formulation. This low toxicity of polymeric micelles towards RBC pleads for their safe use as an i.v. injectable vehicle for docetaxel delivery. Interestingly, micelles derived from diblock PEG45-PCL64 were the most toxic among the three polymeric micelles tested, confirming again the superiority of triblock micelles over diblock one. However, PEG45-PBO6-PCL58 was observed to be less toxic than PEG45-PBO9-PCL53. This suggests that longer PBO might also not be favorable to

RBCs and, thus optimal PBO length is needed for generating drug delivery system with reduced hemolytic activity.

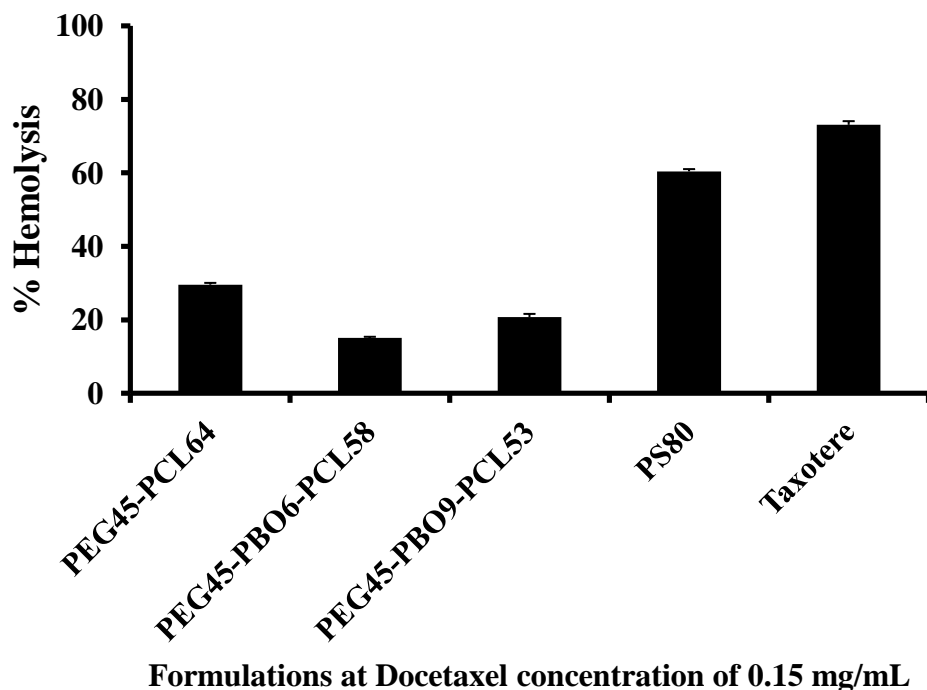


Figure 30: Hemolysis of docetaxel-loaded polymeric micelles at fixed concentration of drug (0.15 mg/mL), in PBS at 37 °C

Conceptually, after crossing the above-mentioned barriers, drug loaded polymeric micelles should release the loaded drug actively or passively at the target site. Thus, the drug can be released from the carrier by one process or by a combination of many processes including diffusion of drugs out of the polymeric micelles; solvent and amphiphilic compound percolation into the nanoparticles, and/or enzymatic degradation of the carrier with release of the loaded drug. Many techniques are reported in literature to study the drug release from the carrier such as membrane diffusion technique[190], sample and separate technique [201], in situ methods[202], etc.

In our case, the drug release process was studied on the same polymer sets, in sink conditions, using the dialysis bag diffusion technique in combination with HPLC quantification of remaining drug in polymeric nanoparticles as described in the literature [188, 190, 203, 204]. The DTX release profile was assessed as a function of polymer structure and supramolecular assembly properties. The drug loaded polymer micelles were placed in inserts having a dialysis membrane bag (3500 MWCO) under sink condition. If the drug is poorly soluble in water, it is permissible to add non-aqueous solvent or solubilization agents to the sink [205]. It must also be emphasized that the serum concentration of albumin is 35 - 50 g/L, which will impact the drug release from the polymeric micelles carrier. As we are using a poorly soluble hydrophobic drug (docetaxel) as a model drug in this study, 1% albumin was added to the sink as a receiving phase. Mention must be made that albumin cannot pass the pores of 3500 MWCO membrane. The PEG45-PCL64 micelles have released 50 % of the drugs within few hours, whereas triblocks PEG45-PBO6-PCL58 and PEG45-PBO9-PCL53 have shown sustained release of the drug for a longer time with a better release profile, as shown in Figure 31. Overall, PEG45-PBO6-PCL53 polymeric micelles have displayed the best drug retention and release over time, allowing for a higher amount of drug to be delivered through EPR to the target site, which will increase the therapeutic efficacy and reduce the systemic toxicity of the treatment.

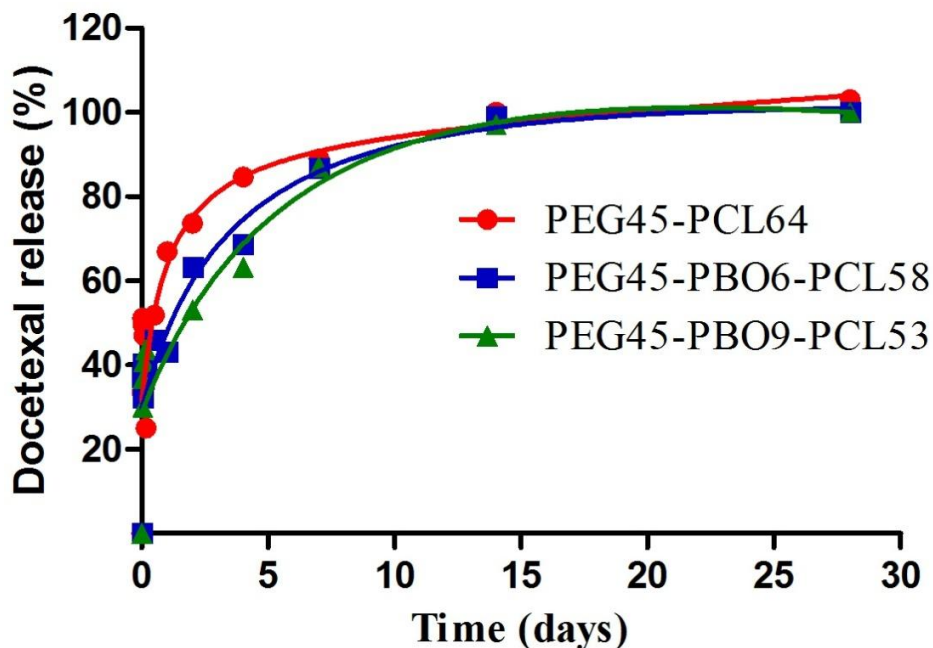


Figure 31: Comparison of in vitro docetaxel release from drug loaded diblock and triblocks polymeric micelles under sink condition at 37 °C

For evaluating the biological activity of the formulation, in-vitro cytotoxic studies were also performed with docetaxel loaded polymeric nanoparticles of similar drug loading, against Taxotere[®], on non-small-cell lung cancer cell line NCI-H23. The viability of the cells post delivery was evaluated via a tetrazolium dye viability assay (MTT, WST-1), according to literature procedures [188, 190, 203, 204] (Figure 32). Data from Figure 32 has shown a lower IC₅₀ for all the docetaxel –loaded PEG₄₅PBO₉PCL₆₁, PEG₄₅PBO₆PCL₅₈ and PEG₄₅PCL₆₂ micelles as compared to the Taxotere[®]. This effect can be explained by a better drug loading, retention and release profile from the polymeric formulation as compared to Taxotere[®]. Taxotere formulation needed higher concentration of formulation to exhibit similar cytotoxicity to polymeric micelles. PEG₄₅PBO₉PCL₆₁ and PEG₄₅PBO₆PCL₅₈ have shown similar IC₅₀ values, which are

intermediate between results achieved with Taxotere[®] and with PEG45-PCL64 micelle. Importantly, the percentage of tumoral cells surviving the treatment was minimal for the PEG45-PBO9-PCL53 micelles, followed by PEG45-PBO6-PCL58 and PEG45-PCL64, revealing the impact of interface tuning on drug release profile of the carrier on the viability of tumor cells.

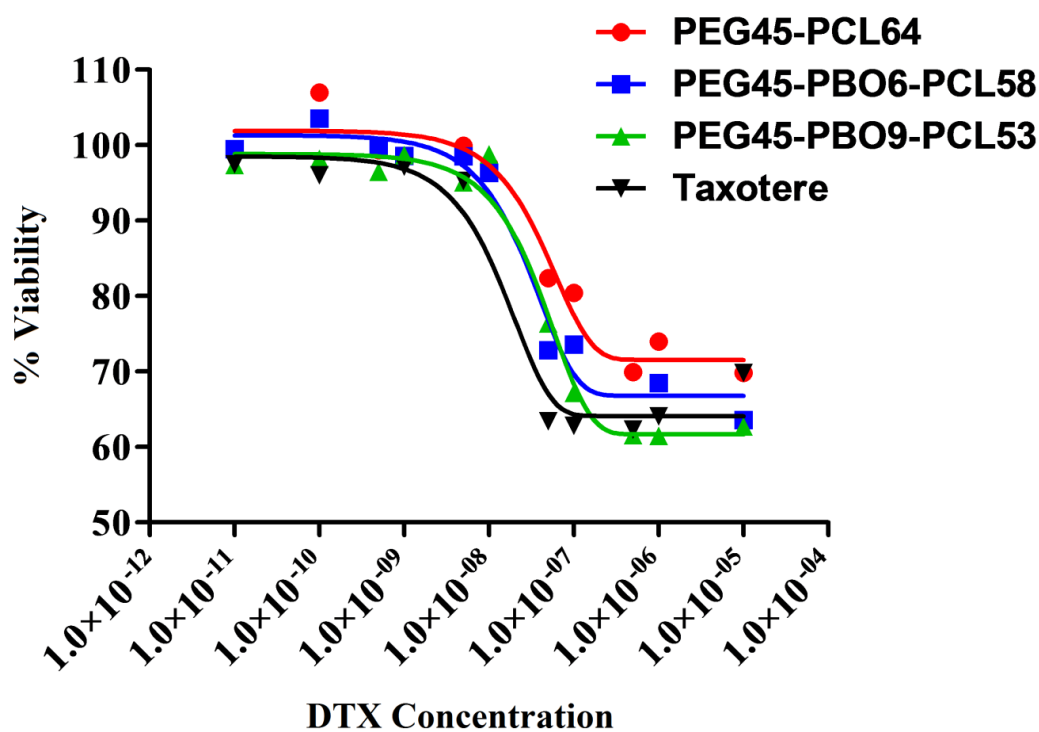


Figure 32: Comparative NCI-H23 lung cancer cells viability exposed to docetaxel-loaded polymeric triblock micelles with tuned interfaces versus standard diblock ones and polysorbate 80/ethanol standard (Taxotere[®]) formulation. The data represent the mean of four experiments. Error bars were removed for clarity.

Another important factor that impacts the applicability of the DDS is the shelf stability of the formulation. The delivery system needs to be stable enough to maintain its efficacy during storage. Consequently, shelf stability studies were performed at room

temperature as well as at 4 °C. In accelerated stability studies, DTX loaded micelles were aged for three weeks and their physicochemical parameters were assessed at specified intervals, as shown in Table 5. The Z_{av} of the diblock micelles has increased from 33.37 nm to 237 nm in 22 days, whereas the triblocks PEG45-PBO9-PCL53-derived micelles have maintained their size (within experimental error). PEG45-PBO6-PCL58 micelles have shown an intermediate size increase from 38.89 nm to 80.1 nm.

Table 5: Aging of drug loaded polymeric micelles as determined by size and zeta potential variation in time

Polymer NP/ degradation time (days)	PEG45PCL62			PEG45PBO6PCL58			PEG45PBO9PCL61		
	Size (Z_{av} , nm, (PDI))	Size (main peak, nm)	Zeta potential (average, mV)	Size (Z_{av} , nm, (PDI))	Size (main peak, nm)	Zeta potential (average, mV)	Size (Z_{av} , nm, (PDI))	Size (main peak, nm)	Zeta potential (average, mV)
0	33.37 (0.355)	25.55	- 1.52	38.89 (0.371)	22.75	- 1.11	39.43 (0.357)	23.55	- 5.44
7	43.89 (0.378)	26.47	0.768	33.57 (0.239)	24.57	- 1.14	32.30 (0.27)	22.74	- 1.78
14	73.84 (0.532)	25.51	- 6.11	47.86 (0.468)	26.62	- 5.88	44.24 (0.42)	24.02	- 7.48
22	237.3 (0.359)	27.35	- 4.47	80.1 (0.300)	27.08	- 4.8	38.31 (0.371)	23.69	- 11.4

Long term stability study was also conducted on the DTX loaded polymeric micelles at 4 °C for 7 months. The polymeric micelles were analyzed in terms of appearance, size, polymer concentration and drug retention (Figure 33). The diblock polymers PEG45-PCL64 were degraded significantly, as evident from their hazy

appearance (Figure 33a), with PEG45-PBO6-PCL58 and PEG45-PBO9-PCL53 micelles evidently less degraded. All these formulations were then filtered through 0.2 μm filters to remove the large aggregates and analyzed for size via DLS. PEG45-PCL64 micelles have shown the maximum increase in the size of polymeric micelle (20 nm), whereas PEG45-PBO9-PCL53 polymeric micelles have resisted the size change within experimental error. The PEG45-PBO6-PCL58 had an intermediate behavior (Figure 33b). The polymer amount was analyzed through a PEG assay. The PEG concentration is not actual polymer concentration in the sample because of the presence of both free PEG and bound PEG in the micellar suspension, However, it can give a good approximation of polymer concentration in the suspension post removal of large aggregates. PEG assay revealed PEG45-PCL64 has formulation dropped its polymer concentration by 50%, whereas in formulation based on triblocks PEG45-PBO6-PCL58 and PEG45-PBO9-PCL53 the polymer content decreased only by approx 10%, (Figure 33c). In term of drug retention, diblock polymeric micelles retained with only 20 % of the drug initially loaded after seven months of storage, while PEG45-PBO9-PCL53 has retained 60-70 % of the initial drug in the same interval (Figure 33d) PEG45-PBO6-PCL58-based micelles had again an intermediate behavior. The experimental results proved the superiority of the triblock copolymers PEG45-PBO6-PCL58 and PEG45-PBO9-PCL53 over the diblock amphiphilic micelles in terms of long term and short term stability.

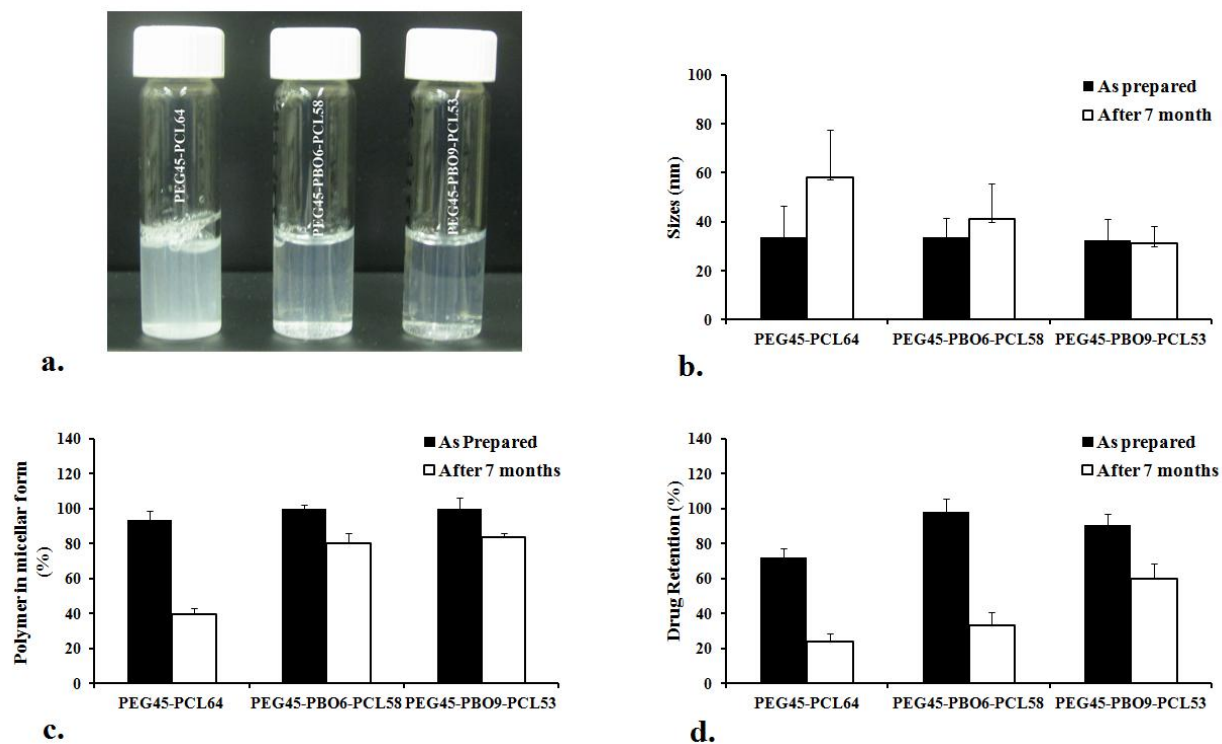


Figure 33: Long term stability of DTX-loaded polymeric micelles after seven months: aspect of formulations (a), size of the polymeric micelles (b), PEG content of formulations (c) and drug loading (d)

Conclusions

The prototype set of copolymers synthesized for this proof-of-concept set of experiments indicate that the interfacial engineering of PEG-PCL diblock copolymers via insertion of a PBO linker between the hydrophilic and hydrophobic blocks of the copolymers impacts enzymatic hydrolytic stability, drug loading, encapsulation efficiency, drug release and stability of formulations. These results reveal how hydrophilic/hydrophobic interface tuning can be used to adjust key properties of polymeric DDSs of this type. Results from this study will advance the development of polymer nanosystems towards exploiting their full capabilities as DDSs.

CHAPTER 5

FUTURE STUDIES OF GENE AND DRUG DELIVERY

The efficient optimized formulations generated from interfacially optimized pyridinium gemini surfactants and their blends with pyridinium cationic lipids highlighted in chapters 2 and 3, are currently being developed further for translating these technologies from in vitro to in vivo, in animal models of lung cancer. Similarly, the optimized polymer DDSs presented in chapter 4 are currently being scaled up in order to be injected in nude mice bearing NCI-H23 tumor xenografts for in vivo evaluation of the drugs delivery system efficiency. If successful, these technologies will constitute a step forward for the treatment of NSCLC.

ABBREVIATIONS

CAC : Critical aggregation concentration

Chol: Cholesterol

CrEL: Cremophor EL

CMC: Critical micelle concentration

DDS: Drug delivery system

DMF: dimethyl formamide

DNA: Deoxyribonucleic acid

DLS: Dynamic light scattering

DOPE: 1,2-dioleoyl-*sn*-glycero-3-phosphoethanolamine

DSC: Differential scanning calorimetry

DTX: Docetaxel

EIPA: 5-(*N*-ethyl-*N*-isopropyl)amiloride

EPR: Enhanced permeation and retention

FBS: Fetal bovine serum

GS: Gemini surfactant

GFP: Green fluorescent protein

GPC: Gel Permeation Chromatography

HPLC: High performance liquid chromatography

LC: Liquid crystal

NMR: Nucleic Magnetic Resonance

PBO: poly(butylene oxide)

PBS: Phosphate buffer saline

PCL: polycaprolactone

PEG: polyethylene glycol

PLA : polylactic acid

RBC: red blood cells

RLU: Relative luminescence units

RNA: Ribonucleic acid

S_A: smectic A

SAXS: Small-angle X-ray scattering

TLC: Thin layer chromatography

TOPM: transmission optical polarized microscopy

WAXS: Wide-angle X-ray scattering

WST: Water soluble tetrazolium salts

BIBLIOGRAPHY

1. American Cancer Society: Cancer Facts and Figures 2012. American Cancer Society, Atlanta, GA, 2012.
2. Nemunaitis, J.J., Gene immunotherapy for non-small cell lung cancer. *Method Mol Biol*, 2009. 542: p. 499-514.
3. Nishio, M., T. Koshikawa, T. Kuroishi, M. Suyama, K. Uchida, Y. Takagi, O. Washimi, T. Sugiura, Y. Ariyoshi, T. Takahashi and R. Ueda, Prognostic significance of abnormal p53 accumulation in primary, resected non-small-cell lung cancers. *J Clin Oncol*, 1996. 14(2): p. 497-502.
4. Muzykantov, V.R., Biomedical aspects of targeted delivery of drugs to pulmonary endothelium. *Expert Opin Drug Deliv*, 2005. 2(5): p. 909-926.
5. Albelda, S.M., Gene therapy for lung cancer and mesothelioma. *Chest*, 1997. 111(6 Suppl): p. 144S-149S.
6. Hoganson, D.K., R. K. Batra, J. C. Olsen and R. C. Boucher, Comparison of the effects of three different toxin genes and their levels of expression on cell growth and bystander effect in lung adenocarcinoma. *Cancer Res*, 1996. 56(6): p. 1315-1323.
7. Carbone, D.P. and J.D. Minna, The molecular genetics of lung cancer. *Adv Int Med*, 1992. 37: p. 153-171.

8. Rami-Porta, R., J.J. Crowley, and P. Goldstraw, The revised TNM staging system for lung cancer. *Ann Thorac Cardiovasc Surg*, 2009. 15(1): p. 4-9.
9. William, W.N., Jr., H. Y. Lin, J. J. Lee, S. M. Lippman, J. A. Roth and E. S. Kim, Revisiting stage IIIB and IV non-small cell lung cancer: analysis of the surveillance, epidemiology, and end results data. *Chest*, 2009. 136(3): p. 701-709.
10. Ilies, M.A. and A.T. Balaban, Recent developments in cationic lipid-mediated gene delivery and gene therapy. *Expert Opin Ther Pat*, 2001. 11(11): p. 1729-1752.
11. Li, W. and F.C. Szoka, Jr., Lipid-based nanoparticles for nucleic acid delivery. *Pharm Res*, 2007. 24(3): p. 438-449.
12. Kay, M.A., State-of-the-art gene-based therapies: the road ahead. *Nat Rev Genet*, 2011. 12(5): p. 316-328.
13. Bennett, J., M. Ashtari, J. Wellman, K. A. Marshall, L. L. Cyckowski, D. C. Chung, S. McCague, E. A. Pierce, Y. Chen, J. L. Bennicelli, X. Zhu, G. S. Ying, J. Sun, J. F. Wright, A. Auricchio, F. Simonelli, K. S. Shindler, F. Mingozzi, K. A. High and A. M. Maguire, AAV2 gene therapy readministration in three adults with congenital blindness. *Sci Transl Med*, 2012. 4(120): p. 120ra15.
14. Dotti, G., B. Savoldo, F. Okur, R. F. Rousseau and M. K. Brenner, Gene therapy for the treatment of cancer: from laboratory to bedside. *Gene Cell Ther*, 2009: p. 1001-1018.

15. Murphy, S.L. and K.A. High, Gene therapy for haemophilia. *Br J Haematol*, 2008. 140(5): p. 479-487.
16. Gao, K. and L. Huang, Nonviral methods for siRNA delivery. *Mol Pharm*, 2009. 6(3): p. 651-658.
17. Cao, H., R. Molday, and J. Hu, Gene therapy: light is finally in the tunnel. *Protein & Cell*, 2011. 2(12): p. 973-989.
18. Li, S.D. and L. Huang, Non-viral is superior to viral gene delivery. *J Control Release*, 2007. 123(3): p. 181-183.
19. Felgner, P.L., T. R. Gadek, M. Holm, R. Roman, H. W. Chan, M. Wenz, J. P. Northrop, G. M. Ringold and M. Danielsen, Lipofection: a highly efficient, lipid-mediated DNA-transfection procedure. *Proc Natl Acad Sci U S A*, 1987. 84(21): p. 7413-7417.
20. Miller, A.D., Cationic liposomes for gene therapy. *Angew Chem Int Ed*, 1998. 37: p. 1768-1785.
21. Kostarelos, K. and A.D. Miller, Synthetic, self-assembly ABCD nanoparticles; a structural paradigm for viable synthetic non-viral vectors. *Chem Soc Rev*, 2005. 34(11): p. 970-994.
22. Nishikawa, M. and L. Huang, Nonviral vectors in the new millennium: delivery barriers in gene transfer. *Hum Gene Ther*, 2001. 12(8): p. 861-870.

23. Pinnaduwaage, P., L. Schmitt, and L. Huang, Use of a quaternary ammonium detergent in liposome mediated DNA transfection of mouse L-cells. *Biochim Biophys Acta*, 1989. 985: p. 33-37.
24. Blessing, T., J.S. Remy, and J.P. Behr, Monomolecular collapse of plasmid DNA into stable virus-like particles. *Proc Natl Acad Sci U S A*, 1998. 95(4): p. 1427-1431.
25. Ilies, M.A., T. V. Sommers, L. C. He, A. Kizewski and V. D. Sharma, Pyridinium Amphiphiles in Gene Delivery - Present and Perspectives, in *Amphiphiles: Molecular Assembly and Applications*, R. Nagarajan, Editor 2011, ACS Symposium Series: Washington, DC. p. 23-38.
26. Bhattacharya, S. and S.K. Samanta, Surfactants Possessing Multiple Polar Heads. A Perspective on their Unique Aggregation Behavior and Applications. *J Phys Chem Lett*, 2011. 2(8): p. 914-920.
27. Ilies, M.A., W.A. Seitz, and A.T. Balaban, Cationic Lipids in Gene Delivery: Principles, Vector Design and Therapeutical Applications. *Curr Pharm Design*, 2002. 8(27): p. 2441-2473.
28. Niculescu-Duvaz, D., J. Heyes, and C.J. Springer, Structure-activity relationship in cationic lipid mediated gene transfection. *Curr Med Chem*, 2003. 10(14): p. 1233-1261.
29. Bhattacharya, S. and A. Bajaj, Advances in gene delivery through molecular design of cationic lipids. *Chem Comm*, 2009(31): p. 4632-4656.

30. Barnard, A., P. Posocco, S. Pricl, M. Calderon, R. Haag, M. E. Hwang, V. W. Shum, D. W. Pack and D. K. Smith, Degradable self-assembling dendrons for gene delivery: experimental and theoretical insights into the barriers to cellular uptake. *J Am Chem Soc*, 2011. 133(50): p. 20288-20300.
31. Esfand, R. and D.A. Tomalia, Poly(amidoamine) (PAMAM) dendrimers: from biomimicry to drug delivery and biomedical applications. *Drug Discov Today*, 2001. 6(8): p. 427-436.
32. Mintzer, M.A. and E.E. Simanek, Nonviral vectors for gene delivery. *Chem Rev*, 2009. 109(2): p. 259-302.
33. Smith, D.K., Dendrimers and the double helix--from DNA binding towards gene therapy. *Curr Top Med Chem*, 2008. 8(14): p. 1187-1203.
34. Hwang, S.J. and M.E. Davis, Cationic polymers for gene delivery: designs for overcoming barriers to systemic administration. *Curr Opin Mol Ther*, 2001. 3(2): p. 183-191.
35. De Laporte, L., J. Cruz Rea, and L.D. Shea, Design of modular non-viral gene therapy vectors. *Biomaterials*, 2006. 27(7): p. 947-954.
36. Midoux, P., C. Pichon, J. J. Yaouanc and P. A. Jaffres, Chemical vectors for gene delivery: a current review on polymers, peptides and lipids containing histidine or imidazole as nucleic acids carriers. *Br J Pharmacol*, 2009. 157(2): p. 166-178.

37. Schaffert, D. and E. Wagner, Gene therapy progress and prospects: synthetic polymer-based systems. *Gene Ther*, 2008. 15(16): p. 1131-1138.
38. Troiber, C. and E. Wagner, Nucleic acid carriers based on precise polymer conjugates. *Bioconjug Chem*, 2011. 22(9): p. 1737-1752.
39. Shuvaev, V.V., M. A. Ilies, E. Simone, S. Zaitsev, Y. Kim, S. S. Cai, A. Mahmud, T. Dziubla, S. Muro, D. E. Discher and V. R. Muzykantov, Endothelial Targeting of Antibody-Decorated Polymeric Filomicelles. *ACS Nano*, 2011. 5(9): p. 6991-6999.
40. Torchilin, V.P., Multifunctional pharmaceutical nanocarriers: promises and problems, in *Nanotechnologies for the Life Sciences*, C. Kumar, Editor 2011, Wiley-VCH: Weinheim. p. 121-155.
41. Reddy, G.R., M. S. Bhojani, P. McConville, J. Moody, B. A. Moffat, D. E. Hall, G. Kim, Y. E. Koo, M. J. Woolliscroft, J. V. Sugai, T. D. Johnson, M. A. Philbert, R. Kopelman, A. Rehemtulla and B. D. Ross, Vascular targeted nanoparticles for imaging and treatment of brain tumors. *Clin Cancer Res*, 2006. 12(22): p. 6677-6686.
42. Menger, F.M. and J.S. Keiper, Gemini surfactants. *Angew Chem Int Ed*, 2000. 39: p. 1906-1920.
43. Zana, R. and J. Xia, eds. *Gemini Surfactants: Synthesis, Interfacial and Solution-Phase Behavior, and Applications*. *Surfactant Science*, ed. A.T. Hubbard. Vol. 117. 2004, Marcel Dekker, Inc: New York. 109-114.

44. Rosenzweig, H.S., V.A. Rakhmanova, and R.C. MacDonald, Diquaternary ammonium compounds as transfection agents. *Bioconjug Chem*, 2001. 12(2): p. 258-263.
45. VanderWoude, I., A. Wagenaar, A. A. Meekel, M. B. ter Beest, M. H. Ruiters, J. B. Engberts and D. Hoekstra, Novel pyridinium surfactants for efficient, nontoxic in vitro gene delivery. *Proc Natl Acad Sci U S A*, 1997. 94(4): p. 1160-1165.
46. Ilies, M.A., W. A. Seitz, B. H. Johnson, E. L. Ezell, A. L. Miller, E. B. Thompson and A. T. Balaban, Lipophilic pyrylium salts in the synthesis of efficient pyridinium-based cationic lipids, gemini surfactants, and lipophilic oligomers for gene delivery. *J Med Chem*, 2006. 49(13): p. 3872-3887.
47. Wettig, S.D., R.E. Verrall, and M. Foldvari, Gemini surfactants: A new family of building blocks for non-viral gene delivery systems. *Curr Gene Ther*, 2008. 8(1): p. 9-23.
48. Biswas, J., S. K. Mishra, P. Kondaiah and S. Bhattacharya, Syntheses, transfection efficacy and cell toxicity properties of novel cholesterol-based gemini lipids having hydroxyethyl head group. *Org Biomol Chem*, 2011. 9(12): p. 4600-4613.
49. Cardoso, A.M., H. Faneca, J. A. Almeida, A. A. Pais, E. F. Marques, M. C. de Lima and A. S. Jurado, Gemini surfactant dimethylene-1,2-bis(tetradecyldimethylammonium bromide)-based gene vectors: a biophysical

- approach to transfection efficiency. *Biochim Biophys Acta*, 2011. 1808(1): p. 341-351.
50. Kirby, A.J., P. Camilleri, J. B. Engberts, M. C. Feiters, R. J. Nolte, O. Soderman, M. Bergsma, P. C. Bell, M. L. Fielden, C. L. Garcia Rodriguez, P. Guedat, A. Kremer, C. McGregor, C. Perrin, G. Ronsin and M. C. van Eijk, Gemini surfactants: new synthetic vectors for gene transfection. *Angew Chem Int Ed Engl*, 2003. 42(13): p. 1448-1457.
 51. Sharma, V.D. and M.A. Ilies, Heterocyclic Cationic Gemini Surfactants: A Comparative Overview of Their Synthesis, Self-Assembling, Physicochemical, and Biological Properties. *Med Res Rev*, 2014. 34(1): p. 1-44.
 52. Menger, F.M. and C.A. Littau, Gemini-surfactants: synthesis and properties. *J Am Chem Soc*, 1991. 113(4): p. 1451-1452.
 53. Israelachvili, J.N., D.J. Mitchell, and B.W. Ninham, Theory of Self-Assembly of Hydrocarbon Amphiphiles into Micelles and Bilayers. *J Chem Soc-Faraday Trans*, 1976. 72: p. 1525-1568.
 54. Danino, D., Y. Talmon, H. Levy, G. Beinert and R. Zana, Branched threadlike micelles in an aqueous solution of a trimeric surfactant. *Science*, 1995. 269: p. 1420-1421.
 55. Zana, R. and Y. Talmon, Dependence of Aggregate Morphology on Structure of Dimeric Surfactants. *Nature*, 1993. 362(6417): p. 228-230.

56. Bernheim-Groswasser, A., R. Zana, and Y. Talmon, Sphere-to-cylinder transition in aqueous micellar solution of a dimeric (gemini) surfactant. *J Phys Chem B*, 2000. 104(17): p. 4005-4009.
57. De, S., V. K. Aswal, P. S. Goyal and S. Bhattacharya, Characterization of new gemini surfactant micelles with phosphate headgroups by SANS and fluorescence spectroscopy. *Chem Phys Lett*, 1999. 303(3-4): p. 295-303.
58. De, S., V. K. Aswal, P. S. Goyal and S. Bhattacharya, Role of spacer chain length in dimeric micellar organization. Small angle neutron scattering and fluorescence studies. *J Phys Chem*, 1996. 100(28): p. 11664-11671.
59. Hattori, N., H. Hirata, H. Okabayashi, M. Furusaka, C. J. O'Connor and R. Zana, Small-angle neutron-scattering study of bis(quaternaryammonium bromide) surfactant micelles in water. Effect of the long spacer chain on micellar structure. *Coll Polym Sci*, 1999. 277(1): p. 95-100.
60. Aswal, V.K., S. De, P. S. Goyal, S. Bhattacharya and R. K. Heenan, Transition from disc to rod-like shape of 16-3-16 dimeric micelles in aqueous solutions. *J Chem Soc-Faraday Transac*, 1998. 94(19): p. 2965-2967.
61. Nagarajan, R., Molecular packing parameter and surfactant self-assembly: The neglected role of the surfactant tail. *Langmuir*, 2002. 18(1): p. 31-38.
62. Nagarajan, R. and E. Ruckenstein, Theory of Surfactant Self-Assembly - a Predictive Molecular Thermodynamic Approach. *Langmuir*, 1991. 7(12): p. 2934-2969.

63. Lin, A.J., N. L. Slack, A. Ahmad, C. X. George, C. E. Samuel and C. R. Safinya, Three-dimensional imaging of lipid gene-carriers: Membrane charge density controls universal transfection behavior in lamellar cationic liposome-DNA complexes. *Biophys J*, 2003. 84(5): p. 3307-3316.
64. VanDerWoude, I., A. Wagenaar, A. A. P. Meekel, M. B. A. TerBeest, M. H. J. Ruiters, J. B. F. N. Engberts and D. Hoekstra, Novel pyridinium surfactants for efficient, nontoxic in vitro gene delivery. *Proc Natl Acad Sci USA*, 1997. 94(4): p. 1160-1165.
65. Meekel, A.A.P., A. Wagenaar, J. Smisterova, J. E. Kroeze, P. Haadsma, B. Bosgraaf, M. C. A. Stuart, A. Brisson, M. H. J. Ruiters, D. Hoekstra and J. B. F. N. Engberts, Synthesis of pyridinium amphiphiles used for transfection and some characteristics of amphiphile/DNA complex formation. *Eur J Org Chem*, 2000: p. 665-673.
66. Quagliotto, P., N. Barbero, C. Barolo, E. Artuso, C. Compari, E. Fisicaro and G. Viscardi, Synthesis and properties of cationic surfactants with tuned hydrophylicity. *J Coll Int Sci*, 2009. 340(2): p. 269-275.
67. Quagliotto, P., G. Viscardi, C. Barolo, E. Barni, S. Bellinvia, E. Fisicaro and C. Compari, Gemini pyridinium surfactants: Synthesis and conductometric study of a novel class of amphiphiles. *J Org Chem*, 2003. 68(20): p. 7651-7660.

68. Bhadani, A. and S. Singh, Novel Gemini Pyridinium Surfactants: Synthesis and Study of Their Surface Activity, DNA Binding, and Cytotoxicity. *Langmuir*, 2009. 25(19): p. 11703-11712.
69. Zhou, L.M., X. H. Jiang, Y. T. Li, Z. Chen and X. Q. Hu, Synthesis and properties of a novel class of gemini pyridinium Surfactants. *Langmuir*, 2007. 23(23): p. 11404-11408.
70. Balaban, A.T. and E. Stepan, Reactions of pyrylium salts with nucleophiles. XIX. Novel bispyridinium salts with potential biological activity. *Rev. Roum. Chim.*, 1987. 32(2): p. 155-177.
71. Dinculescu, A. and A.T. Balaban, Reactions of pyrylium salts with nucleophiles. XIV. New pyridinium salts with potential biological activity. *Rev. Roum. Chim.*, 1980. 25(11-12): p. 1505-1528.
72. Bajaj, A., P. Kondaiah, and S. Bhattacharya, Synthesis and gene transfer activities of novel serum compatible cholesterol-based gemini lipids possessing oxyethylene-type spacers. *Bioconjugate Chem*, 2007. 18(5): p. 1537-1546.
73. Bajaj, A., P. Kondaiah, and S. Bhattacharya, Effect of the nature of the spacer on gene transfer efficacies of novel thiocholesterol derived gemini lipids in different cell lines: A structure-activity investigation. *J Med Chem*, 2008. 51(8): p. 2533-2540.

74. Bajaj, A., P. Kondaiah, and S. Bhattacharya, Gene transfection efficacies of novel cationic gemini lipids possessing aromatic backbone and oxyethylene spacers. *Biomacromolecules*, 2008. 9(3): p. 991-999.
75. Evans, H.C., Alkyl Sulphates .1. Critical Micelle Concentrations of the Sodium Salts. *J Chem Soc*, 1956(Mar): p. 579-586.
76. Berridge, M.V., A. S. Tan, K. D. McCoy and R. Wang, The biochemical and cellular basis of cell proliferation assays that use tetrazolium salts. *Biochemica*, 1996(4): p. 14-19.
77. Ilies, M.A., W. A. Seitz, I. Ghiviriga, B. H. Johnson, A. Miller, E. B. Thompson and A. T. Balaban, Pyridinium cationic lipids in gene delivery: a structure-activity correlation study. *J Med Chem*, 2004. 47(15): p. 3744-3754.
78. Ilies, M.A., W. A. Seitz, M. T. Caproiu, M. Wentz, R. E. Garfield and A. T. Balaban, Pyridinium-Based Cationic Lipids as Gene-Transfer Agents. *Eur J Org Chem*, 2003: p. 2645-2655.
79. Aberle, A.M., M. J. Bennett, R. W. Malone and M. H. Nantz, The counterion influence on cationic lipid-mediated transfection of plasmid DNA. *Biochim Biophys Acta*, 1996. 1299(3): p. 281-283.
80. Davis, P.B. and M.J. Cooper, Vectors for airway gene delivery. *Aaps J*, 2007. 9(1): p. E11-17.

81. Manet, S., Y. Karpichev, D. Bassani, R. Kiagus-Ahmad and R. Oda, Counteranion effect on micellization of cationic gemini surfactants 14-2-14: Hofmeister and other counterions. *Langmuir*, 2010. 26(13): p. 10645-10656.
82. Nostro, P.L., A. L. Nostro, B. W. Ninham, G. Pesavento, L. Fratoni and P. Baglioni, Hofmeister specific ion effects in two biological systems. *Curr Opin Colloid Interface Sci*, 2004. 9(1-2): p. 97-101.
83. Bijma, K. and J.B.F.N. Engberts, Effect of counterions on properties of micelles formed by alkylpyridinium surfactants .1. Conductometry and H-1-NMR chemical shifts. *Langmuir*, 1997. 13(18): p. 4843-4849.
84. Zuidam, N.J. and Y. Barenholz, Electrostatic and structural properties of complexes involving plasmid DNA and cationic lipids commonly used for gene delivery. *Biochim Biophys Acta*, 1998. 1368(1): p. 115-128.
85. Wagner, K., D. Harries, S. May, V. Kahl, J. O. Radler and A. Ben-Shaul, Direct evidence for counterion release upon cationic lipid-DNA condensation. *Langmuir*, 2000. 16: p. 303-306.
86. Kikuchi, I.S. and A.M. Carmona-Ribeiro, Interactions between DNA and synthetic cationic liposomes. *J Phys Chem B*, 2000. 104: p. 2829-2835.
87. Collins, K.D. and M.W. Washabaugh, The Hofmeister effect and the behaviour of water at interfaces. *Quart rev biophys*, 1985. 18(4): p. 323-422.

88. Balaban, A.T., M. A. Ilies, A. Eichhofer and T. S. Balaban, Molecular and crystal structure of a self-assembling pyridinium cationic lipid. *J Molecular Struct*, 2010. 984(1-3): p. 228-231.
89. Earle, M.J. and K.R. Seddon, Ionic liquids. Green solvents for the future. *Pure Appl Chem*, 2000. 72(7): p. 1391-1398.
90. Petrie, S.E.B., Smectic liquid crystals, in *Liquid Crystals*, F.D. Saeva, Editor 1979, Marcel Dekker New York. p. 163-202.
91. Koltover, I., T. Salditt, J. O. Radler and C. R. Safinya, An inverted hexagonal phase of cationic liposome-DNA complexes related to DNA release and delivery. *Science*, 1998. 281(5373): p. 78-81.
92. Regelin, A.E., S. Fankhaenel, L. Gurtesch, C. Prinz, G. von Kiedrowski and U. Massing, Biophysical and lipofection studies of DOTAP analogs. *Biochim Biophys Acta*, 2000. 1464(1): p. 151-164.
93. Heerklotz, H., Interactions of surfactants with lipid membranes. *Quart Rev Biophys*, 2008. 41(3-4): p. 205-264.
94. Conwell, C.C. and L. Huang, Recent Advances in Non-viral Gene Delivery. *Adv Genet*, 2005. 53PA: p. 1-18.
95. Scarzello, M., V. Chupin, A. Wagenaar, M. C. Stuart, J. B. Engberts and R. Hulst, Polymorphism of pyridinium amphiphiles for gene delivery: influence of ionic

- strength, helper lipid content, and plasmid DNA complexation. *Biophys J*, 2005. 88(3): p. 2104-2113.
96. Mingozzi, F. and K.A. High, Therapeutic in vivo gene transfer for genetic disease using AAV: progress and challenges. *Nat Rev Genet*, 2011. 12(5): p. 341-355.
 97. Ewert, K., A. Ahmad, H. M. Evans and C. R. Safinya, Cationic lipid-DNA complexes for non-viral gene therapy: relating supramolecular structures to cellular pathways. *Expert Opin Biol Ther*, 2005. 5(1): p. 33-53.
 98. Kirby, A.J., P. Camilleri, J. B. Engberts, M. C. Feiters, R. J. Nolte, O. Soderman, M. Bergsma, P. C. Bell, M. L. Fielden, C. L. Garcia Rodriguez, P. Guedat, A. Kremer, C. McGregor, C. Perrin, G. Ronsin and M. C. van Eijk, Gemini surfactants: New synthetic vectors for gene transfection. *Angew Chem Int Ed*, 2003. 42(13): p. 1448-1457.
 99. Radler, J.O., I. Koltover, T. Salditt and C. R. Safinya, Structure of DNA-cationic liposome complexes: DNA intercalation in multilamellar membranes in distinct interhelical packing regimes. *Science*, 1997. 275(5301): p. 810-814.
 100. Zhang, Y. and T.J. Anchordoquy, The role of lipid charge density in the serum stability of cationic lipid/DNA complexes. *Biochim Biophys Acta*, 2004. 1663(1-2): p. 143-157.
 101. Crook, K., B. J. Stevenson, M. Dubouchet and D. J. Porteous, Inclusion of cholesterol in DOTAP transfection complexes increases the delivery of DNA to cells in vitro in the presence of serum. *Gene Ther*, 1998. 5(1): p. 137-143.

102. Ilies, M.A., B. H. Johnson, F. Makori, A. Miller, W. A. Seitz, E. B. Thompson and A. T. Balaban, Pyridinium cationic lipids in gene delivery: an in vitro and in vivo comparison of transfection efficiency versus a tetraalkylammonium congener. *Arch Biochem Biophys*, 2005. 435(1): p. 217-226.
103. Lindberg, M.F., N. Carmoy, T. Le Gall, A. Fraix, M. Berchel, C. Lorilleux, H. Couthon-Gourves, P. Bellaud, A. Fautrel, P. A. Jaffres, P. Lehn and T. Montier, The gene transfection properties of a lipophosphoramidate derivative with two phytanyl chains. *Biomaterials*, 2012. 33(26): p. 6240-6253.
104. Berchel, M., T. Le Gall, H. Couthon-Gourves, J. P. Haelters, T. Montier, P. Midoux, P. Lehn and P. A. Jaffres, Lipophosphonate/lipophosphoramidates: a family of synthetic vectors efficient for gene delivery. *Biochimie*, 2012. 94(1): p. 33-41.
105. Montier, T., T. Benvegna, P. A. Jaffres, J. J. Yaouanc and P. Lehn, Progress in cationic lipid-mediated gene transfection: a series of bio-inspired lipids as an example. *Curr Gene Ther*, 2008. 8(5): p. 296-312.
106. Balaban, A.T., Seitz, W. A., Ilies, M. A., Thompson, E. B., Garfield, R. E., Johnson, B. H., Miller, A. L., Wentz, M. J., Pyridinium cationic lipids as gene transfer agents, Patent 2008.
107. Sharma, V.D., E. O. Aifuwa, P. A. Heiney and M. A. Ilies, Interfacial engineering of pyridinium gemini surfactants for the generation of synthetic transfection systems. *Biomaterials*, 2013. 34(28): p. 6906-6921.

108. Balaban, A.T., Seitz, W. A., Ilies, M. A., Thompson, E. B., Garfield, R. E., Johnson, B. H., Miller, A. L., Wentz, M. J., Pyridinium cationic lipids as gene transfer agents, T.A.M. University, Editor 2008.
109. Mallilankaraman, K., R. K. Gandhirajan, B. J. Hawkins and M. Madesh, Visualization of vascular Ca²⁺ signaling triggered by paracrine derived ROS. J Vis Exp, 2011(58): doi. 10.3791/3511.
110. Madesh, M., B. J. Hawkins, T. Milovanova, C. D. Bhanumathy, S. K. Joseph, S. P. Ramachandrarao, K. Sharma, T. Kurosaki and A. B. Fisher, Selective role for superoxide in InsP3 receptor-mediated mitochondrial dysfunction and endothelial apoptosis. J Cell Biol, 2005. 170(7): p. 1079-1090.
111. Rejman, J., A. Bragonzi, and M. Conese, Role of clathrin- and caveolae-mediated endocytosis in gene transfer mediated by lipo- and polyplexes. Mol Ther, 2005. 12(3): p. 468-474.
112. Wang, L.H., K.G. Rothberg, and R.G. Anderson, Mis-assembly of clathrin lattices on endosomes reveals a regulatory switch for coated pit formation. Journal Cell Biol, 1993. 123(5): p. 1107-1117.
113. Rejman, J., V. Oberle, I. S. Zuhorn and D. Hoekstra, Size-dependent internalization of particles via the pathways of clathrin- and caveolae-mediated endocytosis. Biochem J, 2004. 377(Pt 1): p. 159-169.
114. Fretz, M., J. Jin, R. Conibere, N. A. Penning, S. Al-Taei, G. Storm, S. Futaki, T. Takeuchi, I. Nakase and A. T. Jones, Effects of Na⁺/H⁺ exchanger inhibitors on

- subcellular localisation of endocytic organelles and intracellular dynamics of protein transduction domains HIV-TAT peptide and octaarginine. *J Controlled Release*, 2006. 116(2): p. 247-254.
115. Nakase, I., M. Niwa, T. Takeuchi, K. Sonomura, N. Kawabata, Y. Koike, M. Takehashi, S. Tanaka, K. Ueda, J. C. Simpson, A. T. Jones, Y. Sugiura and S. Futaki, Cellular uptake of arginine-rich peptides: roles for macropinocytosis and actin rearrangement. *Mol Ther*, 2004. 10(6): p. 1011-1022.
 116. Farhood, H., N. Serbina, and L. Huang, The role of dioleoyl phosphatidylethanolamine in cationic liposome mediated gene transfer. *Biochim Biophys Acta*, 1995. 1235(2): p. 289-295.
 117. Bhattacharya, S. and S. Haldar, The effects of cholesterol inclusion on the vesicular membranes of cationic lipids. *Biochim Biophys Acta*, 1996. 1283(1): p. 21-30.
 118. Bhattacharya, S. and S. Haldar, Interactions between cholesterol and lipids in bilayer membranes. Role of lipid headgroup and hydrocarbon chain-backbone linkage. *Biochim Biophys Acta*, 2000. 1467(1): p. 39-53.
 119. Munoz-Ubeda, M., S. K. Misra, A. L. Barran-Berdon, C. Aicart-Ramos, M. B. Sierra, J. Biswas, P. Kondaiah, E. Junquera, S. Bhattacharya and E. Aicart, Why is less cationic lipid required to prepare lipoplexes from plasmid DNA than linear DNA in gene therapy? *J Am Chem Soc*, 2011. 133(45): p. 18014-18017.

120. Munoz-Ubeda, M., S. K. Misra, A. L. Barran-Berdon, S. Datta, C. Aicart-Ramos, P. Castro-Hartmann, P. Kondaiah, E. Junquera, S. Bhattacharya and E. Aicart, How does the spacer length of cationic gemini lipids influence the lipoplex formation with plasmid DNA? Physicochemical and biochemical characterizations and their relevance in gene therapy. *Biomacromolecules*, 2012. 13(12): p. 3926-3937.
121. Reilly, M.J., J.D. Larsen, and M.O. Sullivan, Polyplexes Traffic through Caveolae to the Golgi and Endoplasmic Reticulum en Route to the Nucleus. *Mol Pharm*, 2012. 9(5): p. 1280-1290.
122. Gabrielson, N.P. and D.W. Pack, Efficient polyethylenimine-mediated gene delivery proceeds via a caveolar pathway in HeLa cells. *J Control Release*, 2009. 136(1): p. 54-61.
123. Canton, I. and G. Battaglia, Endocytosis at the nanoscale. *Chem Soc Rev*, 2012. 41(7): p. 2718-2739.
124. Wang, T., Z. Ming, W. Xiaochun and W. Hong, Rab7: role of its protein interaction cascades in endo-lysosomal traffic. *Cell Signal*, 2011. 23(3): p. 516-521.
125. Yu, J., E. Deliu, X. Q. Zhang, N. E. Hoffman, R. L. Carter, L. A. Grisanti, G. C. Brailoiu, M. Madesh, J. Y. Cheung, T. Force, M. E. Abood, W. J. Koch, D. G. Tilley and E. Brailoiu, Differential activation of cultured neonatal cardiomyocytes

- by plasmalemmal versus intracellular G protein-coupled receptor 55. *J Biol Chem*, 2013. 288(31): p. 22481-22492.
126. Nemunaitis, J.J.J., *Gene Immunotherapy for Non-Small Cell Lung Cancer*, 2009. p. 498-513.
 127. Grossi, F., K. Kubota, F. Cappuzzo, F. de Marinis, C. Gridelli, M. Aita and J. Y. Douillard, Future scenarios for the treatment of advanced non-small cell lung cancer: focus on taxane-containing regimens. *Oncologist*, 2010. 15(10): p. 1102-1112.
 128. Gelderblom, H., J. Verweij, K. Nooter and A. Sparreboom, Cremophor EL: the drawbacks and advantages of vehicle selection for drug formulation. *Eur J Cancer*, 2001. 37(13): p. 1590-1598.
 129. Ardavanis, A., D. Tryfonopoulos, I. Yiotis, G. Gerasimidis, N. Baziotis and G. Rigatos, Non-allergic nature of docetaxel-induced acute hypersensitivity reactions. *Anti-Cancer Drugs*, 2004. 15(6): p. 581-585.
 130. ten Tije, A.J., J. Verweij, W. J. Loos and A. Sparreboom, Pharmacological effects of formulation vehicles : implications for cancer chemotherapy. *Clin Pharmacokinet*, 2003. 42(7): p. 665-685.
 131. Zhang, H., J. Dou, Y. Zhai, A. Liu and G. Zhai, Advances in the formulations of non-injection administration of docetaxel. *J Drug Target*, 2014. 22(2): p. 87-94.

132. Norris, L.B., Z. P. Qureshi, P. B. Bookstaver, D. W. Raisch, Oliver Sartor, H. Chen, F. Chen and C. L. Bennett, Polysorbate 80 hypersensitivity reactions: a renewed call to action. *Community Oncol*, 2010. 7(9): p. 425-428.
133. Desai, N. V. Trieu, Z. Yao, L. Louie, S. Ci, A. Yang, C. Tao, T. De, B. Beals, D. Dykes, P. Noker, R. Yao, E. Labao, M. Hawkins and P. Soon-Shiong, Increased antitumor activity, intratumor paclitaxel concentrations, and endothelial cell transport of cremophor-free, albumin-bound paclitaxel, ABI-007, compared with cremophor-based paclitaxel. *Clin Cancer Res*, 2006. 12(4): p. 1317-1324.
134. Langer, R., *New Methods of Drug Delivery*. Science, 1990. 249(4976): p. 1527-1533.
135. Jensen, K.D., A. Nori, M. Tijerina, P. Kopeckova and J. Kopecek, Cytoplasmic delivery and nuclear targeting of synthetic macromolecules. *J Control Release*, 2003. 87(1-3): p. 89-105.
136. Bronich, T., *Multifunctional Polymeric Carriers for Gene and Drug Delivery*. *Pharm Res*, 2010. 27(11): p. 2257-2259.
137. Hubbell, J.A., Enhancing drug function. *Science*, 2003. 300(5619): p. 595-596.
138. Ding, B.S., T. Dziubla, V. V. Shuvaev, S. Muro and V. R. Muzykantov, Advanced drug delivery systems that target the vascular endothelium. *Molecular Interventions*, 2006. 6(2): p. 98-112.

139. Khandare, J. and T. Minko, Polymer-drug conjugates: Progress in polymeric prodrugs. *Prog Polym Sci*, 2006. 31(4): p. 359-397.
140. Croy, S.R. and G.S. Kwon, Polymeric micelles for drug delivery. *Curr Pharm Des*, 2006. 12(36): p. 4669-4684.
141. Torchilin, V.P., Micellar nanocarriers: pharmaceutical perspectives. *Pharm Res*, 2007. 24(1): p. 1-16.
142. Elsabahy, M. and K.L. Wooley, Design of polymeric nanoparticles for biomedical delivery applications. *Chem Soc Rev*, 2012. 41(7): p. 2545-2561.
143. Allen, T.M. and P.R. Cullis, Drug delivery systems: Entering the mainstream. *Science*, 2004. 303(5665): p. 1818-1822.
144. Muzykantov, V.R., Biomedical aspects of targeted delivery of drugs to pulmonary endothelium. *Expert Opin drug deliv*, 2005. 2(5): p. 909-926.
145. Pirker, R., J. R. Pereira, A. Szczesna, J. von Pawel, M. Krzakowski, R. Ramlau, I. Vynnychenko, K. Park, C. T. Yu, V. Ganul, J. K. Roh, E. Bajetta, K. O'Byrne, F. de Marinis, W. Eberhardt, T. Goddemeier, M. Emig and U. Gatzemeier, Cetuximab plus chemotherapy in patients with advanced non-small-cell lung cancer (FLEX): an open-label randomised phase III trial. *Lancet*, 2009. 373(9674): p. 1525-1531.
146. Pirker, R., J. R. Pereira, J. von Pawel, M. Krzakowski, R. Ramlau, K. Park, F. de Marinis, W. E. Eberhardt, L. Paz-Ares, S. Storkel, K. M. Schumacher, A. von

- Heydebreck, I. Celik and K. J. O'Byrne, EGFR expression as a predictor of survival for first-line chemotherapy plus cetuximab in patients with advanced non-small-cell lung cancer: analysis of data from the phase 3 FLEX study. *Lancet Oncol*, 2012. 13(1): p. 33-42.
147. Mir, O., P. Boudou-Rouquette, J. Giroux, J. Chapron, J. Alexandre, L. Gibault, S. Ropert, R. Coriat, J. P. Durand, P. R. Burgel, D. Dusser and F. Goldwasser, Pemetrexed, oxaliplatin and bevacizumab as first-line treatment in patients with stage IV non-small cell lung cancer. *Lung Cancer*, 2012. 77(1): p. 104-109.
148. Wang, F., T. K. Bronich, A. V. Kabanov, R. D. Rauh and J. Roovers, Synthesis and evaluation of a star amphiphilic block copolymer from poly(epsilon-caprolactone) and poly(ethylene glycol) as a potential drug delivery carrier. *Bioconjugate Chem*, 2005. 16(2): p. 397-405.
149. Rajagopal, K., A. Mahmud, D. A. Christian, J. D. Pajerowski, A. E. X. Brown, S. M. Loverde and D. E. Discher, Curvature-Coupled Hydration of Semicrystalline Polymer Amphiphiles Yields flexible Worm Micelles but Favors Rigid Vesicles: Polycaprolactone-Based Block Copolymers. *Macromolecules*, 2010. 43(23): p. 9736-9746.
150. Rameez, S., H. Alost, and A.F. Palmer, Biocompatible and biodegradable polymersome encapsulated hemoglobin: a potential oxygen carrier. *Bioconjugate Chem*, 2008. 19(5): p. 1025-1032.

151. Gref, R., Y. Minamitake, M. T. Peracchia, V. Trubetskoy, V. Torchilin and R. Langer, Biodegradable Long-Circulating Polymeric Nanospheres. *Science*, 1994. 263(5153): p. 1600-1603.
152. Yasugi, K., Y. Nagasaki, M. Kato and K. Kataoka, Preparation and characterization of polymer micelles from poly(ethylene glycol)-poly(D,L-lactide) block copolymers as potential drug carrier. *J Control Release*, 1999. 62(1-2): p. 89-100.
153. Hagan, S.A., A. G. A. Coombes, M. C. Garnett, S. E. Dunn, M. C. Davis, L. Illum, S. S. Davis, S. E. Harding, S. Purkiss and P. R. Gellert, Polylactide-poly(ethylene glycol) copolymers as drug delivery systems .1. Characterization of water dispersible micelle-forming systems. *Langmuir*, 1996. 12(9): p. 2153-2161.
154. Wei, X.W., C. Y. Gong, M. Y. Gou, S. Z. Fu, Q. F. Guo, S. Shi, F. Luo, G. Guo, L. Y. Qiu and Z. Y. Qian, Biodegradable poly(epsilon-caprolactone)-poly(ethylene glycol) copolymers as drug delivery system. *Int J Pharm*, 2009. 381(1): p. 1-18.
155. Ghoroghchian, P.P., G. Z. Li, D. H. Levine, K. P. Davis, F. S. Bates, D. A. Hammer and M. J. Therien, Bioresorbable vesicles formed through spontaneous self-assembly of amphiphilic poly(ethylene oxide)-block-polycaprolactone. *Macromolecules*, 2006. 39(5): p. 1673-1675.
156. Wong, S.Y., J.M. Pelet, and D. Putnam, Polymer systems for gene delivery-past, present, and future. *Prog Polym Sci*, 2007. 32(8-9): p. 799-837.

157. Xu, L. and T. Anchordoquy, Drug Delivery Trends in Clinical Trials and Translational Medicine: Challenges and Opportunities in the Delivery of Nucleic Acid-Based Therapeutics. *J Pharm Sci*, 2011. 100(1): p. 38-52.
158. Batrakova, E.V., T. K. Bronich, J. A. Vetro and A. V. Kabanov, Polymer micelles as drug carriers. *Nanopart. Drug Carriers*, 2006: p. 57-93.
159. Otsuka, H., Y. Nagasaki, and K. Kataoka, PEGylated nanoparticles for biological and pharmaceutical applications. *Adv Drug Deliv Rev*, 2003. 55(3): p. 403-419.
160. Kataoka, K., A. Harada, and Y. Nagasaki, Block copolymer micelles for drug delivery: design, characterization and biological significance. *Adv Drug Deliv Rev*, 2001. 47(1): p. 113-131.
161. Schmieder, A.H., L. E. Grabski, N. M. Moore, L. A. Dempsey and S. E. Sakiyama-Elbert, Development of novel poly(ethylene glycol)-based vehicles for gene delivery. *Biotech Bioeng*, 2007. 96(5): p. 967-976.
162. Gaucher, G., M. H. Dufresne, V. P. Sant, N. Kang, D. Maysinger and J. C. Leroux, Block copolymer micelles: preparation, characterization and application in drug delivery. *J Control Release*, 2005. 109(1-3): p. 169-188.
163. Discher, B.M., Y. Y. Won, D. S. Ege, J. C. M. Lee, F. S. Bates, D. E. Discher and D. A. Hammer, Polymersomes: Tough vesicles made from diblock copolymers. *Science*, 1999. 284(5417): p. 1143-1146.

164. Savic, R., L. B. Luo, A. Eisenberg and D. Maysinger, Micellar nanocontainers distribute to defined cytoplasmic organelles. *Science*, 2003. 300(5619): p. 615-618.
165. Bader, H., H. Ringsdorf, and B. Schmidt, Watersoluble Polymers in Medicine. *Angew Chem*, 1984. 123(Aug): p. 457-485.
166. Kabanov, A.V., E.V. Batrakova, and D.W. Miller, Pluronic((R)) block copolymers as modulators of drug efflux transporter activity in the blood-brain barrier. *Adv Drug Deliv Rev*, 2003. 55(1): p. 151-164.
167. Langer, R. and D.A. Tirrell, Designing materials for biology and medicine. *Nature*, 2004. 428(6982): p. 487-492.
168. Oerlemans, C., W. Bult, M. Bos, G. Storm, J. F. Nijsen and W. E. Hennink, Polymeric micelles in anticancer therapy: targeting, imaging and triggered release. *Pharm Res*, 2010. 27(12): p. 2569-2589.
169. Kim, D.W., S. Y. Kim, H. K. Kim, S. W. Kim, S. W. Shin, J. S. Kim, K. Park, M. Y. Lee and D. S. Heo, Multicenter phase II trial of Genexol-PM, a novel Cremophor-free, polymeric micelle formulation of paclitaxel, with cisplatin in patients with advanced non-small-cell lung cancer. *Ann Oncol*, 2007. 18(12): p. 2009-2014.
170. Simone, E.A., T.D. Dziubla, and V.R. Muzykantov, Polymeric carriers: role of geometry in drug delivery. *Expert Opin Drug Deliv*, 2008. 5(12): p. 1283-1300.

171. Greish, K., J. Fang, T. Inutsuka, A. Nagamitsu and H. Maeda, Macromolecular therapeutics: advantages and prospects with special emphasis on solid tumour targeting. *Clin Pharmacokinet*, 2003. 42(13): p. 1089-1105.
172. Geng, Y., P. Dalhaimer, S. S. Cai, R. Tsai, M. Tewari, T. Minko and D. E. Discher, Shape effects of filaments versus spherical particles in flow and drug delivery. *Nature Nanotech*, 2007. 2(4): p. 249-255.
173. Jaye, M., K. J. Lynch, J. Krawiec, D. Marchadier, C. Maugeais, K. Doan, V. South, D. Amin, M. Perrone and D. J. Rader, A novel endothelial-derived lipase that modulates HDL metabolism. *Nat Genet*, 1999. 21(4): p. 424-428.
174. Goldberg, I.J., Lipoprotein lipase and lipolysis: central roles in lipoprotein metabolism and atherogenesis. *J Lipid Res*, 1996. 37(4): p. 693-707.
175. Yasuda, T., T. Ishida, and D.J. Rader, Update on the role of endothelial lipase in high-density lipoprotein metabolism, reverse cholesterol transport, and atherosclerosis. *Circ J*, 2010. 74(11): p. 2263-2270.
176. Nie, T., Y. Zhao, Z. Xie and C. Wu, Micellar formation of poly(caprolactone-block-ethylene oxide-block-caprolactone) and its enzymatic biodegradation in aqueous dispersion. *Macromolecules*, 2003. 36: p. 8825-8829.
177. Gan, Z., T. F. Jim, M. Li, Z. Yuer, S. Wang and C. Wu, Enzymatic Biodegradation of Poly(ethylene oxide-b-caprolactone) Diblock Copolymer and Its Potential Biomedical Applications. *Macromolecules*, 1999. 32: p. 590-594.

178. Samarajeewa, S., R. Shrestha, Y. Li and K. L. Wooley, Degradability of poly(lactic acid)-containing nanoparticles: enzymatic access through a cross-linked shell barrier. *J Am Chem Soc*, 2012. 134(2): p. 1235-1242.
179. Jiang, Z.P., Z. S. Zhu, C. J. Liu, Y. Hu, W. Wu and X. Q. Jiang, Non-enzymatic and enzymatic degradation of poly(ethylene glycol)-b-poly-(epsilon-caprolactone) diblock copolymer micelles in aqueous solution. *Polymer*, 2008. 49(25): p. 5513-5519.
180. Muratov, A. and V.A. Baulin, Degradation versus self-assembly of block copolymer micelles. *Langmuir*, 2012. 28(6): p. 3071-3076.
181. Gref, R., M. Luck, P. Quellec, M. Marchand, E. Dellacherie, S. Harnisch, T. Blunk and R. H. Muller, 'Stealth' corona-core nanoparticles surface modified by polyethylene glycol (PEG): influences of the corona (PEG chain length and surface density) and of the core composition on phagocytic uptake and plasma protein adsorption. *Colloids Surf B Biointerfaces*, 2000. 18(3-4): p. 301-313.
182. Liu, J., F. Zeng, and C. Allen, Influence of serum protein on polycarbonate-based copolymer micelles as a delivery system for a hydrophobic anti-cancer agent. *J Control Release*, 2005. 103(2): p. 481-497.
183. Romberg, B., W.E. Hennink, and G. Storm, Sheddable coatings for long-circulating nanoparticles. *Pharm Res*, 2008. 25(1): p. 55-71.
184. Zhu, X.B., V. D. Sharma, M. Fryd, M. A. Ilies and B. B. Wayland. Enzyme and acid catalyzed degradation of PEG(45)-b-PBO0,6,9-b-PCL60 micelles: Increased

- hydrolytic stability by engineering the hydrophilic-hydrophobic interface, *Polymer*, 2013, 54, 2879-2886.
185. Lam, H., X. Gong, and C. Wu, Novel differential refractometry study of the enzymatic degradation kinetics of poly(ethylene oxide)-b-poly(epsilon-caprolactone) particles dispersed in water. *J Phys Chem B*, 2007. 111(7): p. 1531-1535.
 186. Kohane, D.S. and R. Langer, Biocompatibility and drug delivery systems. *Chemical Sci*, 2010. 1(4): p. 441-446.
 187. Geng, Y. and D.E. Discher, Hydrolytic degradation of poly(ethylene oxide)-block-polycaprolactone worm micelles. *J Am Chem Soc*, 2005. 127(37): p. 12780-12781.
 188. Elsabahy, M., M. E. Perron, N. Bertrand, G. E. Yu and J. C. Leroux, Solubilization of docetaxel in poly(ethylene oxide)-block-poly(butylene/styrene oxide) micelles. *Biomacromolecules*, 2007. 8(7): p. 2250-2257.
 189. Rao, B.M., A. Chakraborty, M. K. Srinivasu, M. L. Devi, P. R. Kumar, K. B. Chandrasekhar, A. K. Srinivasan, A. S. Prasad and J. Ramanatham, A stability-indicating HPLC assay method for docetaxel. *J Pharm Biomed Anal*, 2006. 41(2): p. 676-681.
 190. Ostacolo, L., M. Marra, F. Ungaro, S. Zappavigna, G. Maglio, F. Quaglia, A. Abbruzzese and M. Caraglia, In vitro anticancer activity of docetaxel-loaded micelles based on poly(ethylene oxide)-poly(epsilon-caprolactone) block

- copolymers: Do nanocarrier properties have a role? *J Control Release*, 2010. 148(2): p. 255-263.
191. Gan, Z., B. Jiang, and J. Zhang, Poly(ϵ -caprolactone)/poly(ethylene oxide) diblock copolymer. I. Isothermal crystallization and melting behavior. *J Appl Polym Sci*, 1996. 59(6): p. 961-967.
 192. Floudas, G., G. Reiter, O. Lambert and P. Dumas, Structure and Dynamics of Structure Formation in Model Triarm Star Block Copolymers of Polystyrene, Poly(ethylene oxide), and Poly(ϵ -caprolactone). *Macromolecules*, 1998. 31(21): p. 7279-7290.
 193. Matsumura, Y. and H. Maeda, A New Concept for Macromolecular Therapeutics in Cancer Chemotherapy: Mechanism of Tumoritropic Accumulation of Proteins and the Antitumor Agent Smancs. *Cancer Res*, 1986. 46: p. 6387-6392.
 194. Maeda, H. and Y. Matsumura, Tumoritropic and lymphotropic principles of macromolecular drugs. *Crit Rev Ther Drug Carrier Syst*, 1989. 6(3): p. 193-210.
 195. Mikhail, A.S. and C. Allen, Block copolymer micelles for delivery of cancer therapy: transport at the whole body, tissue and cellular levels. *J Control Release*, 2009. 138(3): p. 214-223.
 196. Iyer, A.K., G. Khaled, J. Fang and H. Maeda, Exploiting the enhanced permeability and retention effect for tumor targeting. *Drug Discov Today*, 2006. 11(17-18): p. 812-818.

197. Kabanov, A.V., I. R. Nazarova, I. V. Astafieva, E. V. Batrakova, V. Y. Alakhov, A. A. Yaroslavov and V. A. Kabanov, Micelle Formation and Solubilization of Fluorescent Probes in Poly(oxyethylene-b-oxypropylene-b-oxyethylene) Solutions. *Macromolecules*, 1995. 28(7): p. 2303-2314.
198. Gopferich, A., Mechanisms of polymer degradation and erosion. *Biomaterials*, 1996. 17(2): p. 103-114.
199. Lenz, R., Biodegradable polymers, in *Biopolymers I*, R. Langer and N. Peppas, Editors. 1993, Springer Berlin Heidelberg. p. 1-40.
200. Li, B., M. Sedlacek, I. Manoharan, R. Boopathy, E. G. Duysen, P. Masson and O. Lockridge, Butyrylcholinesterase, paraoxonase, and albumin esterase, but not carboxylesterase, are present in human plasma. *Biochem Pharmacol*, 2005. 70(11): p. 1673-1684.
201. Tsai, D.C., S. A. Howard, T. F. Hogan, C. J. Malanga, S. J. Kandzari and J. K. H. Ma, Preparation and in vitro evaluation of polylactic acid-mitomycin C microcapsules. *J Microencapsul*, 1986. 3(3): p. 181-193.
202. Wakiyama, N., K. Juni, and M. Nakano, Preparation and Evaluation in Vitro of Polylactic Acid Microspheres Containing Local Anesthetics. *Chem Pharm Bull*, 1981. 29(11): p. 3363-3368.
203. Zheng, D.H., X. L. Li, H. E. Xu, X. W. Lu, Y. Hu and W. X. Fan, Study on docetaxel-loaded nanoparticles with high antitumor efficacy against malignant melanoma. *Acta Biochim Biophys Sinica*, 2009. 41(7): p. 578-587.

204. Zhu, Z., Y. Li, X. Li, R. Li, Z. Jia, B. Liu, W. Guo, W. Wu and X. Jiang, Paclitaxel-loaded poly(N-vinylpyrrolidone)-b-poly(epsilon-caprolactone) nanoparticles: preparation and antitumor activity in vivo. *J Control Release*, 2010. 142(3): p. 438-446.
205. Benoit, J., S. Benita, F. Puisieux and C. Thies, Stability and release kinetics of drugs incorporated within microspheres. *Microspheres Drug Delivery*, Elsevier, Amsterdam, 1984: p. 91-102.